Realistic Chipless RFID: Identification and Localization

Der Fakultät für Ingenieurwissenschaften,
Abteilung Elektrotechnik und Informationstechnik
der Universität Duisburg-Essen

zur Erlangung des akademischen Grades

Doktor der Ingenieurwissenschaften (Dr.-Ing.)

genehmigte Dissertation

von

Abdelfattah Megahed

aus

Kalyobiya, Egypt

Gutachter:

Prof. Dr.-Ing. Thomas Kaiser

Prof. Dr.-Ing. Jürgen Götze

Tag der mündlichen Prüfung: 13.12.2016

Fachgebiet Digitale Signalverarbeitung (DSV)
Universität Duisburg-Essen
Bismarckstrasse 81
47057 Duisburg
Germany
Tel.: +49 (203) 3 79-32 87
Fax : +49 (203) 3 78-34 98

Referent: Prof. Dr.-Ing. Thomas Kaiser
Co-Referent: Dr.-Ing. Jürgen Götze
Vorsitzende: Prof. Dr. István Erlich
Tag der Promotion: 13.12.2016

Mit Unterstützung des Deutschen
Akademischen Austauschdienstes

Acknowledgment

First of all, I would like to express my deepest gratitude and respect to my advisor Prof. Thomas Kaiser for providing me the opportunity to be a doctoral student at DSV and for all support and encouragement throughout the years. Also many thanks to Prof. Dr.-Ing. Jürgen Götze for his kind care in my research and reviewing my thesis. I also want to show my gratitude to Dr. -Ing Mohammed El-Hadidiy, Prof. Hadia El-Henawy, Prof. Dr. ir. A.J. Han Vink and Marc Hoffman for their technical advise and support. For all of them, many thanks for your excellent supervision and professional guidance.

I am also deeply grateful for working with the best team whom I call my brothers, Ahmed El-Awamry and Maher Khaliel. We've been together through thick and thin. Every discussion with you is an inspiration to me, stimulating me to provide innovative solutions for technical challenges. Without anyone of you, I could not have achieved such progress. For all the members of DSV thanks for always lending us a helping hand when we needed it.

Special gratitude is for the committee members who were present in my doctoral defense. They are Prof. Dr. Kokozinski, Prof. Dr. Gerd Bacher, Prof. Dr. István Erlich. It was my honor to communicate with you about my work. Also I am glad to have such a wonderful opportunity to learn from you.

I want to say thanks to my family for their forever encouragement and selfless love. My wife Aya, words cant describe my love and gratitude to you. For all you have done and support you have given to me, thank you I can never repay you. Thanks to my dear daughter, Lara, for upgrading me to a Dad! Without you my life would have not had such happiness and beautifulness you are a blessing from above. For my parents sister, brother and my lovely aunt Fawkia thank you for making me the man I am today.

The dissertation is dedicated to all of you, the people who I will always love, my friends and my family!

Abdelfattah Megahed

Duisburg, Germany

November, 2017

Abstract

For mass deployment of RFID systems, cheap and accurate item level identification and tracking are profoundly needed. Fortunately, unlike conventional chip-based RFID, chipless RFID systems offers low-cost printable tags holding a better chance to enter the era of penny-cost tags. This dissertation concentrated on solving three challenges in the detection of the chipless tag inside an indoor environment.

The first aspect discussed in the thesis are the chipless RFID clutter removal techniques. In chipless RFID the environmental clutter response is defined as the signal reflected from the environment, that does not interact with the tag. This signal has higher power than the backscattered signal from the tag, rendering the tag signature undetectable. Two algorithms to overcome this problem was used, the first is empty room calibration. The first algorithm is based on subtracting the measurement with the tag from the one without. The second algorithm is Rake receiver using PN sequence; this algorithm requires no pre-measurement calibration.

The second aspect is notch detection and identification which is a critical part of the chipless system. This part is responsible for converting the notches into bits. For effective detection, a windowing operation is proposed, where each window may contain a notch or not. Three novel techniques are implemented to detect the notch. The first is matched filter were a reference notch is compared with the incoming signal. The second is window based singular value decomposition, where a constellation is created to detect not only the existence of a notch but also the bandwidth of the notch. The third notch detection technique is dynamic frequency warping. This technique utilizes non-linear warping to detect the notch and the frequency shifts that occurs on the notch.

The third aspect discussed in the thesis is tag localization. In this aspect, two algorithms are implemented and explained. The first is trilateration which requires three different readers. The second localization algorithm exploits received signal strength and angle of arrival to detect the location of the tag accurately.

All the algorithms were tested using a real testbed to validate the reliability of the techniques. The measurements were done using fabricated tags in an indoor environment using Software Defines Radio (SDR).

Abstrakt

Für die weitere Massenverbreitung von RFID Systemen ist ein günstiges und genaues Verfahren zur Objektlokalisierung und –verfolgung zwingend erforderlich. Chiplose RFID Systeme erlauben im Gegensatz zu herkömmlichen chipbehafteten RFID Systemen den Einsatz von einfachen, druckbaren RFID Tags, eine Möglichkeit zum Einstieg in die Ära von extrem billigen RFID Tags. Diese Dissertation konzentriert sich auf die Lösung von drei Herausforderungen bei der Erkennung von chiplosen RFID Tags innerhalb geschlossener Räume.

Der erste in der vorliegenden Arbeit diskutierte Aspekt beschäftigt sich mit Methoden zum Eliminieren des Störechos der Umgebung (clutter removal techniques). Im chiplosen RFID System ist das Umgebungsstörecho definiert durch das von der Umgebung reflektierte Signal, das nicht mit dem RFID Tag interagiert. Die Stärke dieses Signals ist in jedem Fall größer als die des vom RFID Tag zurückgestrahlten (backscattered) Signals, was die Signaturerkennung des RFID Tags unmöglich macht. Zur Lösung dieses Problems schlage ich zwei Algorithmen vor. Der erste ist die Leerraum-Kalibrierung (empty room calibration). Bei diesem Algorithmus werden die Messungen mit RFID Tag von denen ohne RFID Tags abgezogen. Der zweite Algorithmus basiert auf dem Rake-Receiver unter Nutzung einer Zufallsfolge (PN sequence), er erfordert keine zusätzliche Kalibrierung.

Der zweite Aspekt betrifft die Notch Erkennung und Identifikation, ein sehr wichtiger Bereich des chiplosen RFID Systems. Er ist dafür verantwortlich, die Notchs in Bits umzuwandeln. Für eine effektive Detektion werden Windowing (Fenster) Verfahren vorgeschlagen, wobei jedes Fenster einen oder auch keinen Notch beinhalten kann. Insgesamt drei neue Verfahren zur Notch Erkennung wurden implementiert. Als erstes ein Matched Filter (MF), in dem der einkommende Notch mit einem Referenz Notch verglichen wird. Das zweite Verfahren basiert auf einer gefensterten Singulärwertzerlegung, damit kann sowohl der Notch erkannt werden, als auch seine Bandbreite bestimmt werden. Als drittes Verfahren wird das dynamische Frequency Warping vorgestellt. Diese Technik nutzt nichtlineare um die Notche und

die Frequenzverschiebungen, die an den Notches auftreten, zu erkennen.

Als dritter Aspekt wird die Lokalisierung der RFID Tags in dieser Dissertation diskutiert. Dazu werden zwei Algorithmen erklärt und implementiert. Der erste Algorithmus beruht auf der Triangulation durch drei getrennte RFID Lesegeräte, während sich der zweite die Position des RFID Tags aus der Signalstärke und dem Winkel des vom RFID Tag kommenden Signals berechnet.

Alle genannten Algorithmen und Verfahren wurden in einer realen Innenraum Testumgebung mit RFID Tags und einer Software Defined Radio (SDR) Plattform vermessen, um die Zuverlässigkeit der Algorithmen unter normalen Bedingungen zu überprüfen.

Contents

List of Acronyms

RFID	Radio Frequency Identification
HF	High Frequency
UHF	Ultra High Frequency
IoT	Internet of Things
FC	Frequency Coded
UWB	Ultra Wide Band
FCC	Federal Communication Commission
RCS	Radar Cross Section
SDR	Software Defined Radio
WI	Wireless Insite
PN	Pseudo Noise
SVD	Singular Value Decomposition
DTW	Dynamic Time Warping
MPM	Matrix Pencil Method
AWGN	Additive White Gaussian Noise
ASIC	Application-Specific Integrated Circuit
CW	Continues Wave
LFM	Linear Frequency Modulation
FT	Fourier Transform
RT	Ray Tracing
SBR	Shooting and Bouncing Ray method
RA	Reflect Array
VCO	Voltage Controlled Oscillator
FC	Frequency Controller
ADC	Analog to Digital Converter

FPGA	Field Programmable Gate Array
MTD	Moving Target Indicator
LoS	Line of Site
CPW	Coplanar Waveguide
GLFSR	Galois Linear Feedback Shift Register
USRP	Universal Software Radio Peripheral
SNR	Signal to Noise Ratio
STMPM	Short-Time Matrix Pencil Method
WB-SVD	Window Based Signal Variable Decomposition
SSR	Signal Space Representation
NWC	Notch Width Coding
MDVC	Minimum Distance Vector Criterion
RSS	Received Signal Strength
ToA	Time of Arrival
AoA	Angle of Arrival
EIRP	Effective Isotropic Radiated Power
MUSIC	Multiple Signal Classification
ESPRIT	Estimation of Signal Parameters via Rotational Invariance Technique

List of Figures

1 Introduction

Radio Frequency Identification (RFID) has undergone significant development, regarding applications, in the past decade. It now has a large number of tag families, each family serving a specific market and fulfilling very special needs. However, since the adoption of the retailers to RFID tags for shelf-level stock replenishment, the number of tags is expected to grow from 7 to 25 billion in 2020 [2]. Experts also anticipate rapid growth of RFID use in the pharmaceutical market for anti-counterfeiting applications [3]. This extremely wide variety of applications has yielded a significant number of limitations, which differ according to the intended field of use, necessitating the creation of tags of various sizes, able (or not) to resist high mechanical- or temperature-based stresses or to ensure secure data exchange [4].

To meet this exponential rising needs, new RFID technologies have appeared over time, where better tags and systems are developed. This thesis will concentrate on passive tags, which are tags which need no internal batteries to operate. This type of tags is cheap and small, which makes them ideal candidates for mass deployment.

The first passive technology was High Frequency (HF) tags. These tags relied on coupling for identification, which leads to a very low reading range. This was all replaced by Ultra High Frequency (UHF) RFID tags, where the signal is exchanged by wave propagation. Now tags are not only limited to the domain of identification, but new domains are open. Passive RFID are now used for sensing, even integrating with other wireless technologies like WiFi [5], Bluetooth [6] or Zigbee [7]. This is only the beginning, new standards and technologies are emerging every day to achieve full replacement of the optical barcodes and smooth the transition to the age of Internet of Things (IoT). In IoT, all devices will have the capability to sense the environment and interact with it.

In passive UHF RFID, the absence of the battery in the tag results in a lower cost than the active tags. However, when considering the concept of the tag cost, barcodes will always be the

benchmark reference. These led to the introduction of chipless RFID or RF barcodes. These tags do not contain any chip, which makes them much cheaper than the UHF tags. To understand the development of chipless RFID, it is important to view it in comparison to the UHF RFID and barcodes. As mentioned above the RFID has the advantage of having high functionality given by the use of electromagnetic waves for data exchange. These functions are not possible to implement using optical barcodes. Even though, till now 70% of all items are equipped with barcodes [4]. The reason for this is that the optical reader and barcode are extremely cheap. Due to the presence of electronic circuits, UHF tags have a non-negligible cost much higher than that of barcodes. Therefore, the logical step is to produce tags that do not contain chips. The chipless RFID have the advantage of having increased reading range and the possibility to detect multiple 'barcodes' at the same time, which is not possible by using optical barcodes.

1.1 Motivation and Scope

Chipless tags are most often composed of a substrate (like paper) on which specific conductive patterns are placed. The interaction of the indecent electromagnetic wave with the geometry and shape of these patterns will give the tag ID or signature, thus eliminating the need for a chip. This hard coded read-only signature will make the tag hard to tamper with making the tag more secure. The chipless tag may vary in its shape or design which makes the possibility to design any signature possible. Depending on the design of the tag, the signature could be found in either the time response or the frequency response. Each has its features and disadvantages, in this thesis, we will concentrate on the Frequency Coded (FC) tags.

There is much work done related to the design of the FC chipless tags. It FC chipless tags consists of frequency resonators that absorb certain frequencies from the incident Ultra Wide Band (UWB) signal, creating a notch. This notched signal is then reflected back to the reader where it is detected and decoded, just like a radar system. Unfortunately, all the research is focused on the tag side, and little work has been done on the reader side.

The efficiency of the reader will make or break the chipless RFID system. Certain detection challenges must be addressed like:

1. **Reader transmitted signal**: Since the tags are FC, the transmitted signal should have high bandwidth to cover the operation bandwidth of the tag. Ideally a time impulse should include the whole bandwidth needed, but unfortunately, its power has to be under the UWB

Federal Communication Commission (FCC) regulation mask. This means that the signal power should be less than the noise power. Considering that the reflected power from the tag is very low, using the pulse signal will be useless. An investigation on alternative signals must be studied, and the efficiency of the system should be analyzed.

2. **Radar Cross Section (RCS) of the tag**: Its frequency response describes every tag investigated in the literature. Which makes sense, since the objective is to study the efficiency of the resonators at different frequencies. In a real scenario, the tag's RCS has a spacial correlation. Which means that the tag has an RCS radiation pattern, making it hard to detect at certain angles. Therefore, to calculate the interrogation zone both the radiation pattern of the reader antenna and the tag has to be considered.

3. **The channel and clutter effects**: Unlike other wireless systems where the base-station and the users are using different communication domains to communicate (like frequency or time), the reader and the tag use the same frequency and time. This will lead to one of the biggest problems in chipless RFID , which is clutter. Clutter or self-interference is the signal generated by the reader and reflected back from the environment. The clutter response power is usually higher than the signal backscattered from the tag.

4. **Notch detection**: After the reader receives the signal, a notch detection should be applied. This is important to develop an efficient detection algorithm that could detect the notches. This should algorithm should be fast and reliable.

5. **Localization**: More and more applications require localization. For localization to be done accurately, all the above problems have to be addressed.

1.2 Dissertation Contributions and Organization

In this dissertation, each reader aspect mentioned above will be considered. Each problem will be intensively simulated and modeled. Moreover, real-time measurements will be done using conventional measurement equipment and a commercial Software Defined Radio (SDR). The main contribution and chapter organization could be summarized as follows.

1. **Chapter 2: Background on Chipless RFID**
   This chapter presents an introduction to RFID. It begins by categorizing different types of RFID and their related applications. It briefly shows the UHF system and the ON/OFF

keying used. It then goes to explain the chipless system and the gives a short description on the limitation of the reader in the chipless RFID system. It also gives a brief introduction on the test-bed used.

2. **Chapter 3: RFID Channel Modeling, Estimation and Equalization**
   Chapter 3 starts by formulating the chipless RFID channel. It clearly shows the effect of the clutter response on the received signal. Moreover, the equations clearly show the spatial dependence of tag's RCS. It also introduces a novel way, using a ray tracing tool Wireless Insite (WI), to simulate the EM designed tag. The WI uses the frequency dependent RCS radiation pattern to calculate what will the reader detect in an indoor environment. These results are compared with the real measurements taken using an SDR platform. Different techniques are then used to mitigate the clutter effect. The first technique introduced is the empty room calibration, where an empty measurement is subtracted from a tag measurement. Pseudo Noise (PN) sequence and Rake receiver technique were also introduced to remove the environmental effect of the measurement. All techniques are simulated and measured using fabricated FC tags. Both techniques are compared at the end of the chapter.

3. **Chapter 4: Novel Identification Techniques in Multipath Channel**
   Chapter 4 introduces information theory and notch detection techniques to the chipless RFID. The chapter starts by introducing windowing; this technique will allow the detection one notch at a time. A mathematical framework is then introduced of three signal processing algorithm which we will utilize for notch detection. The algorithms introduced are matched filter, Singular Value Decomposition (SVD) and Dynamic Time Warping (DTW). An investigation was made, using the mentioned algorithms, on some key performance issues. These issues include ideal notch width, where various notch widths are tested. This simulation was done to answer a major question, Should a wide or a narrow notch be used?! This issue will be vital when trying to increase the notch capacity. We also investigated the system performance, represented by the probability of detection P_d, when the notch is wider than the window size. The next investigation was single notch detection where every notch represented a logical 1 or a 0. Furthermore, the ability of the techniques to detect notch bandwidth was also studied and the recommendation for the best technique is given. The last contribution in this chapter was the effect of the notch frequency shift, due to tag manufacturing imperfection or uncalibrated reader.

4. **Chapter 5: Localization in Chipless RFID**

   In this chapter, chipless localization is introduced. First different localization techniques will be discussed in details. Then chipless RFID link budget is formulated. A simulation using WI was also created to calculate the interrogation zone of the tag. Two techniques were investigated, the first is the trilateration estimation. It was proved that using this algorithm will not be efficient in all cases. Moreover, a new technique using Matrix Pencil Method (MPM) and Received Signal Strength (RSS) is simulated and measured.

5. **Chapter 6: Conclusions and Future Work**

   This chapter the conclusion to the whole thesis and future work will be discussed.

For convenience, a schematic diagram showing the contributions within the chapters is presented in Fig. (1.1)

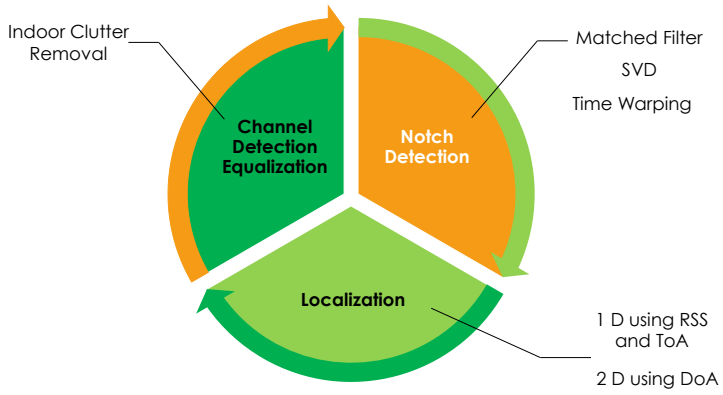

Figure 1.1: Representation of the contribution and the chapters.

2 Background on Chipless RFID

In this chapter the background and the basics of chipless RFID is presented. An overview of different types and application of RFID is also stated. Furthermore, the system components of the chipless RFID are categorized, and their respective function is clearly illustrated. At the end of the chapter, a system diagram with all the Chipless RFID reader components is shown.

2.1 Introduction

The need for identification and localization is growing rapidly in recent years. It started from the punch card [8], the barcode to the invention of RFID technology in 1949. All technologies had one aim was to identify the objects it was attached to. This made it very popular in many service industries, purchasing and distribution logistics, industry, manufacturing companies and material flow systems [9].

There are two broad categories of RFID systems as described in Fig. (2.1), passive and active systems. Active tags have their transmitter and a power source which makes them ideal for long distance tracking or on large assets like containers. They usually operate at VHF and UHF frequency as shown in Fig. (2.2), and they typically have a read range of 20 meters to 100 meters. For a large scale deployment, active RFID will prove to be costly. This advantage leads to the use of passive RFID.

Passive RFID tags do not have a transmitter; they reflect back energy (radio waves) coming from the reader antenna. They are cheaper than active tags and require no maintenance, which is why for massive tagging it is much more efficient. Passive tags can operate at low frequency, high and ultra-high frequency but they have a much shorter read range than active tags. In passive RFID there is two main type chipped and chipless.

In chipped tags, the tag contains a Application-Specific Integrated Circuit (ASIC) chipset

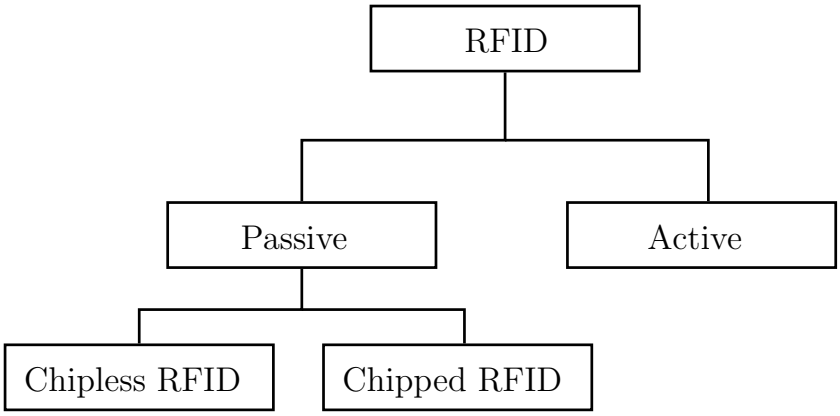

Figure 2.1: Classification of RFID systems.

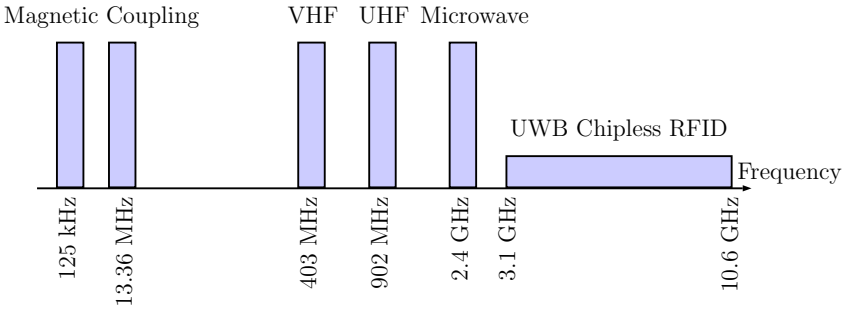

Figure 2.2: Frequency spectrum used by RFID systems.

in the tag [10]. In the chipped system the reader sends a Continues Wave (CW) the modulator inside the chip directly adjusts the antenna load to represent the backscattered data [11] as shown in Fig. (2.3).

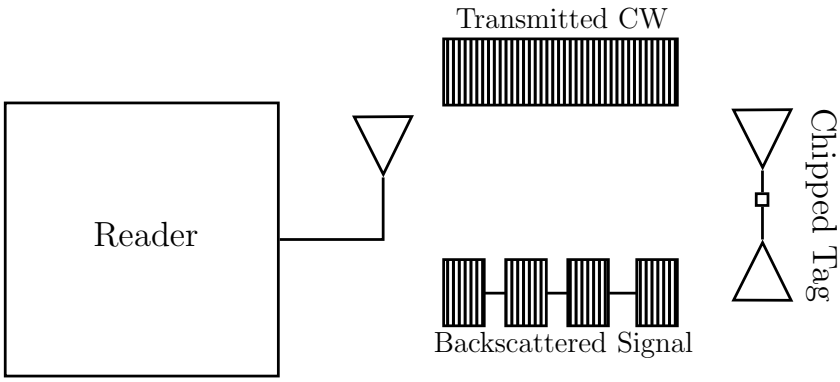

Figure 2.3: Chipped RFID system.

The reader receives and decodes this backscattered signal to identify and detect the tag.

At the chipped RFID technology's early days only internationally available ISM frequencies and the frequency range below 135 kHz could be used due to the nonassignment of separate frequencies [9]. Due to the growing commercial importance of RFID systems and the increasingly liberal frequency regulation in Europe and other regions, new frequencies and standards were created. The most popular standard is the UHF EPC standard, where the tag operates in the 865 and 868 MHz frequency range. Chipped RFID tags have since dominated the market with the ability to detect multiple tags and the range was acceptable. It quit did not replace the barcode system since the cost of the tag was still high for mass deployment.

The other passive solution that will prove to be promising is chipless RFID. A chipless tag costs less than a cent, and these have the potential for mass deployment for low-cost, item-level tagging as the replacement technology for optical barcodes [10]. Chipless RFID tags could be printable just like regular barcodes. It also has more or less the advantage of its chipped counterpart. In the following sections, a full description about the chipless RFID will be explained.

2.2 Chipless RFID

Given the high cost of silicon chip RFID tags (compared to the printable barcodes), efforts to design low-cost RFID tags was the main target of the research community. The idea was to remove the silicon chip and use the tag electromagnetic properties of materials and/or design various conductor layouts/shapes to achieve particular electromagnetic properties/behavior [12]. There are two main types of chipless RFID:

- TDR-based chipless
- Spectral-based chipless RFID

TDR-based chipless: these RFID tags are interrogated by sending a signal from the reader in the form of a pulse and listening to the echoes of the pulse sent by the tag as shown in Fig. (2.4). A train of pulses is then created which can be used to encode data [12]. These tags are sometimes called SAW tags or delay line based tags. The signature of the tag is determined by the time delay [13–15]. Some disadvantage of such tags is the size of the tag and the inaccuracy of the delay concept in a real channel.

The second type of chipless RFID and the one discussed in this thesis is spectral based RFID. In the spectral based RFID, the data is encoded using resonators. Each resonator absorbs

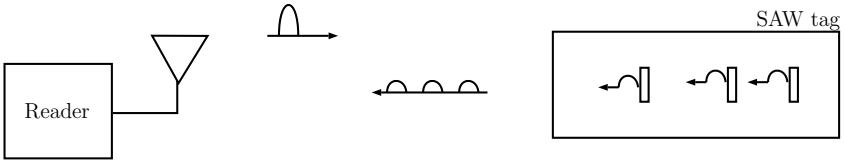

Figure 2.4: SAW tags RFID system.

some of the transmitted power at a certain frequency. To get the full signature of the tag, the reader has to transmit an UWB signal. The tag the creates notches at the required frequency. Unlike the chipped RFID, the chipless RFID does not need any charging to work.

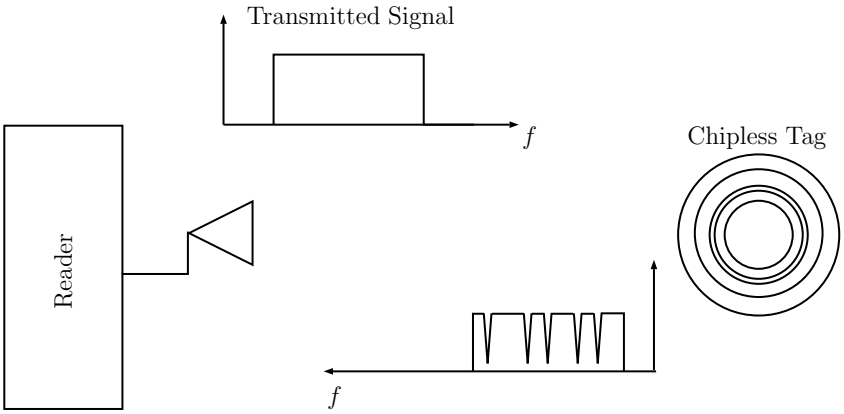

Figure 2.5: Spectrum based chipless RFID system

To replace the barcode for item level labeling, the chipless tag has to have the advantages of both the chipped tag and the optical barcode. This will require the chipless tag to be able to detect multi tags, high reading range, high capacity and high probability of detection. Chipless tags could be categorized into two broad categories:

2.2.1 Spectral Signature based tags

Several attempts were done to design the chipless tag [16–22]. All of the tags have the same functionality but with different designs. Every new design was made to solve a disadvantage in the chipless system.

- Multiresonator based tags
- Multiscatterer based tags

Multiresonator based tags

The multi resonating chipless tag comprises three main components. The transmitting and receiving antennas and multi-resonating circuit as shown in Fig. (2.6). The transmitter and the receiving antenna must be UWB antennas to receive all the incoming frequency range. The resonator circuit is designed to absorb certain frequencies representing the notch. The signal is then passed to the transmitter where it retransmits the signal in a different polarization. The receiving and retransmitting tag antennas are cross-polarized to minimize interference between the interrogation signal and the retransmitted encoded signal containing the spectral signature [16–19].

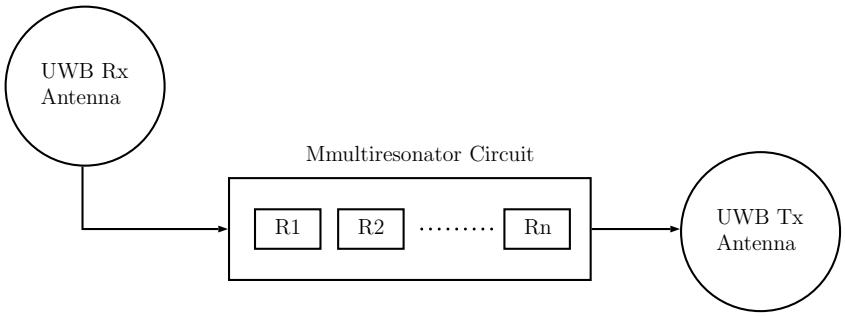

Figure 2.6: Spectrum based chipless RFID system

Multiscatterer based tags

Multi scatterer based tag consists only of scatterers with different dimensions [22–24]. Each scatterer serves as a receiving antenna, a filter and a transmitting antenna as shown in Fig. (2.7). These scatterers act like radar targets, and they will generate a unique spectral ID to encode data. This type of tags has an advantage of being smaller since it does not require the use of antennas for reception and retransmission. The identity of the tag will be presented by its RCS. Understanding the RCS behavior is important for the efficient design and detection of chipless RFID tags. This thesis will all be based on this type of tags.

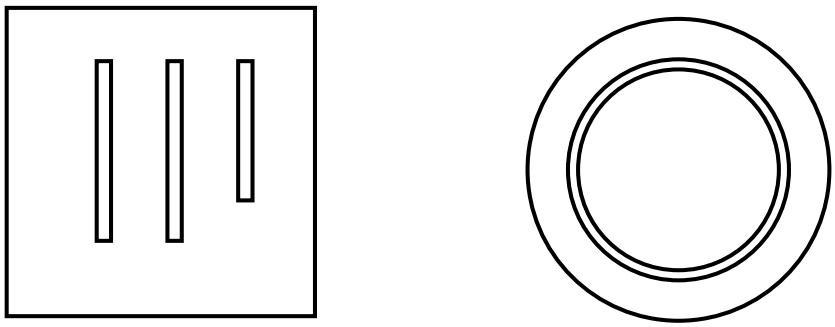

Figure 2.7: Two Multiscatterer based tags

2.2.2 Spectral Signature Based Reader

To replace the barcode and have the same performance as the chipped RFID system, the reader should be able to detect and decode the tag efficiently and reliably in any environment. Another requirement is that the reader be cheap and small. Moreover, it should be able to operate effectively in all the UWB frequency range of the tag. It also has a very low reading sensitivity and high antenna gain to detect long range tags. To achieve all those targets every aspect and function of the reader should be optimized to give the best performance The following sections will provide a short description of each function.

Reader Antenna

Reader antenna must support the UWB frequency range. There are two choices for the selection of the reader antenna, either omni-direction or directional antenna. As later explained in chapter 5, omnidirectional will yield in much lower range than the directional. So it is always recommended to use a high gain directional antenna since the reflected signal power is low. The frequency response of the antenna should almost be constant over the whole range of the UWB frequency to avoid fluctuating result, which might be considered as a notch by the detector.

Transmitted Signal

The first task of the reader is to interrogate the tag with an UWB signal. This signal could be a pulse that covers the whole frequency or a sinusoidal like Linear Frequency Modulation (LFM) signal. UWB pulses have the disadvantage of needing high sampling rate at the reader side for detection. This will require the reader to be expensive. Another challenge is in the FCC

regulations, the power transmitted should be less than the noise level which will lead to low detection range.

One of the most widely used pulse compression waveforms is LFM waveform or the chirp waveform. The frequency of LFM linearly increases (up-chirp) with time. LFM function sweeps linearly across a total bandwidth of b Hz during the t-second pulse duration. Therefore, the waveform is feasible to be achieved by the simple analog circuits.

Detection

If the tag is in the interrogation zone of the reader, the tag will reflect the incoming signal with its signature. The second requirement of the reader is to analyses this signal to be able to detect and identify the tag.

The signal received by the reader antenna includes the scattered signal from the chipless RFID tag located in the interrogation zone, reflections from background objects (clutter), the reader antenna transfer function and noise. Therefore, the detection process is a challenging aspect of the design of chipless RFID systems. In most situations, the reflections from background objects are stronger than the tag response [11]. Therefore an effective clutter equalization technique could be applied to suppress all the unwanted signals.

After the signal is cleared Fourier Transform (FT) should be applied to the signal to detect the existence of a notch or not. This is a major function of the detector. The whole detection chain is shown in Fig. (2.8)

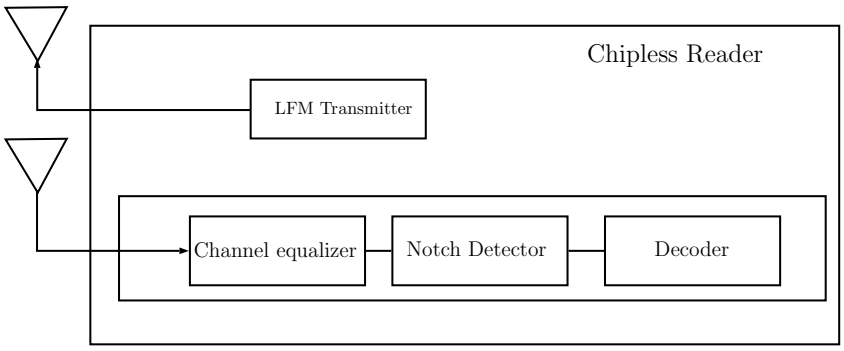

Figure 2.8: Chipless RFID block Diagram

3 RFID Channel Modeling, Estimation and Equalization

In this chapter, FC chipless RFID channel modeling and equalization is presented. The chipless tag is modeled by its 3D RCS and using ray-tracing tools, an analysis of the received signal is calculated. Moreover, a test bed is created using SDR to detect the backscattered signal from the tag. Thus creating a measurement platform for online channel measurement and equalization. In this chapter two algorithms is introduced, empty room calibration and Rake Receiver with PN-Sequence. Both algorithms mathematical framework and results are shown and discussed.

3.1 Introduction

RFID systems are expected to provide both identification and high-definition localization of objects with improved reliability and security while maintaining low power consumption and cost. UWB FC chipless systems are a promising solution for next generation RFID systems to overcome most of the limitations of the current narrow band chipped UHF RFID technology such as high tag cost and complexity, insufficient ranging resolution for accurate localization, sensitivity to interference and scarce multiple-access capability [25]. The main performance criteria for RFID tags are the reading range, speed and accuracy. For many applications, such as warehouses, the read range should be maximized to reduce the number of readers required [26] [27]. The tag selected is FC orientation independent, small in size and easy cheap to fabricate and using UWB signals, the reader can rapidly detect the code of the tag dependent on the RCS of the tag at a selected frequency.

However, in a practical environment, there are multi-path interferences in the intercepted signals [28]. The multi-path interferences will change the amplitude, phase and frequency of the transmitted signals, which will lead the decrease of correct recognition of the tag [29]. Several

attempts to mitigate channel effects in UHF Gen2 chipped RFID, has been investigated [30] [31]. In [26], the authors attempt to increase the reading range of a UHF RFID system, by considering a stochastic model to describe the surrounding environment effects based on a simple two-slope path-loss model. A multiple antenna based RFID system was investigated in [32] using switch-controlled phase shifter in the feeding of a double antenna configuration. Blind filtering equalization using stochastic multipath Rician fading channel based on the successive interference cancellation was investigated in [33]. However, these channel mitigation models restrict the use of single band UHF RFID system. The goal of this chapter is to maximize the UWB chipless tag identification percentage in a real-time environment. This goal is achieved by using chipless RFID system which mitigates the environment effects on the tag and the reader using channel equalizers.

3.2 Channel Simulation and Ray Tracing Analysis

In a chipless RFID system, a tag reflects the UWB signal sent from the reader transceiver. The ID information of the RF tag depends on the RCS of the tag. As illustrated in Fig. 3.1, the channel- frequency response is the summation of 3 terms, one due purely on the background (clutter), the clutter and the other due to the presence of the tag.

To fully understand the problem, the complete frequency domain chipless RFID scheme is shown in Fig. 3.2. The transmitter – receiver setup, in this case, is quasi-monostatic. The signal $X(f)$ is transmitted via the transmit antenna $H_{Tx}(f, \theta_{Tx}, \phi_{Tx})$. The interrogation signal $X(f)$ could be a pulse that covers all the frequency range, or a narrow band signal that sweeps all the operating frequency. This interrogation signal propagates via the forward channel $H_F(f, R)$ to the tag with a 3D RCS pattern $\Gamma(f, \theta_{RCS}, \phi_{RCS})$. The scattered signal arrives at the receiver antenna $H_{Rx}(f, \theta_{Rx})$ via the backward channel $H_B(f, R)$, in this work the backward and the forward channels are assumed to have a reciprocity property, as described in subsection 3.2.1. In addition to the signal received from the tag, two unwanted signals arrive at the receiver side. The first is due to coupling between the transmitting and the receiving antenna $H_{coupl}(f, \theta, \phi)$. This could be mitigated by increasing the distance between both antenna, using high beam width antennas or changing the position of the transmitter and the receiver. The other additive signal is clutter $H_C(f, \theta, \phi)$. Clutter usually has a higher signal strength than the one reflected back from the tag.

In RFID environment the received signal at the reader end is given by (3.1). [34] [35]

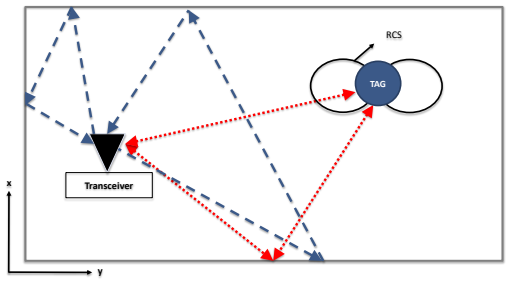

Figure 3.1: Simplified 2D backscattering channel representation.

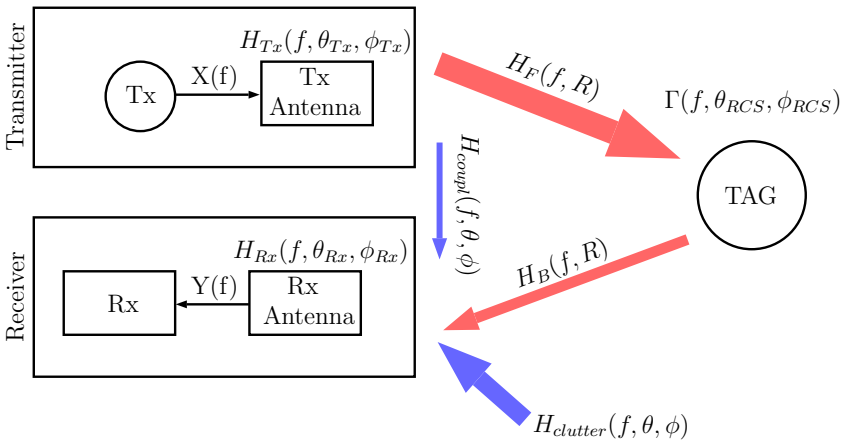

Figure 3.2: Chipless RFID frequency domain, quasi-monostatic radar system

$$
\begin{aligned}
Y(f) = {} & H_{Rx}^{T}(f,\theta_{Rx},\phi_{Rx}) \\
& .\{H_{coupl}(f,\theta,\phi) + H_C(f,\theta,\phi) + H_F(f,R).\Gamma(f,\theta_{RCS},\phi_{RCS}).H_B(f,R)\} \\
& .H_{Tx}(f,\theta_{Tx},\phi_{Tx})X(f) + N(f)
\end{aligned}
\tag{3.1}
$$

where $N(t)$ is the additive noise added at the receiver side.

3.2.1 Channel Reciprocity

In this work the forward and the backward channel is considered as reciprocal. In a time-dependent environment, the channel changes over time which causes loss of reciprocity. To counter the loss of reciprocity, it is assumed that the backward tag reflection occurs within the coherence time of the channel as shown in (3.2).

$$H_F(f) = H_B(f)^T \tag{3.2}$$

where $H_{t_f}(f)$ is the forward channel and $H_{t_b}(f)$ is the backward channel.

3.2.2 Tag Radar Cross Section

The selected tag was designed by [36], to resonate at selected frequency causing it not to appear in the backscattered signal. The number of bits representing the tag may vary depending on the number of rings (resonators). This creates the frequency coding in the chipless RFID and that could be represented using the RCS, a 3-bit RCS is illustrated in Fig.3.3. RCS of a radar target is a far-field quantity and is defined as the scattered over the incident power.

$$\Gamma = \lim_{r\to\infty} 4\pi r^2 \frac{|E^s|^2}{|E^i|^2} \tag{3.3}$$

where E^i is the incident electric field and E^s is the scattered electric field.

The total tag scattered RCS is given by:

$$\Gamma_t = \frac{1}{4\pi} \int_{\phi_s=0}^{2\pi} \int_{\theta_s=0}^{\pi} \Gamma(\theta_s, \phi_s) sin\theta_s d\theta_s d\phi_s \tag{3.4}$$

were the angles (θ_s,ϕ_s) define the direction of propagation of the scattered waves. In theory Γ_t represents the total amount of scattered waves. In real world scenario, various factors affect the amount of waves received by the reader antenna. These factors include polarization and the sensitivity of the reader antenna and the amount of resolvable paths from the tag to the receiver antenna.

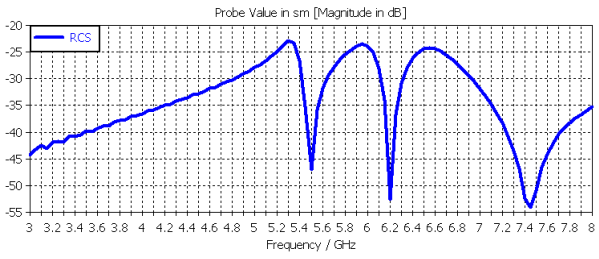

Figure 3.3: 2D RCS plot at a selected angle.

3.2.3 Ray-Tracing

Investigating the indoor chipless RFID channel properties are imperative for the design of the equalizer. Various factors have to be taken into consideration when simulating the tag channel. The most important factor is that the FC chipless RFID operates in the UWB frequency range where the channel and tag properties change according to the frequency. More factors like receiver and tag location; orientation and the high number of multipath created in an indoor environment must be taken into consideration. All these properties will be analyzed using ray tracing, which allows full signal analysis and environment specification; therefore it can facilitate more comprehensive channel characterization, with the additional benefit of efficiency and convenience.

The backscattered radio channel from the tag experienced at a receiver's location $\mathbf{L^I} = (x_\mathrm{I}, y_\mathrm{I}, z_\mathrm{I})$ and tag location $\mathbf{L^T}_\mathrm{n} = (x_{\mathrm{T}_n}, y_{\mathrm{T}_n}, z_{\mathrm{T}_n})$,in a given environment is modeled as a time-invariant linear filter with location-dependent impulse response, $h^b(t, \mathbf{L^I}, \mathbf{L^T}_\mathrm{n})$. In the same prospective, the forward channel from the reader at the tag is modeled as $h^f(t, \mathbf{L^I}, \mathbf{L^T}_\mathrm{n})$. The impulse response provides the characterization of the propagation channel and contains the necessary information to analyze any type of signal transmission over that channel [37].

In a typical wireless system, the UWB impulse response of the channel a transmitted signal $x(t)$ whose spectrum, $X(f)$ is considered. $X(f)$ is sampled at the discrete frequencies $[f_1, ..., f_{nf}]$, where nf is the number of frequency points at a given bandwidth B. The received signal $Y(f)$ is given by:

$$Y(f_k) = X(f_k)H(f_k) \tag{3.5}$$

The samples frequency response, $H(f_k)$, can be determined by employing a Ray Tracing (RT) simulator, where the signal source is a CW at frequency f_k.

The RT tool "Wireless InSite 2.5" is used in this work as a three-dimension (3-D) simulator based on Full 3D indoor propagation model. In the model, ray paths are identified using the Shooting and Bouncing Ray method (SBR).A complex vector electromagnetic field components are evaluated in terms of plane waves undergoing multiple phenomena of reflection, transmission and diffraction. The reflected field is evaluated through optical geometry based on the objects placed in the indoor model. Moreover, the first order diffracting edges are found by searching for adjacent rays which follow different paths through the building geometry, since such occurrences identify discontinuities in the fields.Apparently, the procedure described above can be highly CPU-intensive, depending on the number, nf, of frequency samples. Therefore in this work, the

Material	Conductivity [S/m]	Permittivity	Thickness [cm]
Ceiling (concrete)	0.01	9	15
Floor (concrete)	0.01	9	-
Wall (concrete)	0.01	9	15
Benches, door, table (wood)	10^{-5}	13	3
Window (glass)	10^{-12}	7.6	3

Table 3.1: Material electric properties

samples of only one window (a single notch) is taken into consideration when simulating the channel on the RT tool.

Frequency-domain UWB channel measurements were conducted in a typical indoor environment, with dimensions of $10m \times 10m \times 2.6m$. The scenario has been reconstructed in WI as shown in Fig. 3.4 Particular care has been used for including windows, doors and furniture with appropriate electrical properties, as summarized in Table 3.1. An assumption has been made in this study that the electrical properties do not depend appreciably on the frequency.

In this setup, a horn antenna was used as the reader antenna with a 12 dB gain. The choice of the interrogating antenna is critical and directly affects the amount of clutter received and the reading range. The selection of a narrow-beam antenna like horn [38] or Reflect Array (RA) [39] antennas, will dramatically decrease the clutter and the range will increase since the antenna gain will be high. On the other hand, the number of tags that could be interrogated will decrease. The transmitted power was set to 0 dBm with a reader sensitivity of -70 dBm. It should be noted that although a low transmitted power of 0 dBm from the reader's transmitting antenna was used, the reading range could not be increased by using a higher transmitted power. As the transmitted power increase, the clutter power will increment causing the tag detection to become more challenging. The number of rays are set to 10 and diffractions to 3. Understandably as the number of rays and diffraction increase, the computation complexity will increase. An example of an indoor scenario is shown in Fig.(3.4). In WI, the tag side could not be simply be placed as an object in the environment. This is because of its frequency-dependent backscattering property. Our approach, described in Algorithm 3.1, is to set the position of the tag as a receiver in the backscattering mode; in this mode, the reader is in the transmission mode. Furthermore, when the reader is in the receiving mode, the tag will be in the transmission mode. These modes will be executed every frequency point, where each point will have its RCS radiation pattern. These RCS patterns are extracted from the CST software. Although WI is advanced software, it does not support frequency scanning and mode changing. Matlab was used as a controlling software,

Algorithm 3.1 Simulate tag response in an indoor environment

procedure WI TXMODE(L^I,L^T,RCS,f)
    $Reflections = 10$
    $Diffractions = 1$
    Set Reader Antenna = ARP
    Set Tag RP = RCS
    Set Operating Frequency = f
    Set Tx Signal= $sin(2\pi f)$
    Calculate Forward Ray Model
    Return $h_f(t)$
    Return Received Signal
end procedure
procedure WI RXMODE(L^I,L^T,RCS,Received Signal,f)
    $Reflections = 10$
    $Diffractions = 1$
    Set Reader Antenna = RCS
    Set Tag RP = RP
    Set Operating Frequency = f
    Set Tx Signal= Received Signal
    Calculate Forward Backward Model
    Return $h_b(t)$
end procedure ▷ Main Code
$Frequencies = [f_l, ..., f_h]$
$L^I = [x_\mathrm{I}, y_\mathrm{I}, z_\mathrm{I}]$
$L^T = [x_\mathrm{T}, y_\mathrm{T}, z_\mathrm{T}]$
Extract RCS from CST-MS
for each Frequency f in $Frequencies$ **do**
    WI Txmode (L^I,L^T,RCS,f)
    Calculate $h_f(t)$
    WI Rxmode (L^I,L^T,RCS,Received Signal,f)
    Calculate $h_b(t)$
end for

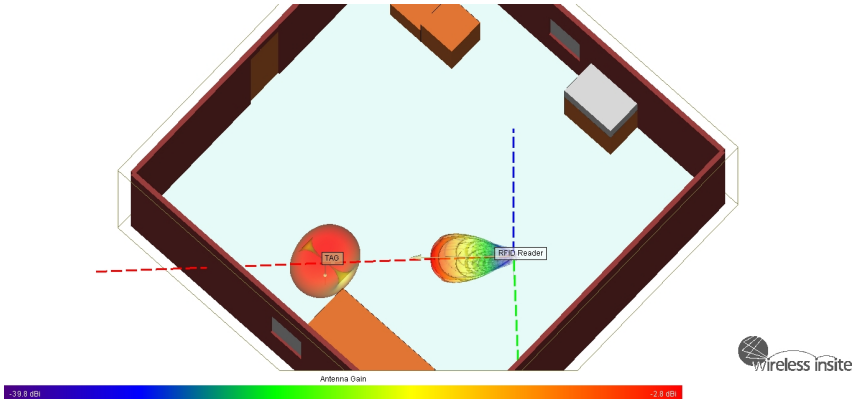

Figure 3.4: Top view of the WI office environment.

where it could change the operating frequency of the WI and organize the output data in a matrix format.

3.3 Chipless RFID Test-Bed

In this work all the proposed algorithms and signal processing techniques must be verified using real tags. This proves that the all the techniques are valid in a real environment where clutter and interference from other sources exists. Unlike other latest work in the same field [40] [41], a testbed in a real environment was performed not in an iconic chamber. The device that were used as the reader was USRP N210.

USRP N210, shown in Fig.(4.28), is an SDR platform designed by Ettus Research. An interesting feature it incorporates is that it can be connected to an RF front end equipment, thus enabling wireless communication. An advantage of such system is that every aspect of the reader could be controlled such as the transmitted signal modulation, sampling rate, bandwidth, carrier frequency and power. It also offers real time signal processing, which gives an incite on the execution time of the algorithm. Unlike measurement systems like spectrum analyzers and generators, USRP is cheap and the chips on the USRP will be similar as a commercial reader.

Figure 3.5: USRP without its top cover showing the RF front end and the motherboard under it.

As shown in Fig. (3.6), the first step in the USRP is the down-conversion. The frequency is determined by a Voltage Controlled Oscillator (VCO). In the tag detection process, the Frequency-Controller (F-C) in the PC sweeps the operating frequency. In the receiver side, the time samples are converted to a digital signal via the Analog to Digital Converter (ADC). Since the amount of data converted is high, the Field Programmable Gate Array (FPGA) is responsible for down-sampling the data. The samples is then sent to the PC via USB or Ethernet. In the transmitter side a continuous wave it transmitted over all the frequencies. The time duration of the CW is $10ms$ at each frequency. This number is chosen based on the recommendation from Ettus research, as it is the minimum delay time for frequency shifts to have a stable performance. The transmitting and the receiving process is chosen to be performed by a single USRP for synchronization. If more than one antenna is needed (as will be described in Chapter 5) multiple antennae will be used with an external clocking system. Furthermore, the signal processing is done in the PC side.

Since the tag ID is in the frequency response, the arriving signal is converted to the frequency domain using FFT. At the same time, an equalization process happens to remove clutter effects and USRP effects. In this work the equalization is done using two techniques:

- Empty Room Calibration.

- Rake receiver using PN-Sequence.

Empty room calibration is based on performing measurements without the tag first, while the Rake receiver does not need a predetermined information about the channel. Both have their advantages and their disadvantages depending on the application. Both are explained in details in the following sections.

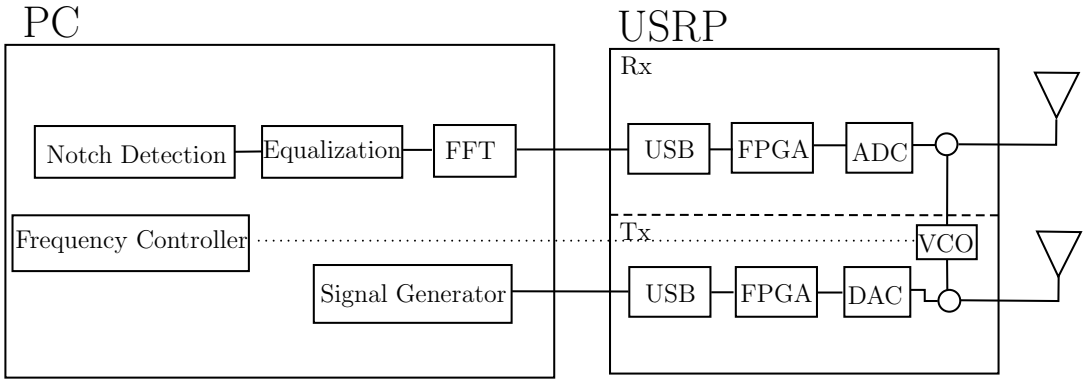

Figure 3.6: Block diagram of USRP testbed including the connection between the PC and USRP.

After equalization process, the frequency response is analyzed using signal processing tools described in Chapter 4. Furthermore, at the transmitter side, a CW signal is generated which is later up-converted to the operating frequency.

3.4 Empty Room Calibration

The detection of a chipless tag in a clutter environments is much more challenging in chipless RFID than in UHF RFID due to the absence of modulation in time, i.e., the absence of two different states in the backscattering signal [42]. The first method suggested is empty room calibration.

Empty room calibration is subtracting the value of the measurements with the tag from the without tag scenario. Equation (3.6) represents the received signal without the tag. This signal contains the value of the clutter and the coupling plus the effect of the transmitting and receiving

antenna.

$$\begin{aligned} Y_{\text{notag}}(f) = H_{Rx}^{T}(f,\theta_{Rx},\phi_{Rx}) \\ .\{H_{coupl}(f,\theta,\phi) \\ .H_{Tx}(f,\theta_{Tx},\phi_{Tx}).X(f)+N(t) \end{aligned} \tag{3.6}$$

To get the response of the tag without the noise and clutter, equation (3.1) will be subtracted from (3.6). In a real world scenario averaging is needed to calculate the channel and remove the noise accurately.

Since the response of the system is periodic, it is possible to reduce the noise and enhance the signal using the statistical technique of signal averaging [43] as represented in (3.7). Fig(3.7) shows a simulated tag, with code $[10101010]$. The SNR value chosen was $0\,dB$, the idea is to see how much averaging of the signal is needed to get an accurate reading. Six different averaging was done on the signal $2, 20, 40, 80, 100, 200$. It is shown that as averaging increases the signal becomes clearer and therefore easy to be detected. The difference in the clarity of the signal between 100 averages and 200 is not that great, so in the real time measurements, one hundred averages are chosen.

$$\hat{\Gamma}(f) = \frac{\sum_{a=1}^{A} Y(f) - Y_{\text{notag}}(f)}{A} \tag{3.7}$$

To evaluate the empty room calibration algorithm, a test bed is created. The test bed is made using USRP N210 using the algorithm described in (3.2). The frequency chosen is based on the CPX daughter board frequency range. The transmitter gain is set to the maximum to increase the tag illumination. The receiver gain is chosen in $0\,dB$ to decrease the noise added to the signal by the receiver.

The results in Fig. (3.8) (3.9) shows the results of an all ones tag without and with calibration respectively. It is clear that the clutter and noise are dominant over the tag response. After applying averaging and empty room calibration, the results tag response is now more clearer. It has the disadvantage of having very low notch amplitude of -2 dBm on average. This is due of inaccurate removal of the clutter response. Another factor that is evident is the inconsistency of the notch. This is due to the USRP carrier synchronization, even though one USRP is used but there is some misalignment in the carrier response. Another factor is the inconsistency of

Algorithm 3.2 Measuring tags in an indoor environment using Empty Room Calibration technique

```
Frequencies = 3.9 GHz : 10 MHz : 6 GHz
Sampling rate = 1 MS/sec
Transmitter gain= 31.5 dB
Receiver gain= 0 dB
No tag measurements
for a=1:A do
    for each Frequency f in Frequencies do
        Transmit a CW at frequency f
        Hold transmission for 10 ms
        Receive a signal at frequency f
        Calculate power of signal
        Save value in P_A
    end for
end for
Calculate average of P_A
Store in P_C
With tag measurements
for a=1:A do
    for each Frequency f in Frequencies do
        Transmit a CW at frequency f
        Hold transmission for 10 ms
        Receive a signal at frequency f
        Calculate power of signal
        Save value in P_r
    end for
end for
Calculate average of P_r
Store in P_R
Tag Response= P_R-P_C
```

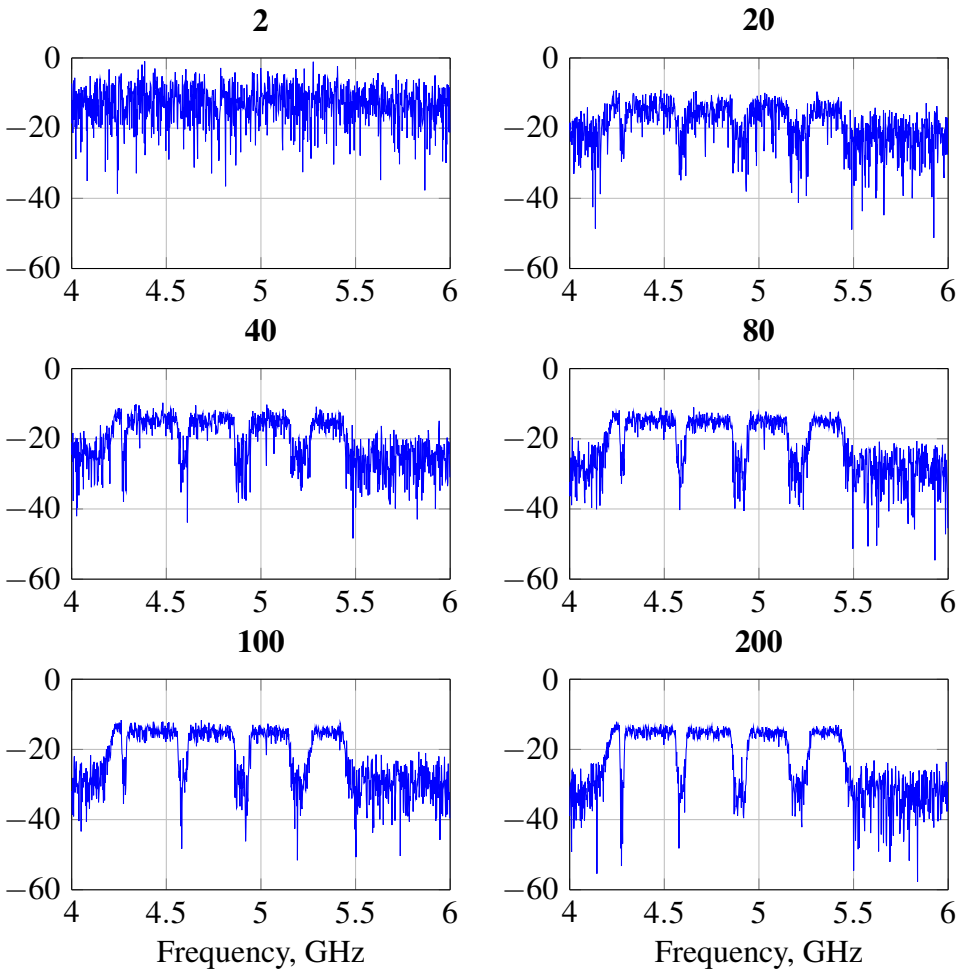

Figure 3.7: Averaging effect on the received signal.

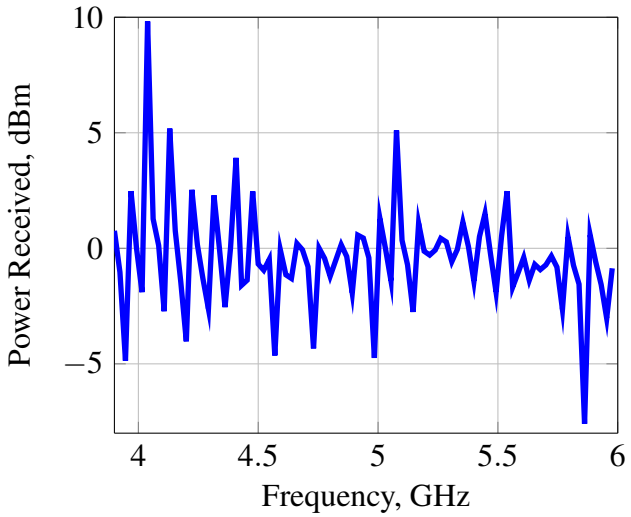

Figure 3.8: Measurements using USRP 210 before calibration.

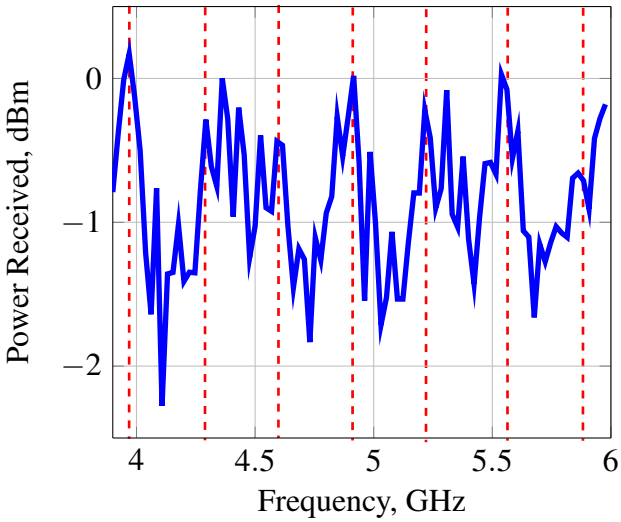

Figure 3.9: Measurements using USRP 210 after calibration.

the transmitted power along the frequency access, where the frequency response is not constant along the frequency access. This could be solved by increasing the averaging but on the cost of elongating the reading time.

The calibration process before any tag reading makes it impracticable in many applications. The calibration process should be done if any position change of the transmitting or the receiving antenna. Furthermore, during the calibration process, the environment os assumed to be constant, which is not a valid assumption in a real scenario. In the following section, we will investigate another clutter removal technique that will not need any calibration and could work in any environment by using PN-sequence and rake receivers.

Parameter	**Value**
Sampling Rate	1 M samples / second
Transmitter Gain	31.5 dB
Receiver Gain	0 dB
Start Frequency	3.9 GHz
End Frequency	6 GHz
Frequency Step	10 MHz
Frequency Sweep	
Averaging	100

Table 3.2: USRP parameters

3.5 PN-Sequence

Different techniques are reported in the literature for the detection of single FC chipless RFID by analyzing the backscattered signal. In [38], [44] and [45] a threshold based detection aided by calibration values is used for determining the existence of a tag resonance at a certain frequency. However, this approach is based on fixed thresholds, which will proof to be insufficient to variant clutter and environmental effects. Furthermore, the cross polarization response of the tag is exploited for removing the clutter effects [46] [47]. In this detection technique, the tag response will vary when the orientation of the tag is altered. In [48] clutter is suppressed by choosing a data sequence with zero mean (or quasi-zero mean) this assumption assumes perfect pulse synchronization. In the radar community, Moving Target Indicator (MTD) was investigated in [49] [50] where clutter is removed from Doppler readings by advanced filtering techniques. The empty-room technique, used in [51] [52] subtracts the channel response measured in the absence of the target from any received signal comprising of both target response and clutter. Unfortunately, this technique is sensitive to environment changes since any change renders the previously measured empty-room response inappropriate.

In this section a novel PN random sequence transmitter and Rake receiver design is implemented, as presented in Fig.3.10, to detect an omni-directional RCS chipless tag. This setup excludes the clutter response created by the environment by considering the Line of Site (LoS) component scattered from the tag. Unlike previous work done in chipless RFID, no calibration or empty room subtraction needed to successfully detect the tag. This approach is more realistic, since there will be no need to remove the tags from the room to measure the no-tag response. Furthermore, there will be successful detection at any tag orientation, since the tag used is orientation independent.

3.5.1 Clutter Description

In this subsection, clutter response is further described. As illustrated in Eq.(3.8) the received signal consists of the summation of two components, one due purely on the background (clutter) and the other due to the RCS generated in response to the transmitter microwave excitation [53].

$$Y[f] = X[f]\,(\Gamma[f]\,H_{\mathbf{T}}[f] + H_{\mathbf{C}}[f]) + N \tag{3.8}$$

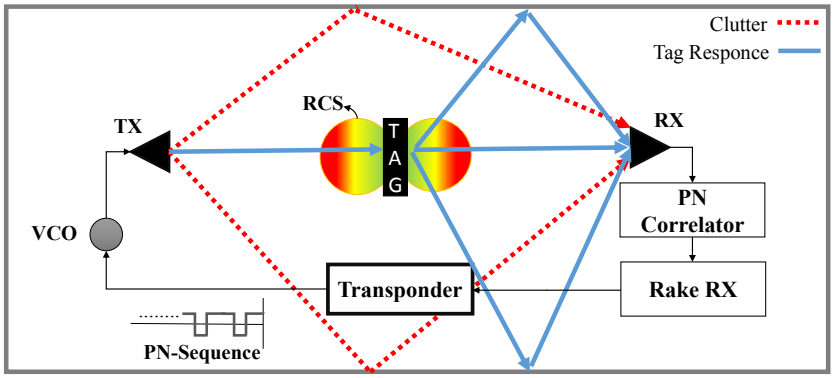

Figure 3.10: Proposed chipless RFID system model.

Where $X[f]$ is the transmitted signal and N is additive white Gaussian noise. $H_{\mathbf{T}}[f]$ and $H_{\mathbf{C}}[f]$ are the tag and clutter channel response respectively. $H_{\mathbf{T}}[f]$ could be discretized into M frequency samples.

$$H_{\mathbf{T}}[f] = \begin{bmatrix} R_1^{\mathbf{T}} & R_2^{\mathbf{T}} & \dots & R_M^{\mathbf{T}} \end{bmatrix} \tag{3.9}$$

Where every sample is the summation of all the time invariant paths received from the tag at frequency f_m as shown in Fig.3.11.

$$R_m^{\mathbf{T}} = \sum_i a_i^{\mathbf{T}} e^{-j2\pi f_m \tau_i^{\mathbf{T}}} \tag{3.10}$$

Where $a_i^{\mathbf{T}}(t)$and $\tau_i^{\mathbf{T}}(t)$ are respectively the attenuation and propagation delay from the tag to the receiver on path i. Similarly the clutter could be presented by Eq. (3.11) and Eq. (3.12).

$$H_{\mathbf{C}}[f] = \begin{bmatrix} R_1^{\mathbf{C}} & R_2^{\mathbf{C}} & \dots & R_M^{\mathbf{C}} \end{bmatrix} \tag{3.11}$$

$$R_m^{\mathbf{C}} = \sum_i a_i^{\mathbf{C}} e^{-j2\pi f_m \tau_i^{\mathbf{C}}} \tag{3.12}$$

Where $a_i^{\mathbf{C}}(t)$and $\tau_i^{\mathbf{C}}(t)$ are the attenuation and propagation delay from the environment to the receiver.

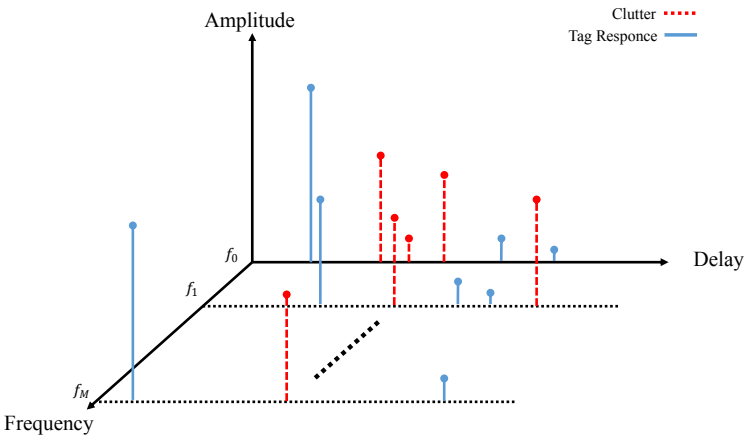

Figure 3.11: CIR in a chipless RFID system.

3.5.2 Tag Design

The tag consists of Coplanar Waveguide (CPW) slot ring resonators without ground plane as presented in [54]. An 8-bit three different single and array tags are designed and simulated using CST-Microwave Studio 2014. The substrate employed in the design is RO4003C with a permittivity of 3.38, a loss tangent of 0.0027 and a thickness of 1.52 mm. Furthermore, the no-resonance 3-D RCS shown in Fig.3.13 shows a gain of more than 17 dB from its resonance state shown in Fig. 3.12. Moreover, the 3-D RCS radiation pattern illustrating the angular dependency of the tags, which should be considered in the ray-tracer to simulate the CIR [55] accurately.

3.5.3 PN Sequence Transmitter

In this paper a modulated PN random sequence is used as the interrogation signal $x(t)$. An important characteristic of a PN sequence, is its periodic autocorrelation property as shown in Fig. 3.14. Similar to white noise, the autocorrelation of a PN N-sequence has a single very sharp peak at the zero shift point [56]. In Eq. (3.13) $R_{ss}(\tau)$ represents the autocorrelation of the PN sequence.

$$R_{ss}(\tau) = \begin{cases} 1 - \frac{N+1}{NT_b}|\tau| & ,\tau = T_s \\ -\frac{1}{N} & ,\tau \neq T_s \end{cases} \tag{3.13}$$

where T_b and T_s is the bit and whole N sequence duration respectively, N is the number of bits in the PN sequence and τ represents the correlation shift. This property allows the receiver to detect

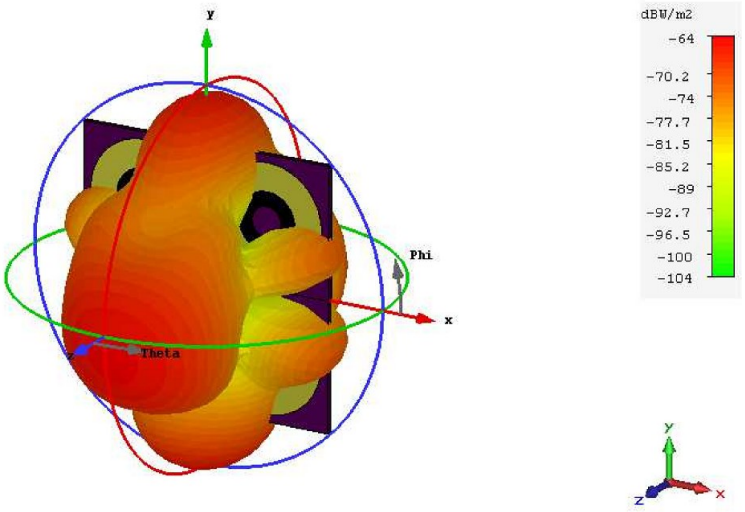

Figure 3.12: 3D RCS radiation pattern of the tag at resonance frequency.

each multipath component separately using the Conventional Matched-Filter (CMF) technique [57] as illustrated in Eq.(3.14). In this equation $y(t)$ will be the superposition, attenuated, phase shifted and delayed copies of the transmitted PN sequence $s(t)$.

$$r(t) = \int_{-\infty}^{\infty} s(\lambda)\, h_{MF}(\tau)\, d\lambda = \sum_i a_i e^{j\theta_i} R_{ss}(t-\tau_i) \tag{3.14}$$

where the impulse response of the matched filter in the receiver is given by

$$h_{MF}(\tau) = s(-\tau) \tag{3.15}$$

In the interrogator a Galois Linear Feedback Shift Register (GLFSR) [58] generator is implemented with a degree n of 10 and length $N = 1023$ where $N = 2^n - 1$. Since the chipless RFID is an UWB technology, the synchronized integrator transmits a modulated PN sequence at every frequency f_m. The number of samples M determines the resolution accuracy of the detected tag's frequency signature.

3.5.4 Rake Receiver

A Rake receiver consists of a number of channels, also referred to as fingers or branches each of which tracks and selects power from one of the received multipath components [59]. In a normal communication system an ideal Rake will combine all resolvable multipath. This ideal

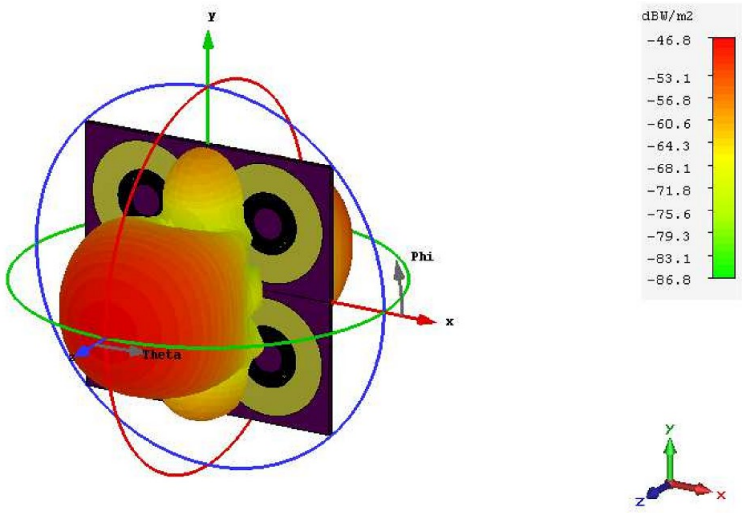

Figure 3.13: 3D RCS radiation pattern of the tag at no resonance frequency.

configuration is often unrealistic due to the complexity and the huge number of channel paths. Usually, a subset of the best L_s paths out of all L resolved path is taken, this is known as *SRake*. Since we are concerned with the LoS scenario, a first arrival local maxima search algorithm is implemented to identify the tag's frequency signature. A proof of concept to validate this hypothesis was implemented using a ray tracing software WI, for channel and *Matlab* for system design.

3.6 Simulation Results

3.6.1 Ray Tracer

Deterministic channel simulation was done using WI software to measure the deterministic channel as illustrated in Fig. 3.15.

In this WI simulation a 4.5 x 4 meter 3D office model was designed so simulate the real testbed setup shown in Fig.3.19. Two horn antennas were placed in the model to simulate the Tx and the Rx antenna respectively at a distance of 35 cm, with a transmitting power of 0 dBm. The tag was represented by a frequency dependent 3D RCS radiation pattern imported from CST. Since WI is a ray tracing tool, the CIR resulted was exported to Matlab where a Rake receiver selects the maximum first path. For simplicity only the frequency range of 4.8 to 5.2 GHz was taken into consideration as illustrated in Fig.3.16

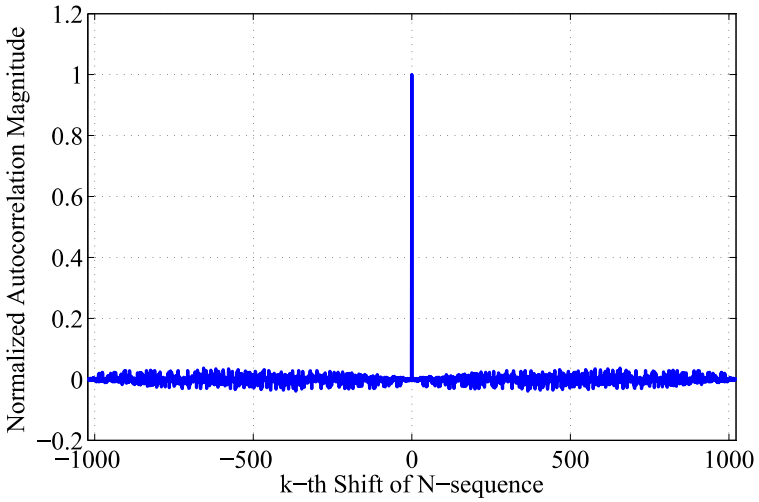

Figure 3.14: Autocorrelation property of PN sequence.

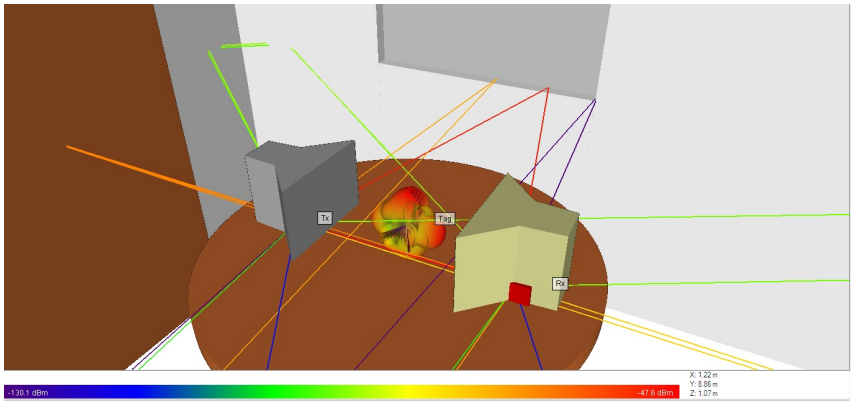

Figure 3.15: Ray-tracer system setup considering multipath and clutter effects.

3.6.2 Phase

Detecting the frequency signature of a chipless tag by extracting the phase information from the backscattered signal is discussed in [60] [61] [62]. This subsection illustrates the effect of multi-path channel at the performance of notch phase property.

Consequently, a chipless tag is implemented using a bank of notch filters and then a Rayleigh channel is defined as a statistical channel with ten paths. It is observed, from Fig. 3.17, that the phase response is significantly affected by the environmental multi-path. Any phase detection technique will fail to detect the presence of the notches in this case, without using an extra step to remove the effects of multi-path. By applying PN-sequence with Rake receiver the phase

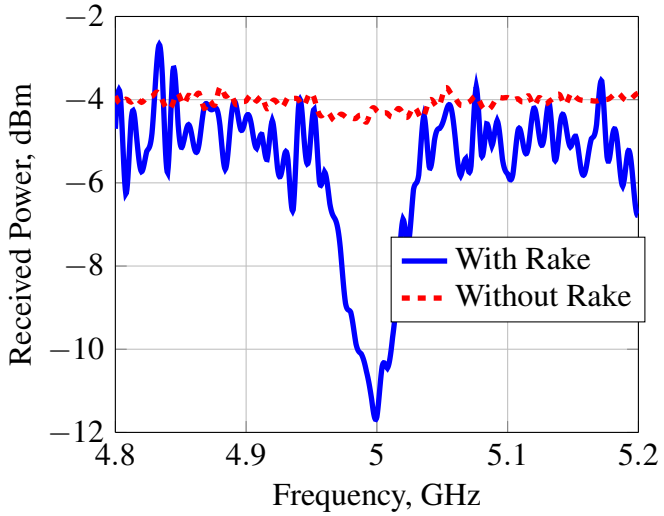

Figure 3.16: Received power using ray-tracer simulation for the indoor environment.

information, similar to the magnitude, will be easily retrieved as shown in Fig. 3.18.

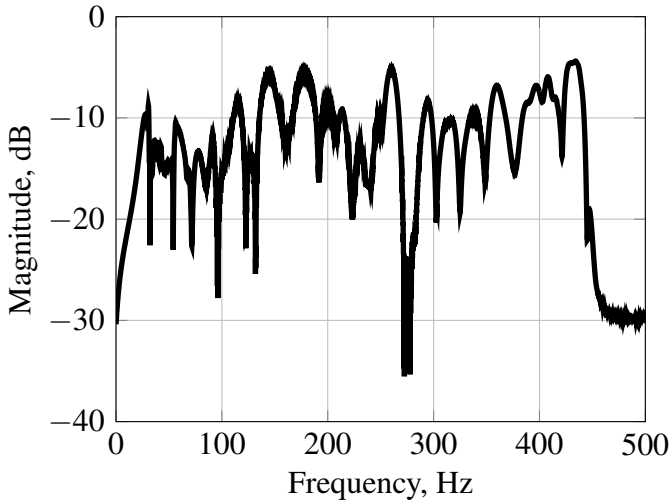

Figure 3.17: Magnituderesponse of tag frequency signature before applying Selective Rake

3.7 Measurement Results

The hardware platform used in the measurement setup is the Universal Software Radio Peripheral 2 (USRP2) developed by Ettus Research. The daughter board used was CBX with a frequency range of 1 to 6 GHz. Since the USRP2 is a narrow band transponder, the generated baseband transmitted signal is multiplied by the variable carrier frequency. The setup of the antennas is

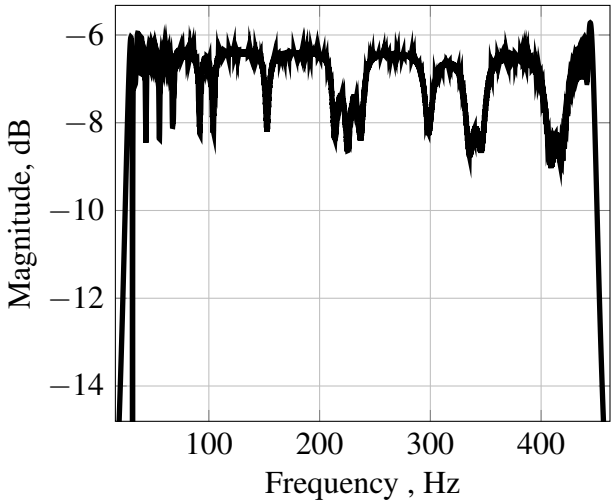

Figure 3.18: Magnitude response of tag frequency signature after applying Selective Rake

illustrated in Fig. 3.19, the two horn antenna are in the LoS setup to ensure that the first received channel component from the tag is the maximum and the first to arrive.

Figure 3.19: USRP test-bed designed to in an indoor office setup.

In this measurement two scenarios are implemented to test the efficiency of the proposed system. The first was done using a regular frequency sweep code where all the multi-path components are summed up to calculate the frequency response of the tag. In this setup averaging was done to minimize the effect of the additive noise caused by the USRP hardware. The second setup is the implementation of PN sequence transmitter with the LoS selection Rake receiver. In both scenarios no calibration or empty room subtraction was done. The simulation parameters of both scenarios are described in Table (3.3).

Parameter	Value
Sampling Rate	1 M samples / second
Transmitter Gain	31.5 dB
Receiver Gain	0 dB
Start Frequency	3.9 GHz
End Frequency	6 GHz
Frequency Step	10 MHz
Frequency Sweep	
Averaging	100
GLFSR PN Sequence	
Degree	10
Mask	0

Table 3.3: USRP parameters

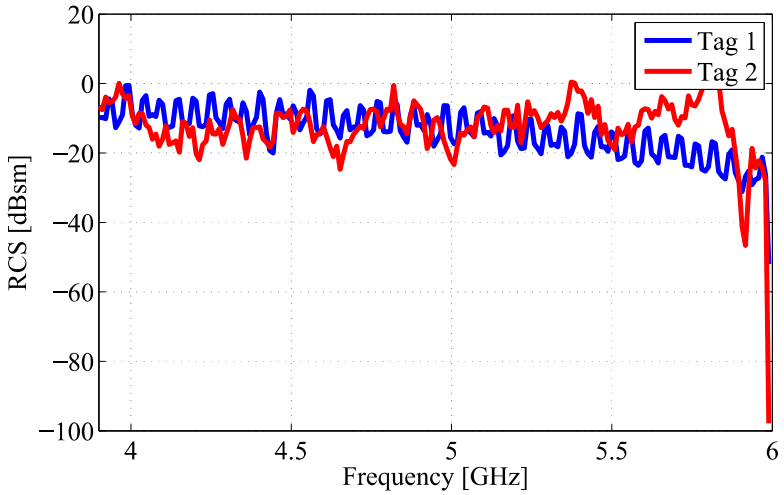

Figure 3.20: USRP results for Tag 1 and Tag 2 using frequency sweep code.

The result of the frequency sweep implementation is shown in Fig. 3.20. As shown in the figure, it is impossible to detect the tag without using post-processing algorithms. The result proves that the clutter and the environmental effects cause the received signal to be distorted and the tag to be undetectable.

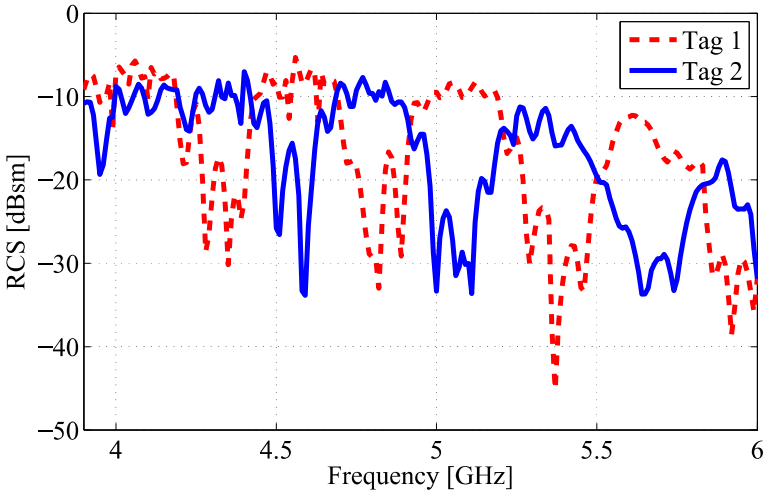

Figure 3.21: USRP results for Tag 1 and Tag 2 using PN sequence implementation.

As expected, Fig. (3.21) depicts the results of the algorithm proposed in this paper. The measurement result show the detection of tag 1 and 2 using an open source low cost SDR. The fluctuations shown in the results are caused by the inconsistency of the transmitted power by the USRP. Utilizing notch detection algorithms, like the one described in the following chapter, will detect the deformed notches.

In the next chapter, the notch detection will be discussed. The next chapter will describe how the system will detect the notches and translate them into bits.

4 Novel Identification Techniques in Multipath Channel

Notch detection and identification is presented in this chapter. In this chapter, three algorithms are used to detect the notch. The three algorithms are matched filter, WB-SVD, and DTW. To investigate the efficiency of all algorithms for notch detection, different real cases is analyzed. Those cases include notch width, bandwidth, and frequency shift. The results of all algorithms are presented, and a comparison with a real-time test bed is shown at the end of the chapter.

4.1 Introduction

The FC chipless RFID system relies on a frequency signature induced by the tag on the excitation of UWB transmitted signal. The chipless RFID tag is detected by analyzing the backscattered signal. The signal processing involved in the detection is quite challenging, since the received signal power is very weak and dramatically affected by undesired interference, environmental clutter and noise caused by the receiver. Furthermore, manufacturing defects on the tag's side may cause the notch to shift its frequency position or even change its shape. Another factor is the transmitting and/or the receiving antenna frequency response which is superimposed on the received signal, and this also could modify the notch shape. All the mentioned factors could render the chipless RFID tag undetectable. In this chapter, notch detection techniques will be introduced to detect the ID of the interrogated tag accurately. Each algorithm is tested by comparing its probability of error (P_e) against the received Signal to Noise Ratio (SNR). It will be shown that having an efficient notch detection algorithm could boost the encoding capacity of the chipless RFID system.

Different techniques are reported in the literature for the detection of single FC chipless RFID by analyzing the backscattered signal. In [38], [44] and [45] a threshold based detection

aided by calibration values is used for determining the existence of a tag resonance at a particular frequency. However, this approach will give inaccurate results due to any tag fabrication and calibration errors. Short-Time Matrix Pencil Method (STMPM) is presented in [63] [64] [65] to distinguish the late-time of the scattered signal. This method requires time synchronization and efficient channel equalization algorithms. Furthermore, the cross polarization response of the tag is exploited for removing the clutter effects [46]. In this detection technique, the tag will not be detected if its orientation is altered. Moreover, signal space representation is used in [66] for identifying different tag frequency signatures. Using singular value decomposition a set of orthonormal basis functions, which are capable of describing all combinations of the tag signatures. Unfortunately, if the tag has a high number of notches (greater than 3), the training sequence will be large, thus making this algorithm very computationally expensive.

4.2 Windowing

Windowing is a vital process in all proposed detection techniques. In this work windowing is done in the frequency domain by multiplying the received signal $Y(f)$ by a shifting window function as illustrated in Eq. (4.1) and Fig. 4.1.

$$\mathbf{r} = Y(f).\text{rect}(\frac{N}{f_{\text{max}} - f_{\text{min}}} - k.N) \text{ where } k = 1,..,K \tag{4.1}$$

Where N is the number of samples in the window, K is the total number of windows and $f_{\text{max}} - f_{\text{min}}$ is the bandwidth of the window. In this work, the window is shifted by N samples.

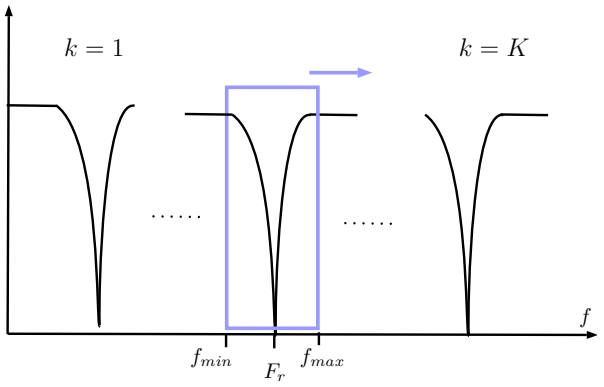

Figure 4.1: Windowing process of the received signal $Y(f)$.

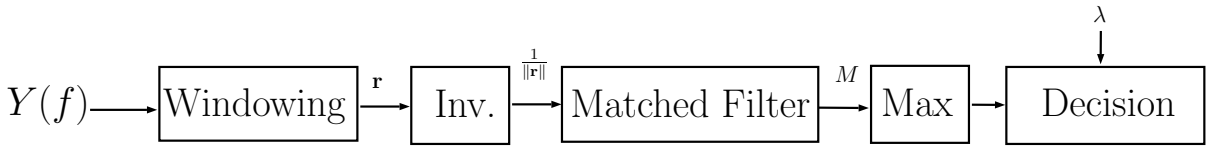

Figure 4.2: Matched filter detection block diagram.

The number of samples are determined by the bandwidth of the largest notch.

4.3 Matched Filter

Matched filter is an ideal filter which calculates the maximum SNR of a received signal in the presence of additive stochastic noise [67]. It is commonly used in radar [68] [69] and digital communication systems [70], where the original waveform is known and the objective is to detect the presence of this signal against the background noise. The transfer function of the matched filter, in the frequency domain, at sampling frequency f_0 may be stated as:

$$H(f) = \kappa \frac{\gamma^*(f)}{P(f)} \mathrm{e}^{-jwt_0} \tag{4.2}$$

where $\gamma(f)$ is the complex conjugate of a known notch response extracted from the fabricated tags. $P(f)$ is the Power Spectral Density (PSD) of the noise associated with an input windowed signal and κ is an arbitrary constant. Assuming an AWGN and selecting a convenient value of κ to represent the operating environment, $P(f)$ could be removed from the matched filter transfer function shown in 4.2. The output of the filter M is given by

$$M = H(f) \star \mathbf{r}(f) = \int_{f_{min}}^{f_{max}} H(\tau) r(f-\tau) d\tau \tag{4.3}$$

4.3.1 Decision in Matched Filter

The detection problem is to distinguish between the hypothesis

$$H_1 : \mathbf{r}[n] = \gamma[f] + w[f] \tag{4.4}$$

$$H_0 : \mathbf{r}[n] = w(f) \tag{4.5}$$

where $w[n]$ is a wide-sense stationary random process which represents the noise. The received windowed signal that contains a notch is represented by H_1 and the absence by H_0.

The decision is done based on Neyman Pearson (NP) detector, where it decides H_1 if likelihood ratio exceeds a threshold λ as shown in Eq.(4.6),

$$L = \frac{p(\mathbf{r};H_1)}{p(r;H_0)} > \lambda \tag{4.6}$$

where $p(r;H_1)$ and $p(r;H_0)$ is described in Eq. (4.7) and (4.8) respectively.

$$p(\mathbf{r};H_1) = \frac{1}{2\pi\sigma^2}\exp[-\frac{1}{2\pi}\sum_{n=0}^{N-1}(\mathbf{r}[n]-\gamma[n])^2] \tag{4.7}$$

$$p(\mathbf{r};H_0) = \frac{1}{2\pi\sigma^2}\exp[-\frac{1}{2\pi}\sum_{n=0}^{N-1}\mathbf{r}^2[n]] \tag{4.8}$$

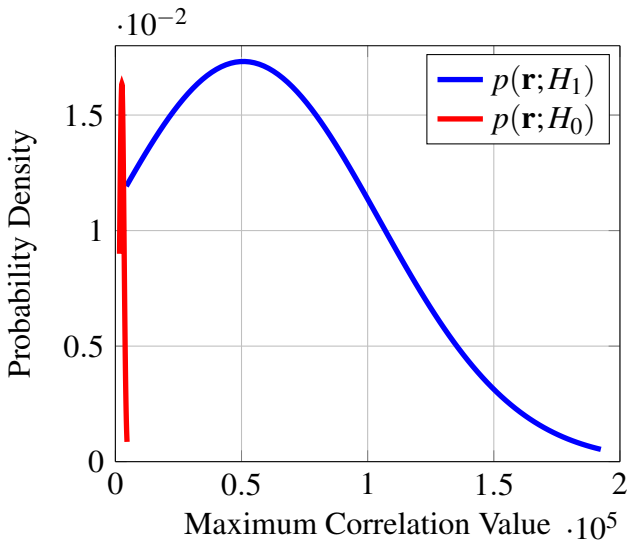

Figure 4.3: Simulated PDFs of the two hypothesis

Fig. (4.3) makes evident that the performance of the detection is determined by the received signal energy versus the noise variance. Using Fig. (4.3) the threshold (λ) could be calculated by the intersection between the two curves.

4.4 Window Based Singular Value Decomposition

The SVD algorithm mentioned in [66] used 2^b combination to create the detection constellation points, where b is the total number of notches. When the number of notches increment, the number of constellation points will directly rise thus decreasing the probability of detection. Moreover, the size of the matrix used to calculate the constellation coordinates will rapidly expand thus making the detection computationally expensive.

Window Based Signal Variable Decomposition (WB-SVD), is a fast and enhanced method to detect the notch using Signal Space Representation (SSR). In WB-SVD only four training sequence are taken for any amount of notches, creating a rank 4 matrix Γ as illustrated in Eq. (4.9).

$$\Gamma = \mathbf{U}\Sigma\mathbf{V}^{\mathbf{T}} = [\gamma_1, \gamma_2, \gamma_3, \gamma_4]_{m\times 4} \tag{4.9}$$

Where $[\gamma_1, \gamma_2, \gamma_3]$ represents three predefined notches with different pattern bandwidth and γ_4 constitutes a no-notch representation. U and V are unitary matrices composed of orthonormal column vectors $\mathbf{u_i}$ and $\mathbf{v_i}$. Moreover, Σ is a diagonal matrix consisting of 4 constant values of σ_i as presented in Eq. (4.10).

$$\Gamma = \begin{bmatrix} \mathbf{u}_1 & \dots & \mathbf{u}_4 \end{bmatrix}_{N\times 4} \begin{bmatrix} \sigma_1 & 0 & 0 & 0 \\ 0 & \sigma_2 & 0 & 0 \\ 0 & 0 & \sigma_3 & 0 \\ 0 & 0 & 0 & \sigma_4 \end{bmatrix}_{4\times 4} \begin{bmatrix} \mathbf{v}_1^T \\ . \\ . \\ . \\ \mathbf{v}_4^T \end{bmatrix}_{4\times 4} \tag{4.10}$$

Further simplification of (4.10) gives the inner product between vectors $\gamma_\mathbf{k}$ and $\mathbf{u_i}$.

$$\gamma_k^T \mathbf{u}_i = \sigma_i v_k^i \tag{4.11}$$

where v_k^i is the k-th element in the column vector $\mathbf{v}_i$. It could be shown that,

$$\gamma_k = \sum_{i=1}^{4} \langle h_k, u_i \rangle u_i = \sum_{i=1}^{4} (\sigma_i v_k^i) u_i \tag{4.12}$$

Since,u_i, where $i = 1,..,4$ serves as a basis for each notch state. This will construct a signal subspace C where the 4 notch states shown in 4.4 are represented by 4 constellation points c_k

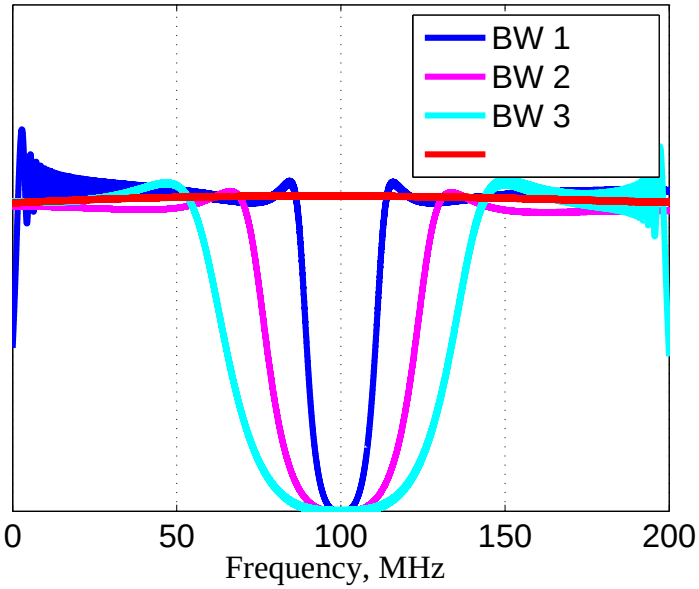

Figure 4.4: 4 notch bandwidth states represented by the constellation

where

$$s_k = [c_1^k, ..., c_4^k] \text{ with } c_i^k = \langle \gamma_k, \mathbf{u}_i \rangle \tag{4.13}$$

These 4 points C will serve as a base for the detection of the unknown FC chipless RFID signature. As shown in Fig. (4.6), the constellation points will be calculated off-line from the predefined γ retrieved from the notch properties of the manufactured tags. In this work four notches with different bandwidths have been considered. As shown in Fig. (4.6.4) the selected bandwidths are

- Smallest bandwidth(BW 1).
- Intermediate bandwidth(BW 2).
- largest bandwidth (BW 3).
- Zero Notch.

Let $Y(f)$ represent the tag backscattered signal which is affected by noise, clutter, multipath, path-loss and even fabrication errors. As shown in Fig. (4.7), the signal $Y(f)$ is windowed into a fixed bandwidth signal $\mathbf{r}$. Then the received signal points are calculated using the inner product between $\mathbf{r}$ and the matrix U. Using Eq.(4.14) the Minimum Distance Vector Criterion (MDVC) between the received point and the precalculated constellation C coordinate is calculated. In the end, a decision is taken based on the type of coding methodology.

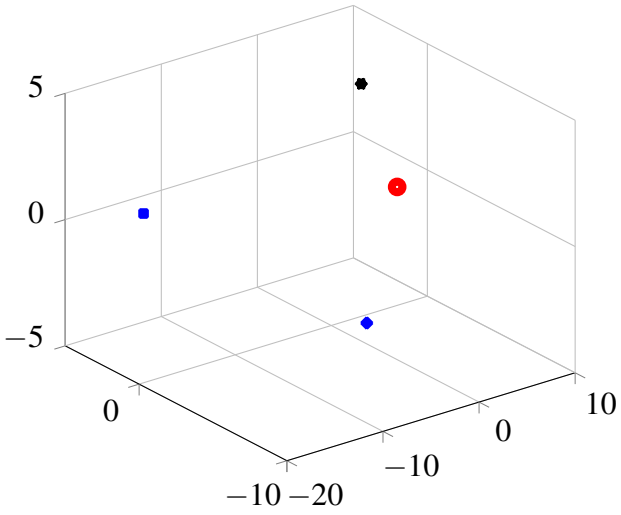

Figure 4.5: WB-SVD constellation points.

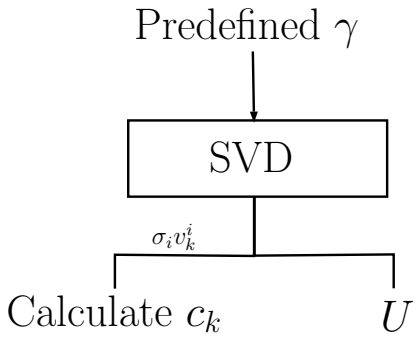

Figure 4.6: Off-line constellation calculation process.

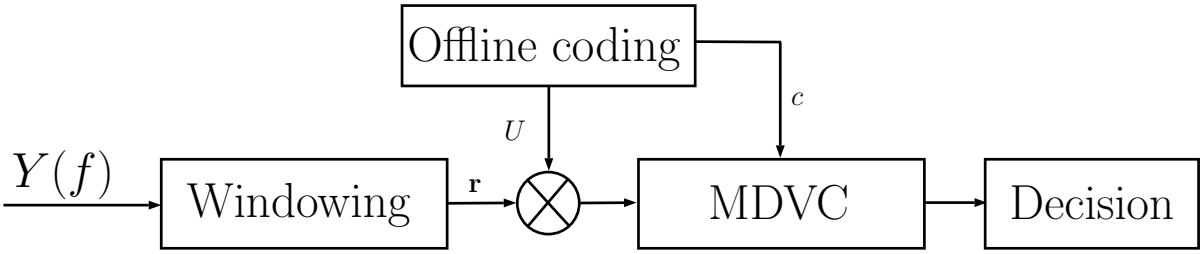

Figure 4.7: WB-SVD block diagram.

$$d_k = \min\left\{ || \langle Y_k(f), U \rangle - c_j ||^2 \right\} \; j = 1..4 \tag{4.14}$$

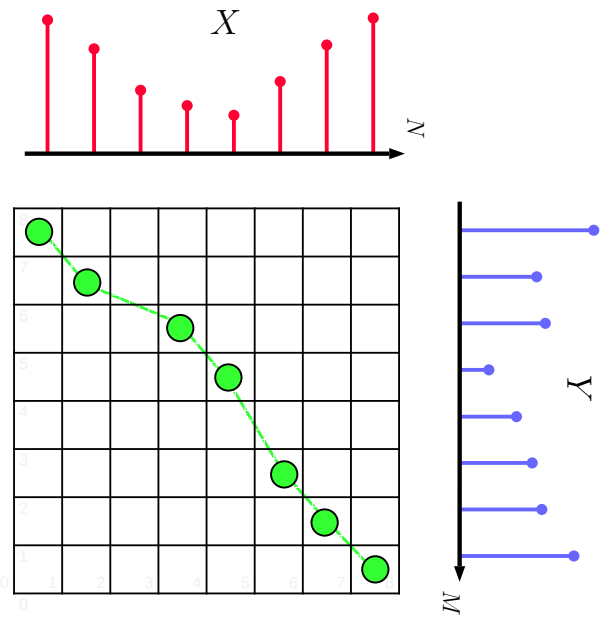

Figure 4.8: Example of DTW cost matrix X (vertical axis) and Y (horizontal axis)

4.5 Dynamic Time Warping

The objective of DTW is to compare two dependent sequences. The sequences are warped in a nonlinear fashion to match each other. A non-linear alignment produces a more intuitive similarity measure, allowing similar shapes to match even if they are shifted time or frequency axis. Originally, DTW has been used to compare different patterns in automatic speech recognition [71], handwriting matching [72].

Let's consider two sequences $X := (x_1, x_2, ...x_N)$ of length N and $Y := (y_1, y_2, ...y_M)$ of length M. These sequences are discrete and represent the reference notch and the received windowed signal respectively. A cost matrix C of size $N \times M$ is obtained by evaluating the cost measure for each element of the sequences X and Y. The goal is to find an alignment between X and Y that has the minimum total cost as shown in Fig. (4.8).

The next definition formalizes the notion of an alignment [73]. An(N,M)-warping path is a sequence $p = (p_1, ..., p_L)$ with $p_l = (n_l, m_l) \in [1:N] \times [1:M]$ for $l \in [1:L]$ satisfying the following three conditions.

1. Boundary condition: $p_1 = (1,1)$ and $P_l = (N,M)$.

2. Monotonicity condition: $n_1 \leq n_2 \leq ... \leq n_L$ and $m_1 \leq m_2 \leq ... \leq m_L$.

3. Step size condition: $p_{l+1} - p_l \in (1,0),(0,1),(1,1)$ for $l \in [1 : L-1]$

An (N,M) warping path p defines an alignment between two sequences X and Y by assigning the element x_{n_l} of X to the element y_{m_l} of Y.The total cost $c_p(X,Y)$ of a warping path p between X and Y with respect to the local cost measure c is defined as:

$$c_p(X,Y) = \sum_{l=1}^{L} c(x_{n_l}, y_{m_l}) \tag{4.15}$$

Furthermore, an optimal warping path between X and Y is a warping path $p^\star$ having minimal total cost among all possible warping paths. Such an optimal path runs along a "valley" of low cost within the matrix C with the optimal warping path $p^\star$ is shown in the red line as seen in Fig. 4.9b.Optimal alignment of the sequence X with a subsequence of Y aligned points are indicated by the red lines shown in Fig. 4.9a.

The operation of the DTW detection method will be performed by comparing the widowed received signal with the stored notch. The cost matrix and the optimal path $p^\star$ will be calculated. The total value of the cost will be compared to the threshold λ_{DTW} to decide code of the received signal.

4.5.1 Decision in DTW

Similar to the matched filter, the value of the threshold was calculated using the PDFs derived from equations (4.7) (4.8). The selected value for the threshold is determined by the intersection between the two PDFs as shown in Fig. 4.10. Unlike the matched filter method, the cost value for $p(\mathbf{r};H_1)$ is expected to be lower than $p(\mathbf{r};H_0)$. This is also illustrated in Fig. 4.9d.

4.6 Simulation Results and Performance Analysis

The performance of WB-SVD, MF and DTW detection algorithms are analyzed through MATLAB simulations. The objective is to analyze the performance of each algorithm for:

- Robustness against notch shape distortion caused by channel effects and noise.
- Ability of the algorithm to detect and identify the variation of the notch bandwidth for Notch Width Coding (NWC) [74].

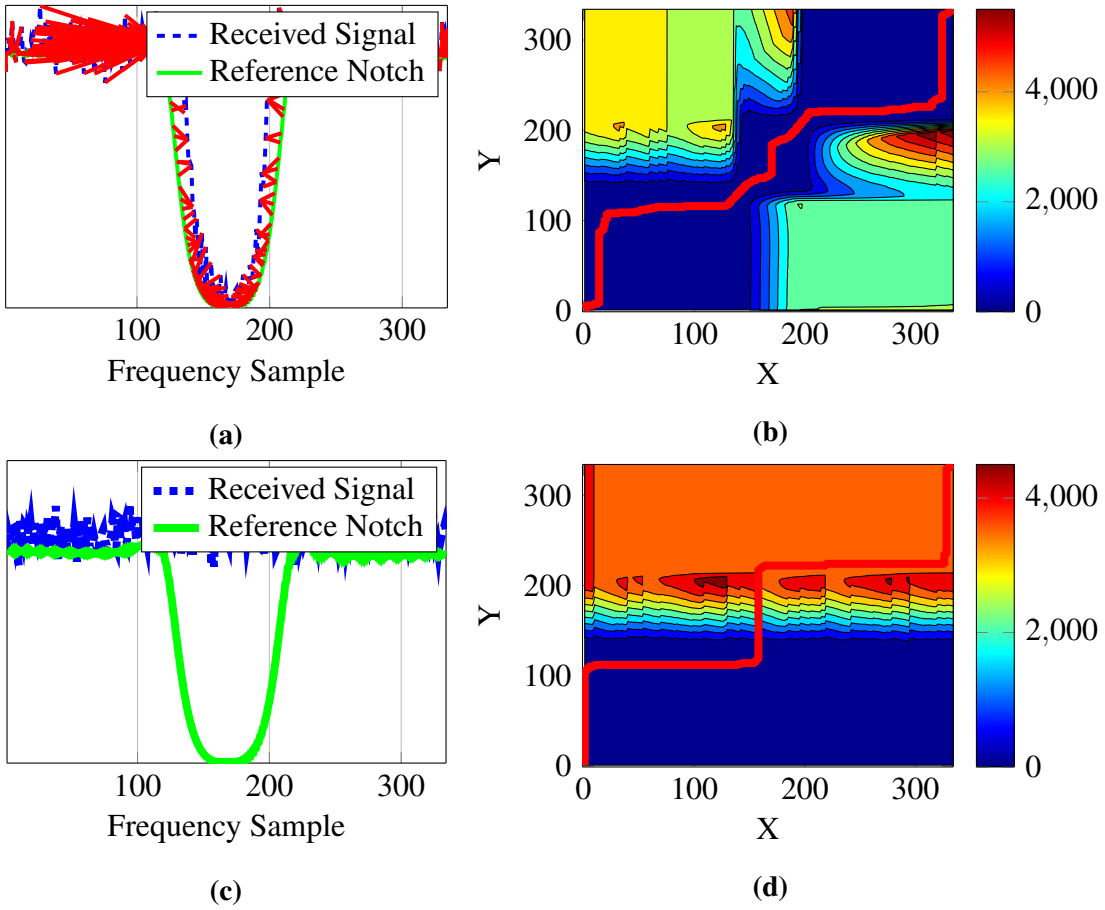

Figure 4.9: **(a)** A non-linear alignment of the received signal (SNR=20 dB) and the reference notch **(b)** Cost matrix *C* of the two signals X (received signal) and Y (reference notch) Regions of low cost are indicated by blue and regions of high cost are indicated by red **(c)** No notch received signal compared with the reference notch **(d)** Applying the DTW algorithm between No notch (X) and the reference (Y).

- Notch detection efficiency in the change of the resonance frequency caused by fabrication errors.

The tag backscattering responses, needed for evaluating the detection efficiency, are extracted from the output of cascaded notch filters each representing a notch frequency with a specific resonance and 3 dB bandwidth as represented in Fig. (4.11) and equation (4.16). Another source is the RCS response of a tag designed in a microwave simulation tool CST. Both sources accurately mimics the backscattered signal from the tag after channel equalization. The variation of the SNR values for the detection algorithm validation, are used to alter the shape of the notch. The distortion of the notch shape after equalization simulates:

- Errors in channel equalization at a specific band.

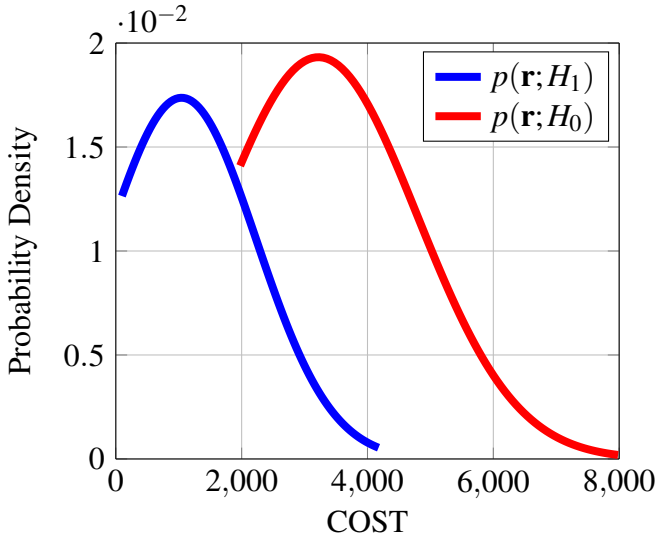

Figure 4.10: PDF of the two hypothesis using DTW algorithm

- Low backscattered power from the tag due to the distance from the reader.
- Fabrication errors in the tag causing the notch shape to change from the design.
- Noise from the receiver due to over heating.

$$H_{\mathrm{c}}(k) = \prod_{k=1}^{K} H_k(z) = \prod_{k=1}^{K} \frac{1 - 2\cos(w_k)z^{-1} + z^{-2}}{1 - 2b\cos(w_k)z^{-1} + r^2 z^{-2}} \tag{4.16}$$

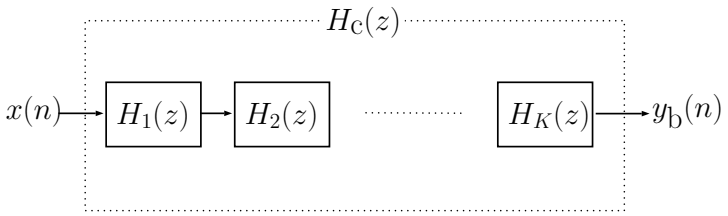

Figure 4.11: Cascaded notch filter for simulating the tag backscattering response

where $x_{\mathrm{f}}(n)$ and y_{b} represent the interrogation after the forward channel and the backscattered signal at the tag respectively. Moreover, $H_k(z)$ is the notch filter representation at resonance frequency w_k where r is the pole radius which controls the notch bandwidth. The choice of the bandwidth will be discussed in the following subsection.

4.6.1 Ideal Notch Width

The notch bandwidth usually is controlled by the physical construction of the tag [75]. It also depicts the maximum and the minimum bandwidth of the notch. The question that should be

answered, in the given bandwidth restrictions; will the wider notch yield in a better probability of detection than the narrow bandwidth. This information is required not to test the detection algorithm, but as a design guideline to be considered in the final coding of the chipless RFID tag. For the sake of increasing the coding capacity of the tag, it is logical to use more narrow notches to increase the number of notches in a given operating bandwidth.

To answer that question, 5 code words each containing 5 slots was constructed using equation (4.16). As seen in Table (4.1) there will be one notch present, represented by 1, in each codeword to avoid any neighboring notch interference. The window size(represented by the red lines in Fig. (4.12-4.13)) and the total bandwidth of the codeword will be constant in both cases, wide notch Fig. (4.13) and the narrow notch Fig.(4.12). Both figures show the increase in bandwidth as frequency increases, this was expected and also simulates real tag resonance response. This also could be shown by the Quality factor (Q) equation(4.17). For also evaluating the effect of the detection window, the wide notches was designed to be bigger than the window size. This will also set design guidelines for the proper window size to be considered in the detector.

Code 1	1 0 0 0 0	Code 2	0 1 0 0 0
Code 3	0 0 1 0 0	Code 4	0 0 0 1 0
Code 5	0 0 0 0 1		

Table 4.1: All code words used for the ideal notch width investigation

$$Q = \frac{f_0}{BW} \tag{4.17}$$

It is seen in that for a designed tag at a fixed resonance frequency (f_0) and Q, which causes the BW to change.

For the detection, an ideal matched filter was used with an additive white Gaussian noise as the source of the notch shape distortion. The output codeword of the detector was compared with the original, where a single bit in error will cause the whole code word to be considered as wrong.

Fig. (4.14) and (4.15) shows the output of the matched filter for the narrow and wide notch respectively. Fig. (4.14) shows that *Code 5* has a better P_d than any other code. This is because it has the widest bandwidth size. So this gives the first recommendation, as the notch bandwidth increases the P_d increases. However, if the bandwidth of the notch increases to the point that it exceeds the bandwidth of the receiver window, then the probability of detection decreases

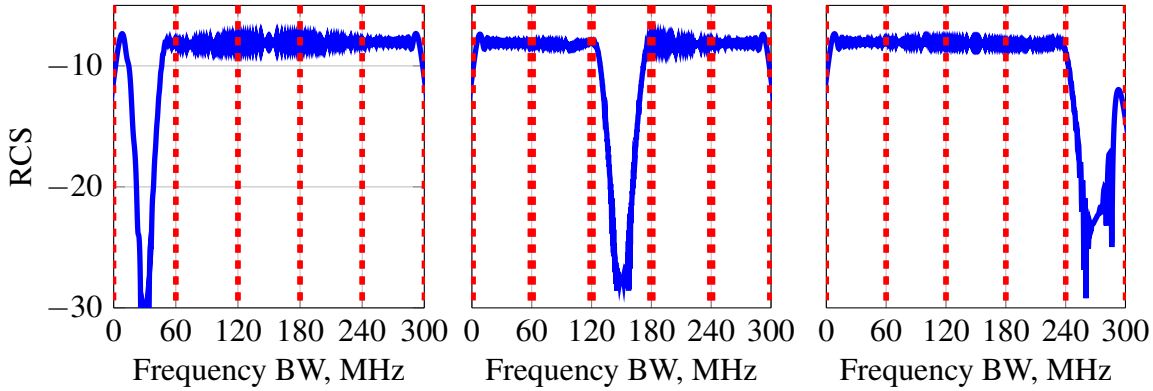

(a) Code 1 **(b)** Code 3 **(c)** Code 5

Figure 4.12: The output of 3 codes representing the narrow bandwidths chosen.

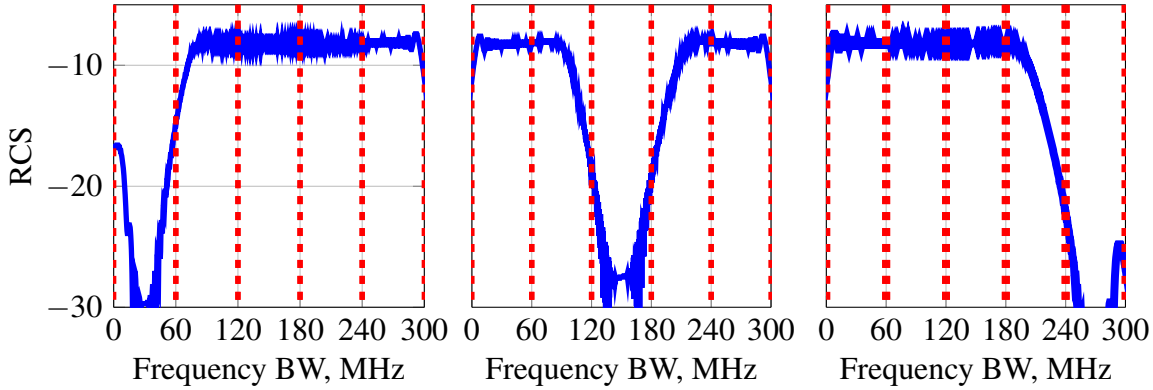

(a) Code 1 **(b)** Code 3 **(c)** Code 5

Figure 4.13: The output of 3 codes representing the wide bandwidths chosen, the notches is wider than the window bandwidth

dramatically as shown in Fig. (4.16). The above conclusion could also be verified mathematically using equations (4.18) and (4.19). Both equations proofs that as Λ increases the P_e decreases.

$$P_e^1 = \frac{1}{2}\,\mathrm{efrc}\left(\sqrt{\frac{\Lambda}{N_o}}\right) \tag{4.18}$$

$$P_e^2 = \frac{1}{2}\,\mathrm{efrc}\left(\sqrt{\frac{\Lambda-\Lambda_1}{N_o}}\right) \tag{4.19}$$

where $P_e = 1 - P_d$ and represents the probability of error. Moreover, Λ is the area of the notch Λ_1 is the area of the notch outside the window. efrc is presented in equation (4.20). P_e^1 is the P_e of the narrow notches where all the bandwidth of the notch is in the detection window, unlike P_e^2

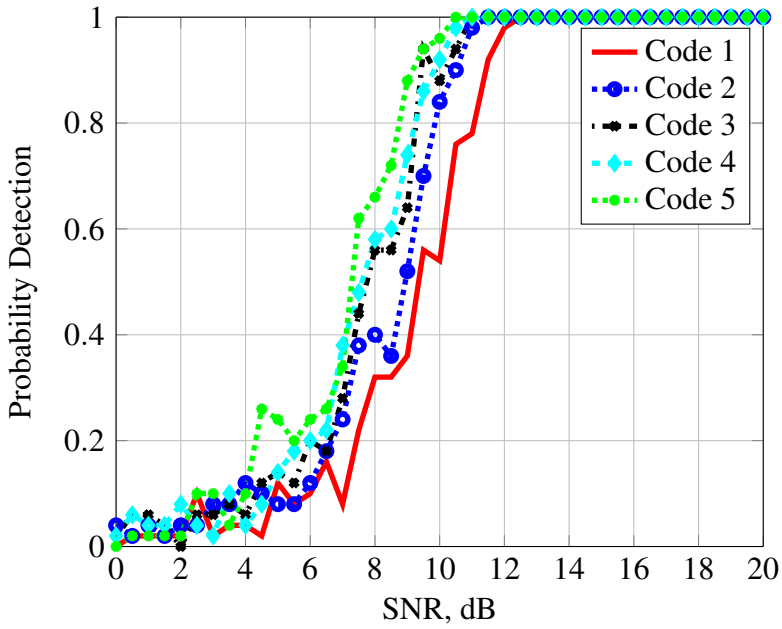

Figure 4.14: Probability of detection of the narrow bandwidth codes.

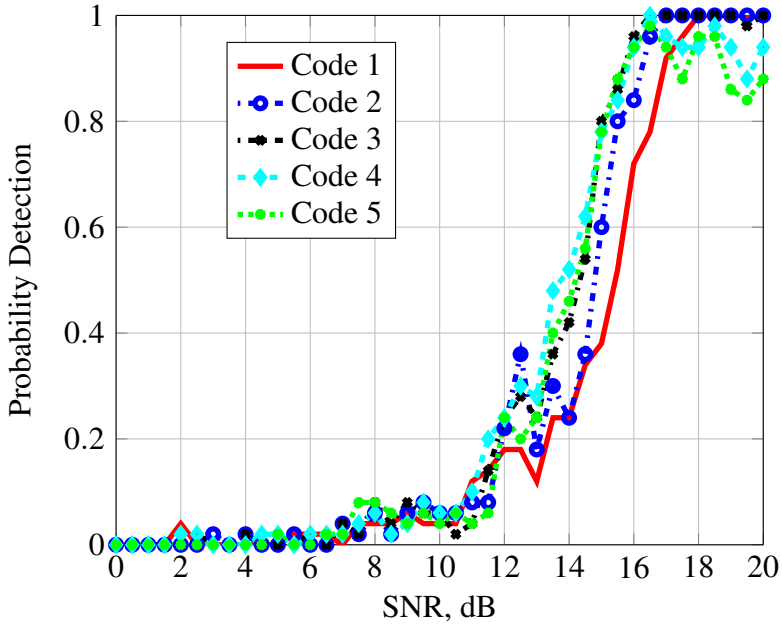

Figure 4.15: Probability of detection of the wide bandwidth codes.

where the area outside the window has a negative effect on the total P_d.

$$erfc(a) = \frac{2}{\sqrt{\pi}} \int_a^{\infty} \exp(-x^2)\, dx \tag{4.20}$$

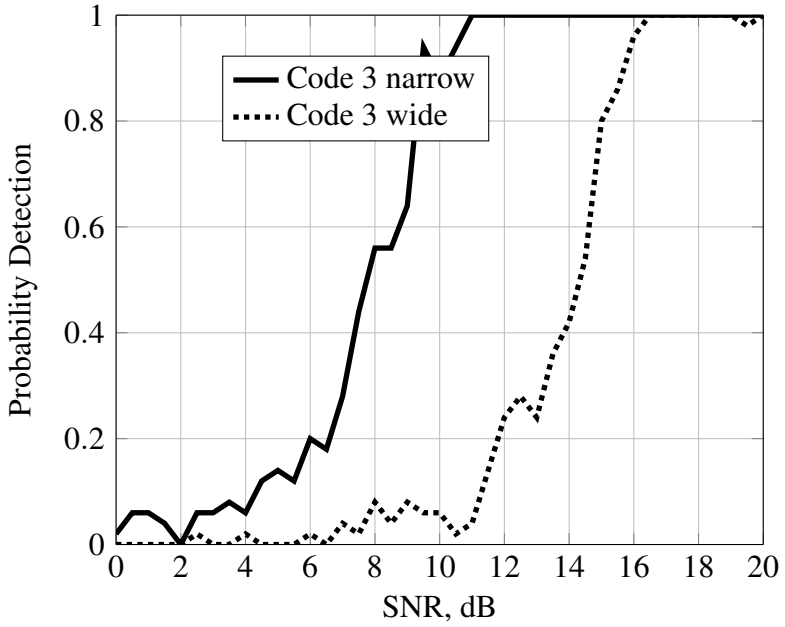

Figure 4.16: Probability of detection of Code 3 in both codes.

4.6.2 Notch Detection

A validation of the performance of the proposed detection algorithm is done by a using simulated tags. A single notch, in both approaches, represents a logical '1', while the absence of the notch represents a '0'. In all used detection techniques, there is no limitation on the number of bits used. The detected signal is windowed depending on the number of bits and the maximum bandwidth of the notch, which is also assumed to be known. This information could be retrieved from the preamble of a protocol based tag, designed by our team [76]. In this protocol, the algorithm scans only the preamble frequency and accordingly it determines the number of tags and the maximum number of notches in the tag. The highest number of notches could also be given by the tag designer. In all cases, the final output is provided in the form of ones and zeros.

In all simulations, 10 bit tags are used with various codes. In the simulation part, where the codes are fabricated using equation (4.16). This code will pass through our detector with a variant SNR to distort the notch shape. The output will be compared with the original code sent, where a single bit will cause the whole code to be considered as an incorrect code. Future research could add error correcting capability in chipless RFID technology, but due to the limitation of the number of bits on the tag, it is currently unavailable.

In this simulation, LFM signal was used as the transmitted signal.

$$x(t) = Acos(2\pi f(t) + \phi) \tag{4.21}$$

where

$$f(t) = \frac{k}{2}t + f_o \tag{4.22}$$

and

$$k = \frac{f_1 - f_2}{T} \tag{4.23}$$

For LFM If the instantaneous phase $\theta(t)$ is constant, the frequency is zero. If $\theta(t)$ is linear, the frequency is fixed (constant), furthermore if $\theta(t)$ is quadratic, the frequency changes linearly with time. In this work, the quadratic phase is used to sweep from the operation band of the tag as described in Fig. (4.17).

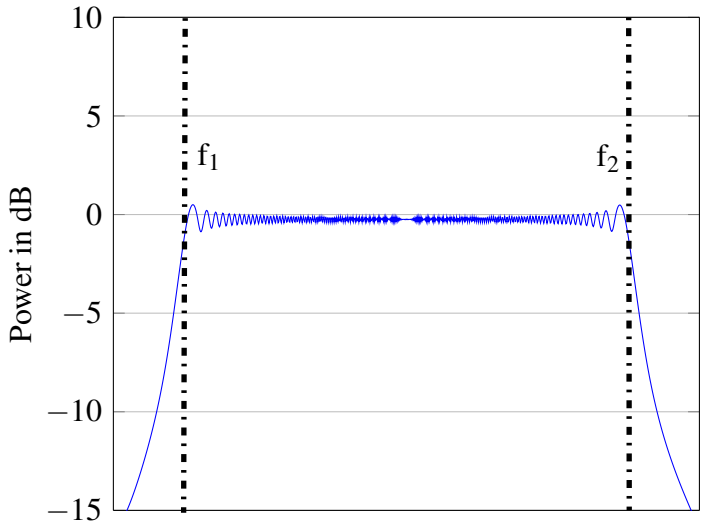

Figure 4.17: Frequency representation of the transmitted signal from f_1 to f_2.

Using equation 4.16 all a random ten bits tag are realized. All the algorithm are tested using the same condition.

For the decision between a logical $'1'$ and $'0'$ is determined differently in each algorithm. In the SVD algorithm, the four predefined sequence are defined with three different bandwidths to counteract the increase of notch width. If the detector chooses any of the three notches, the reader will decide it is a '1'. This could be shown in Fig. (4.18) where the gray area represents the notch. For the other detection algorithms matched filter and DTW are determined by calculating

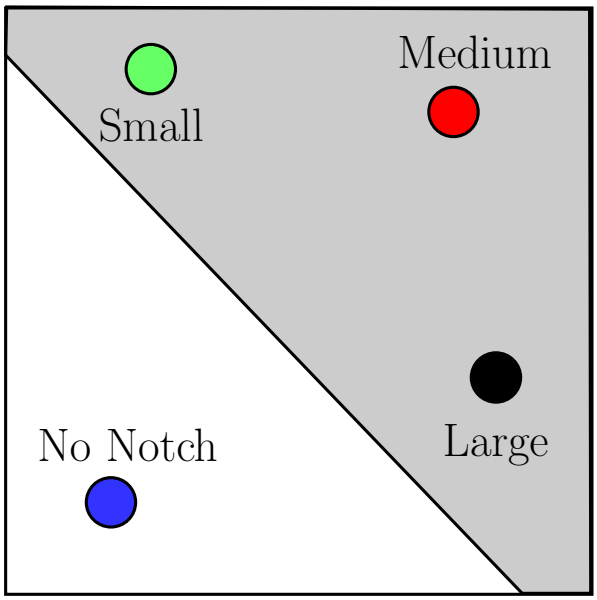

Figure 4.18: WB-SVD constellation for BW detection.

the threshold.

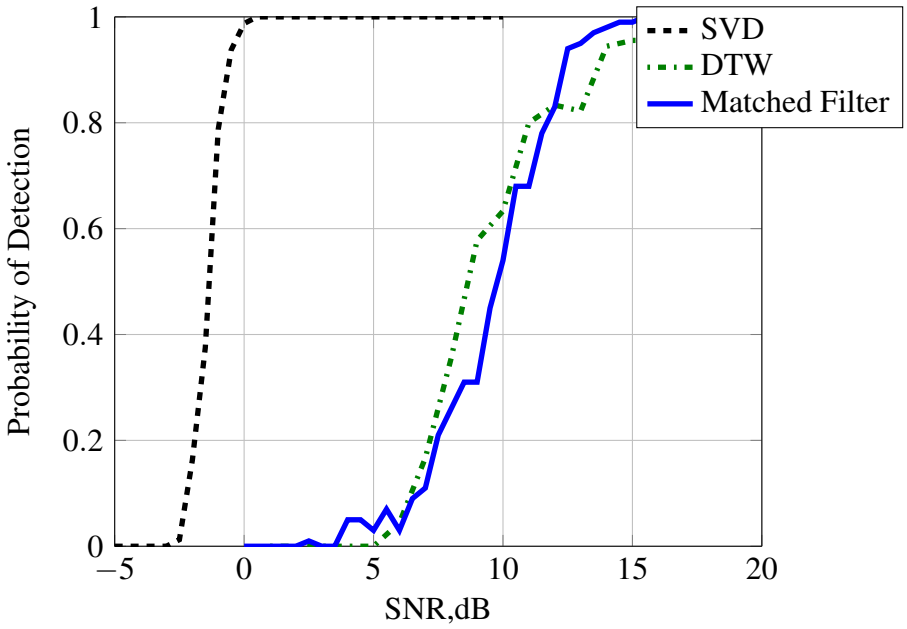

Figure 4.19: Simulated probability of detection for the 3 algorithms.

Fig (4.19) shows the single bit detection of all three algorithms. It is shown that the SVD has the best performance due to its three-notch predefined training sequence. Comparing the other two algorithms they seem to have the same performance except at high SNR where the matched filter proves to be better.

4.6.3 Notch Bandwidth

It is always a target for chipless RFID tag designers to increase the overall coding capacity of the tag. Various attempts were done in the literature to exploit every physical aspect of the tag like angle [77], polarization [78], co/cross properties [79] and tag resonators design [80–82]. Another interesting property is utilizing the notch width and position to boost the total capacity of the tag [83]. Adding information in the bandwidth of the notch adds an extra challenge in the detection of the notch. Not only should the detector detect the existence of a notch, but also identify the bandwidth.

To test the efficiency of the detection algorithm, a tag was designed, using CST, with variable bandwidths. The bandwidth offered by the tag are fixed, the coder of the tag would place the different bandwidths of the tag, shown in Fig. (4.20), depending on the final code of the tag.

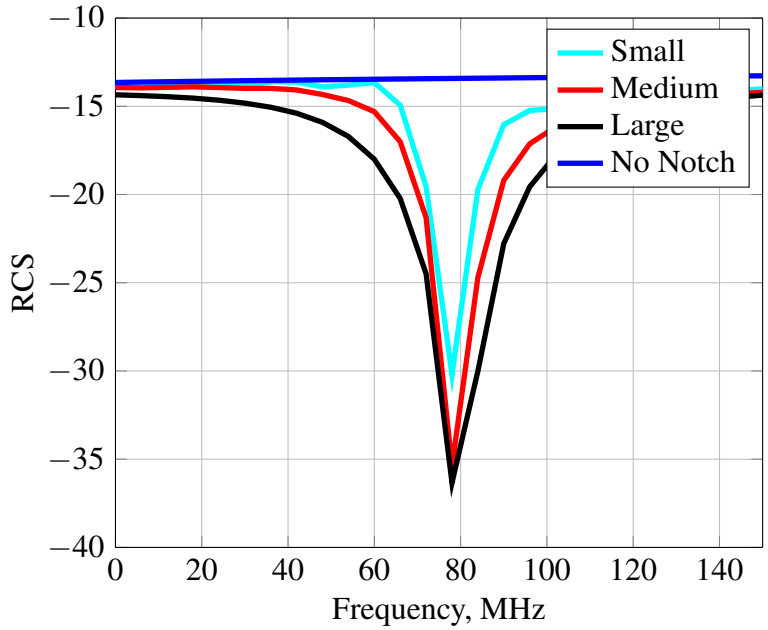

Figure 4.20: Three different notch bandwidth designed using CST.

Matched Filter

To evaluate MF for notch bandwidth detection, the received windowed signal would be compared with four filters. Each filter will represent one of the four states represented in Fig. (4.20). The correlation results are compared together using equation (4.3). All the results were then compared together where the highest correlation between the four filters is chosen as the received width. The width was then compared with the original transmitted signal for the final BER curve.

Unlike the regular notch detection, there are three states and a zero. The three different BWs have small variations in energy, which lead to the unsuitability of the results, where the detector failed to differentiate between the various BWs even at high SNR. The results concluded that using MF in detecting BW variation is not recommended.

WB-SVD

WB-SVD is based on calculating the constellation points for every notch shape. In this section, all four constellation points have been computed off-line. The received constellation point have been calculated using eq.(4.11). Unlike the regular notch detection, the decision is calculated according to the proximity to each constellation point independently as detected by the colored regions in Fig. (4.21).

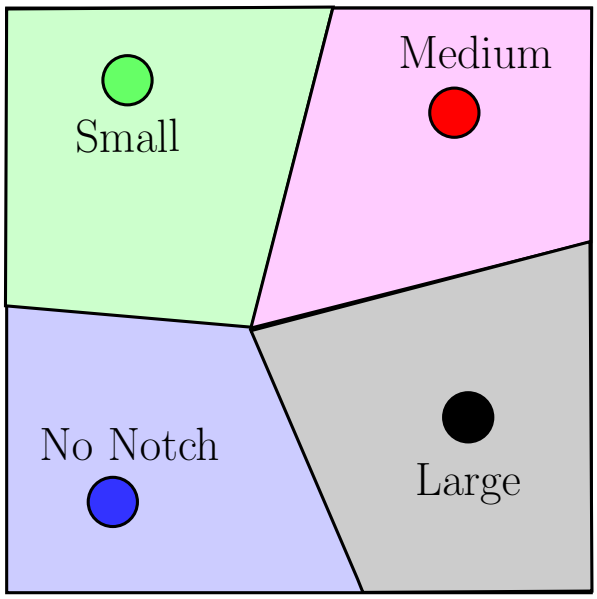

Figure 4.21: WB-SVD constellation for BW detection.

As expected, the results are very promising. The algorithm could easily detect the various bandwidths efficiently and effectively. Fig. (4.21) shows the results of each bandwidth separately. The P_d efficiency was all due to the position of the pre-calculated constellation point and its proximity to its neighboring points. Therefore, the worst performance in all the bandwidths was the medium and the best was the small bandwidth.

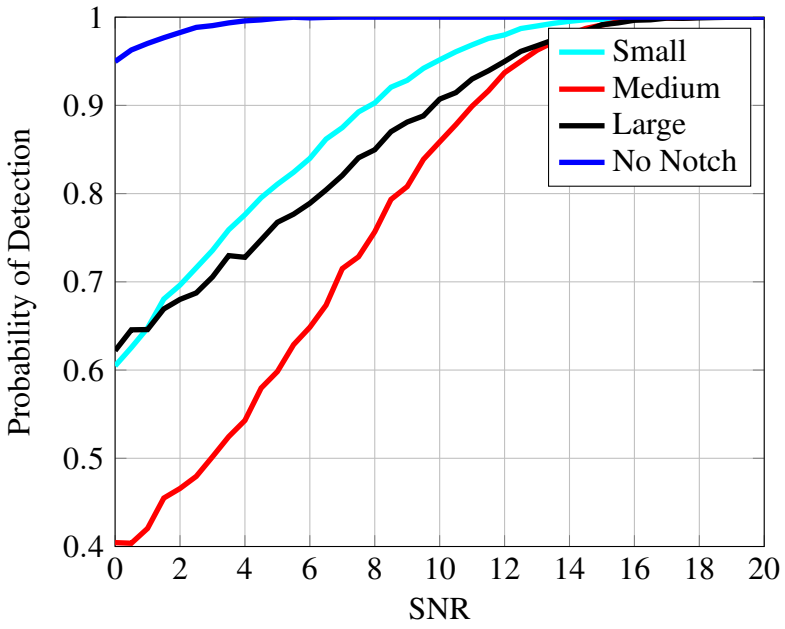

Figure 4.22: Comparing the P_d of all the possible backscattered notch bandwidths using WB-SVD

DTW

Similar to the matched filter approach, four predefined sequences were used as the reference signals. The received signal is compared to each reference signal, and the lowest is considered as the received BW. The results of the DTW algorithm are shown in figure (4.23).

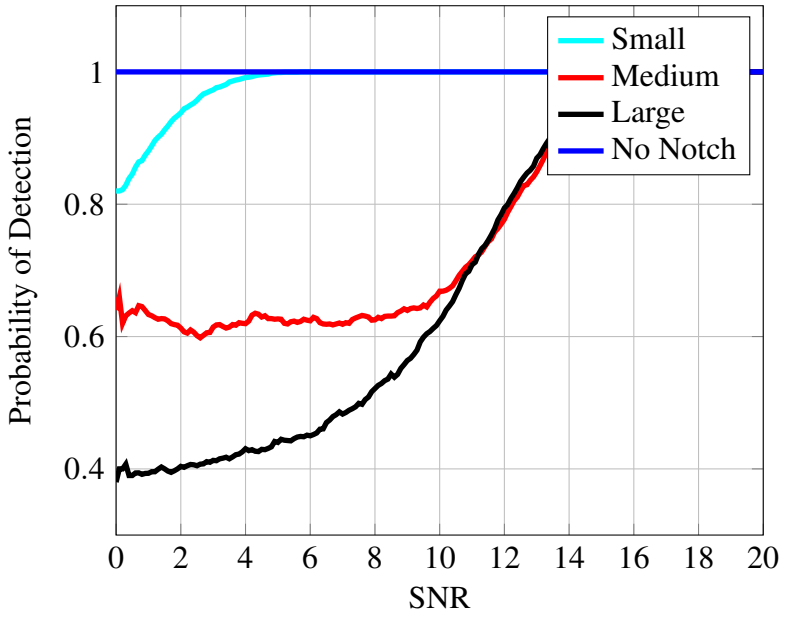

Figure 4.23: Results of detecting the notch and the bandwidth using DTW algorithm.

The results are better than the WB-SVD and the MF. The small BW shows the best results and the medium and large BWs exhibits similar behavior.

4.6.4 Notch Frequency Shift

In chipless RFID tags, the physical dimensions of the tag determine the properties of the backscattered signal [84]. These properties include the operating and resonance frequencies, notch bandwidth and notch width. Usually, the resonant frequencies of the designed notches in the tag are fixed. Unfortunately, due to fabrication errors, tagging effects and uncalibrated detectors the notch resonance frequency could shift in the detection window. In this subsection, the three algorithms would be tested in case of a notch frequency shift.

For this investigation, a variable notch width tag response would be used [75]. The information of this tag is in both its bandwidth and resonance frequency position [74]. Fig. () shows the three bandwidths and the zero level that would be used for the frequency shift investigation, where the noise level would be constant in all simulation for a fair comparison.

Matched Filter

The results show a good shift property but for one notch bandwidth. In this simulation, only the medium notch is compared with the no notch. Since matched filter is based on convolution, the shift in the notch does not affect the response of the system.

WB-SVD

In the WB-SVD the shifted notch constellation point was compared with the other predefined notch bandwidth points.

Fig. (4.25) shows the performance of the WB-SVD algorithm in case of frequency shifts. It is clear that the algorithm shows a poor performance when the received notch is shifted.

DTW

DTW algorithm was also tested using shifted notches. Since the algorithm is using non-linear sequence alignment, it was predicted that the algorithm would have the best performance out of all the three algorithms. Fig. (4.26d) shows the DTW results when two shifted notches was compared with a reference notch.

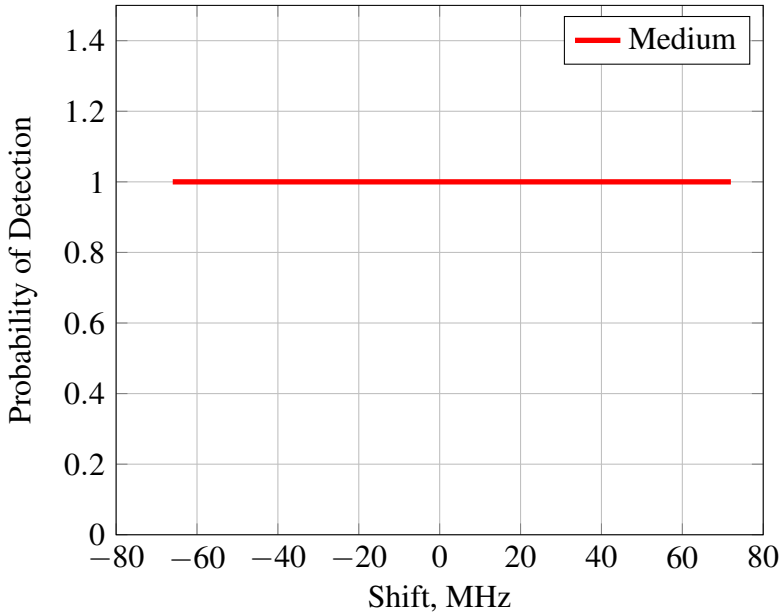

Figure 4.24: Results of detecting the notch and shift using matched filter algorithm.

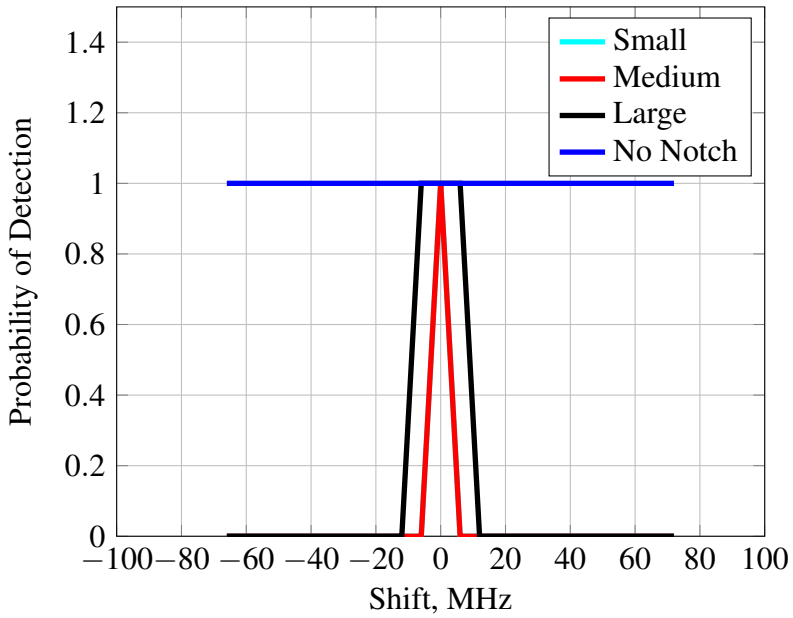

Figure 4.25: Results of detecting the notch and shift using SVD algorithm.

Fig. (4.27) shows an excellent performance for detecting the shift of the notch. According to the figure, the notch would be successfully detected with a shift up to 60 MHz in one direction.

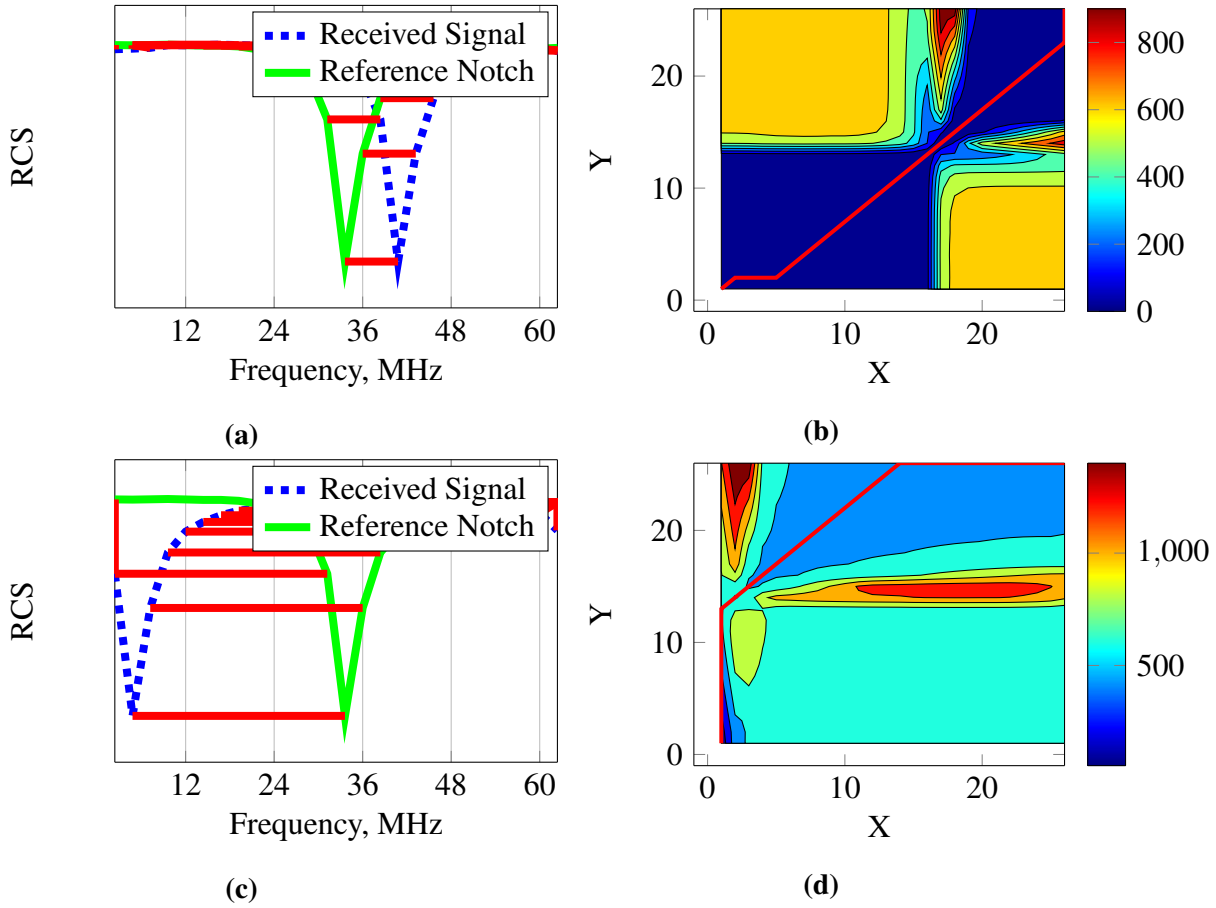

Figure 4.26: **(a)** A small shift detected by the DTW algorithm the red line represents the non-linear matching of both signals **(b)** Cost matrix C of the two signals X (shifted received signal) and Y (reference notch) the red line represent the lowest cost path **(c)** A much bigger shift where the algorithm successfully matched the two signals **(d)** Cost matrix C in case of high shift it shows a higher cost than (b).

4.7 Comparison of Detection Algorithms

In this chapter, an intensive study was made on the three algorithms. All the algorithms use windowing to detect the backscattered signal arriving from the tag. Based on the simulation, the first conclusion derived is that the detection window should not be less than the notch size. If the notch is bigger than the window the performance of the whole system will decrease by 80%, since an interference will occur with the neighboring notch.

The second study was done on a single bit detection were one notch represents either '0' or '1'. It was shown that the WB-SVD has the best performance compared to the matched filter. This is due to the high number of training sequence used (3 notches). Both matched filter

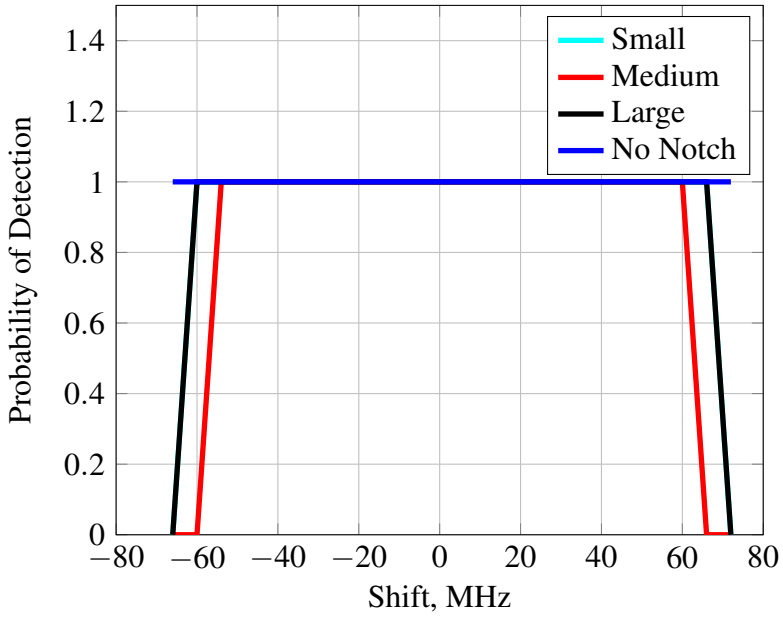

Figure 4.27: Results of detecting the notch and bandwidth using DTW algorithm.

and DTW show similar performance except at high SNR, where matched filter probability of detection exceeds the one of the DTW algorithm.

In an effort to increase the capacity the bandwidth of the notch has been utilized. In this method of coding, it is important to know the bandwidth of the notch. Here a tag was designed by the team to suit the requirement mentioned above. In the detection matched filter proved to be unreliable to detect the small difference in the notch bandwidth. Again SVD proved to be the best in identifying the different bandwidths. The performance of each bandwidth is evaluated separately. In the SVD the medium notch had the worst performance, this is due to its location in the constellation.

In the many measurements performed on manufactured tag, using USRP or measurement equipment. It was noticed that sometimes a shift of resonance occur in the response of tag. This shift was tested by moving the notch over the window bandwidth. It was concluded that the SVD performs so poorly in the case of frequency shift. The best detection algorithm was DTW. Matched filter is applicable for frequency shift for just one bandwidth.

Table (4.2) shows a comparison between all the three algorithms. It also shows the complexity of the algorithm as expected the highest complexity in the DTW and the lowest is the matched filter. As a conclusion, the algorithm should be chosen based on the application if the receiver has a fast processor then DTW is recommended. If a moderate complexity is needed, then SVD but the tags should be well designed and the reader calibration should regularly be

	Matched Filter	WB-SVD	DTW
Single bit detection			
Bandwidth detection			
Notch shift			
Complexity	Uncomplicated	Moderately Complicated	Highly Complicated

Table 4.2: comparing performance of all 3 algorithms red means bad performance and green indicates good while yellow is average

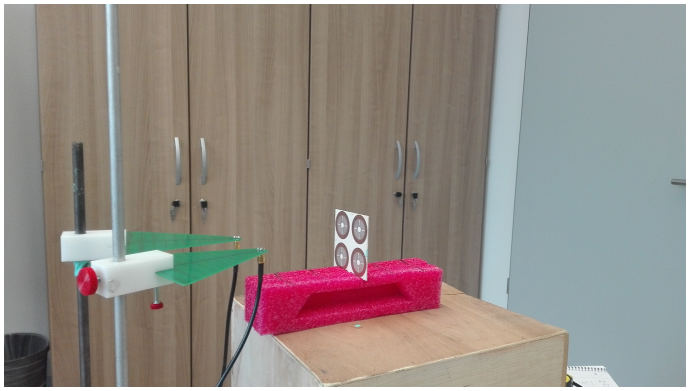

Figure 4.28: USRP Test bed using 2 Log periodic antennas and chipless RFID

performed to avoid notch shift. If a notch represents a single bit, then the recommendation is matched filter.

To test the efficiency of the detection algorithm, a test-bed was created using Universal Software Radio Peripheral 2 (USRP2) developed by Ettus Research. The daughter board used was CBX with a frequency range of 1 to 6 GHz. Since the USRP2 is a narrow band transponder, a frequency sweep transmission is performed. On the other hand, the receiver calculates the power received at each frequency. If the tag exists in the interrogation zone of the tag, the received frequency power spectrum would contain notches representing the ID of the tag.

Fig. (4.28) shows the measurement setup in an indoor environment, where two log periodic antennas are used as the transmitting and receiving antennas. For clutter removal, which is necessary for chipless tag detection, PN sequence was used with Rake receiver as explained in [85]. The USRP parameters could also be found in [85].

As shown in Fig. (4.29) the code of the 7 bit tag is 1010101. The red dotted lines in the figure represent the virtual window size taken by the notch detector. Furthermore, it could be seen from the same figure the increase in the notch bandwidth as frequency increase.

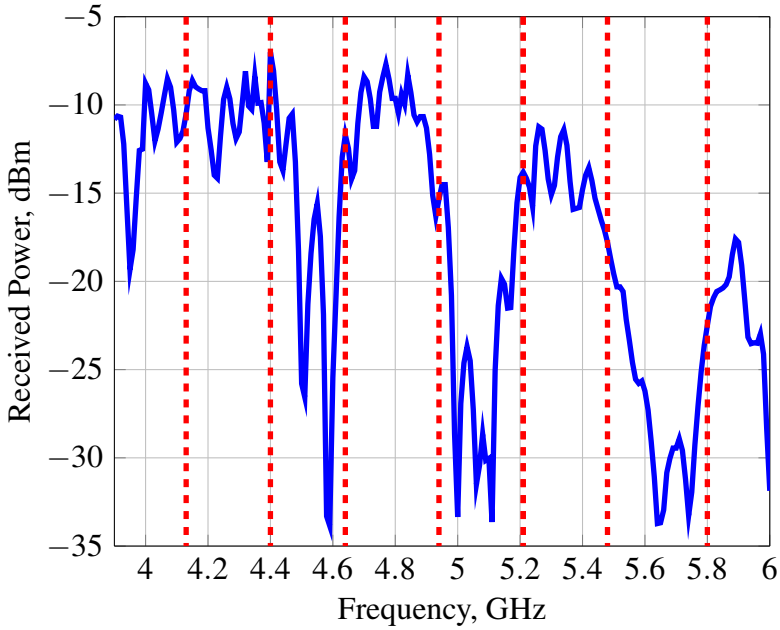

Figure 4.29: Measurement result of the tag using USRP of the 7 bit tag.

	1	0	1	0	1	0	1
Matched Filter	0.5	1	1	0.9	1	0.9	1
WB-SVD	0.05	1	1	1	1	1	1
DTW	1	1	1	1	1	1	0.95

Table 4.3: Probability of detection for 20 measurements done using USRP

Table (4.3) shows the probability of detection results of 20 measurements done using USRP. The reference notches were taken from the CST results. A better results could be achieved if the references was extracted from a reference measurement, but that requires calibration of the system. The results show that the first notch was detected successfully using matched and DTW. Unfortunately due to the notch shift the WB-SVD failed. The rest of the results were very promising.

5 Localization in Chipless RFID

Chipless tag localization techniques and strategies are presented in this chapter. A clear description of the well-known localization technique is presented. Furthermore, chipless RFID link budget using ray tracing and 3D RCS is calculated to estimate the interrogation zone. Two techniques are analyzed for tag localization, trilateration, and AoA based techniques. Both algorithms are analyzed and a testbed created to measure the efficiency of all algorithms.

5.1 Introduction

Spatial awareness is becoming an essential requirement in many indoor applications. These application could include locating fire victims [86], finding assets in a warehouse [87], guiding museum visitors [88], locating patient/elderly in a hospital [89] and motion detection in gaming [90].

Chipless RFID could be used for indoor localization, since it is easily worn by the people or attached to the objects to be tracked. Moreover, chipless RFID enjoys the benefit of on-demand printability on papers with conventional printing methods and conductive inks, which makes it ideal for mass deployment in low-cost item tagging for a wide range of applications [91].

Even-though chipless RFID has many advantages, detecting and localizing the tags could prove to be challenging. As described in the past chapters, the indoor signal propagation environments are often complex because of the presence of obstacles and, of course, any human occupants. Moreover, the signal backscattered from the tag is weak which adds another challenge in the localization process.

Another challenge is the UWB RCS property of the FC RFID tag. As described in chapter 3, the chipless RFID tag has a 3D RCS which changes in frequency. This would affect the power received at the reader side based on its location relative to the tag.

In this chapter, we will test the performance of the chipless tag using different localization techniques. First, a 1D tag localization will be performed to get the range of the tag. Using multiple antennas and AoA signal processing techniques a 2D tag detection will be realized.

5.2 Localization Techniques

In this section, the most common methods which have been proposed in the literature for localization estimation are presented, and their main properties are emphasized. Fig. (5.1) shows the classification of localization techniques.

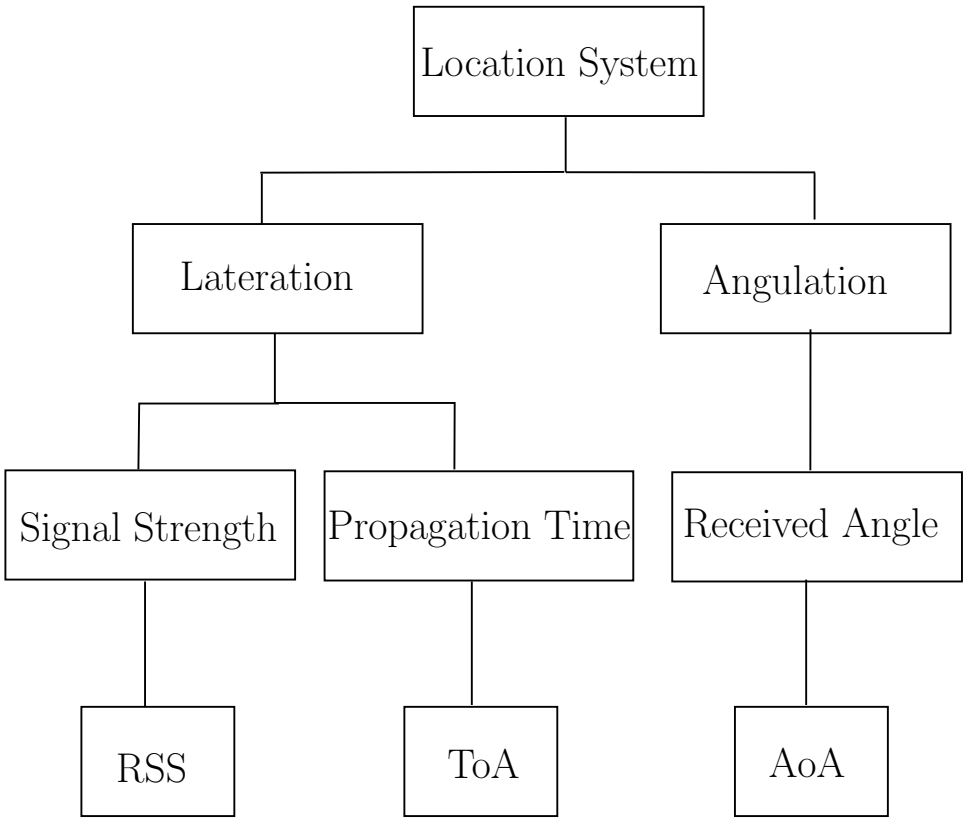

Figure 5.1: Classification of localization techniques

5.2.1 Signal Strength Based Methods

RSS based techniques exploit the distance dependency of the signal to estimate the range. In general, the received signal power decays with the increase in the distance. Given a reference signal power $P_{r,0}$ at a reference distance $d_{r,0}$ the received signal power at distance d is usually

approximated as

$$P_r = P_{r,0} - 10\eta \log(\frac{d}{d_{r,0}}) \tag{5.1}$$

where the P_r and $P_{r,0}$ are calculated in dB.

Unfortunately, P_r strongly depends on the number of multipath in the environment. This will lead to an increase or a decrease in power depending on constructive or destructive interference. This requires accurate calibration of the parameters η and $P_{r,0}$ for different environments, and a priori knowledge (or an accurate estimate) of the environment. This affects the accuracy of the RSS techniques [92–94].

In chipless RFID the backscatter signal will be analyzed for its RSS. Since the received signal will not only contain the tag ID, additive signals like the clutter response should be removed. Moreover, the tag must be calibrated to accurately calculate the tag signal strength.

5.2.2 Time Based Methods

Time based positioning techniques rely on the measurement of the travel time of the signal propagating from the transmitter to the receiver. In a perfect world scenario, the reader will calculate the time of transmission and the Time of Arrival (ToA) of the backscattered signal from the tag. The reader then can directly calculate the tag's distance from the transmitter, by multiplying the estimated ToA by the speed of light [95].

In chipless RFID many aspects have to be considered before considering using ToA as a ranging technique. The first is the high sampling rate at the receiver side since the reflection from the tag is usually fast. Another aspect is the interrogation signal used by the transmitter, which is preferred to be an UWB pulse. As any other localization algorithm, the channel should be acquired so that interfering signals could be removed. Other aspects should also be considered, like the delay caused by the reader hardware. These delays are usually random and hard to calibrate.

5.2.3 Angle of Arrival Based Method

AoA provides the direction information of an incoming signal. In all AOA techniques, antenna array must be used at the receiver side. Commonly the algorithms utilize the difference in time of arrival (phase difference) between the antennas to determine the AOA [96].

In a radar system like the one used in the chipless RFID, the incoming signal is highly

correlated. This will prove to problematic in most of the AOA algorithms.

5.3 Chipless RFID Link Budget

Link budget calculation in communications specifies the reading range based on power budget for the transmitter, the antenna gain, and Effective Isotropic Radiated Power (EIRP) of the reader antenna. Moreover, the link budget helps to calculate the required antenna gain and related specification to obtain a robust and viable communication in the specific conditions of wireless communications.

In backscatter radio, the reader communicates wirelessly with the tag by scattering electromagnetic waves. This communication system allows the tag to communicate while consuming very little or no power. Unlike the chipped RFID the chipless does not require charging, it reflects the incident power. Theoretically, this will increase the reading range [97].

In chipless RFID the system design is challenging because of the complex electromagnetic interactions between the reader, tag, and the radio channel. As described in the previous chapters, these interactions limit the amount of power received by the tag and/or the amount of power backscattered to the reader. If either of these powers drops below a certain threshold, the reader will be unable to detect the backscattered signal reliably. Therefore, it is imperative for the design and operation of modulated backscatter systems that these received powers be predicted.

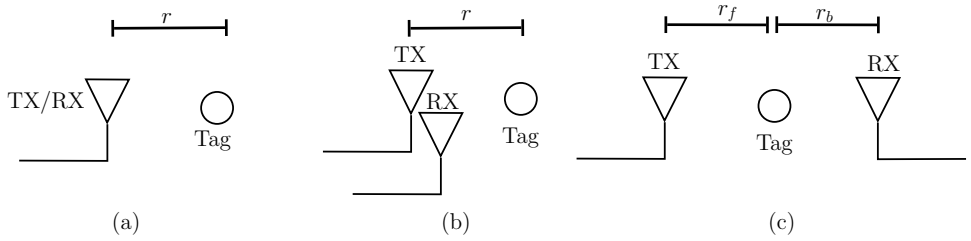

Figure 5.2: The three main antenna configurations in the backscatter link:(a)monostatic, (b) bistatic collocated, and(c) bistatic dislocated [1].

The first link budget in Eq.(5.2), describes the forward channel power flow from the transmitter of the reader to the chipless tag.

$$P_{tag} = \frac{P_T G_T \lambda^2 X_f}{(4\pi r_f)^2 B F_b} \tag{5.2}$$

where

P_{tag}= is the power received at the tag

P_T= is the power transmitted by the reader (W)

G_T= is the gain of the TX antenna

λ= is the is the carrier frequency wavelength (m)

X_f= is the forward polarization mismatch

r_f= is the reader to tag distance (m)

B_f= is the forward blockage loss

F_b= is the power-up link, small-scale multipath fading loss

Equation (5.2) depends on the tag-reader separation distance, antenna gain and transmitted power. In chipless RFID, unlike the chipped, there is no minimum power P_{tag}. All the limitation is in received power at the receiver side, as presented in equation(5.3).

$$P_R = \frac{P_T G_T G_R \lambda^4 X_f X_b \Gamma(\Theta, \Phi)}{(4\pi r)^4 r_f r_b B_f B_b F} \tag{5.3}$$

where

r_b= is the tag-to-reader separation distance (m)

X_b= is the reverse-link polarization mismatch

G_R= is the gain of the RX antenna

r_f= is the reader to tag distance (m)

B_b= is the backward blockage loss

F_b= is the power-up link, small-scale multipath fading loss

Γ= is the RCS of the tag which depends on angle of arrival θ_f ; $\phi_b$and departure θ_b and ϕ_b of the indecent signal.

The unit-less loss terms B, F and X that appear in Eq. (5.3) and (5.2) are explained in details in [97]. These terms and the other will vary depending on the antenna configuration of the RF tag reader, shown in Fig (5.2). In the monostatic configuration, the reader uses a single antenna to transmit and receive.In the monostatic case $r_f = r_b$, $X_f = X_b$, $B_f = B_b$. Moreover, this configuration requires a circulator which will add an extra power loss [98].

The FC chipless has two major backscattering states, *total reflection* and *absorption*. In the total reflection state, the tag will reflect back the incident power depending on its RCS (Γ). In the absorption state, the tag absorbs some of the power and reflects the rest. For the tag to be detected both states must be above the reader sensitivity as shown in Fig (5.3).

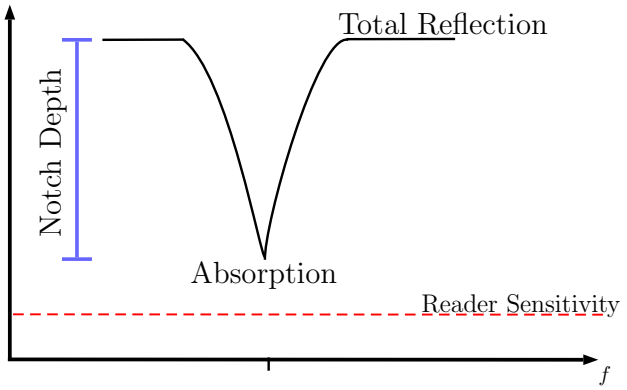

Figure 5.3: A description drawing showing the two backscattering states and the reader sensitivity

In chipless RFID the notch depth of the tag is determined by the design of the tag. The notch depth changes depending on the position of the tag relative to the reader. The clarity of the notch is determined by the RCS radiation pattern of the tag. The reader sensitivity is stated by the reader. Both the reader sensitivity and the notch depth are important when determining the maximum range of the tag.

To show the location dependence of the tag a WI simulation was made where a regular office was designed using the same electric parameters described in Table (3.1). A groundless tag was used with a backscattering power of 0 dB. As shown in Fig (5.5) (5.4) the tag placed in the middle in the total reflection state and 3D RCS was extracted from CST.

The tag was surrounded by readers. The simulation was done twice, once by using a high

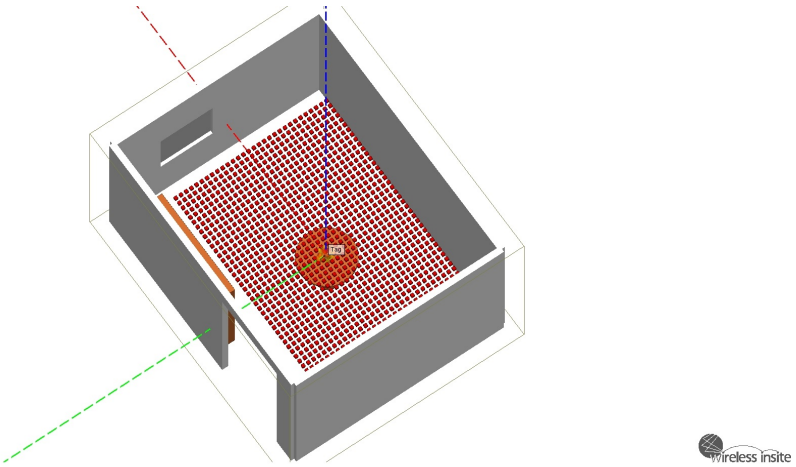

Figure 5.4: WI setup for a room with a tag in the middle surrounded by reader 3D view

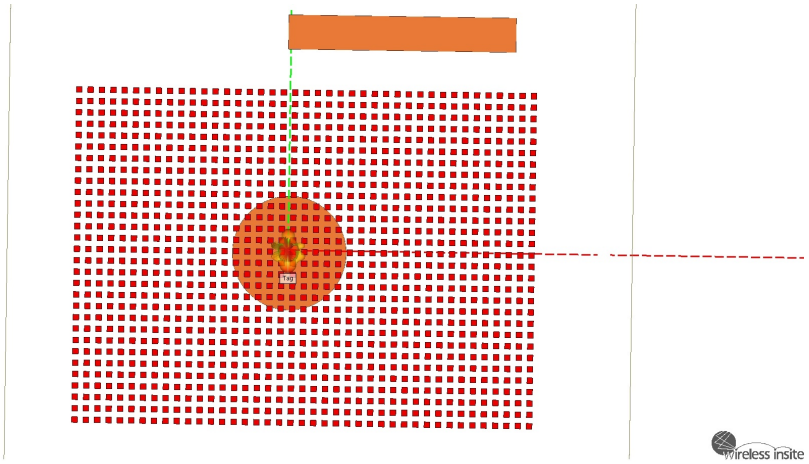

Figure 5.5: WI setup for a room with a tag in the middle surrounded by reader top view

directive horn antenna and another by using a conventional omni-directional antenna, to show the effect of the reader gain factor. In the directional antenna case, all the readers were designed that the maximum gain is directed towards the tag.

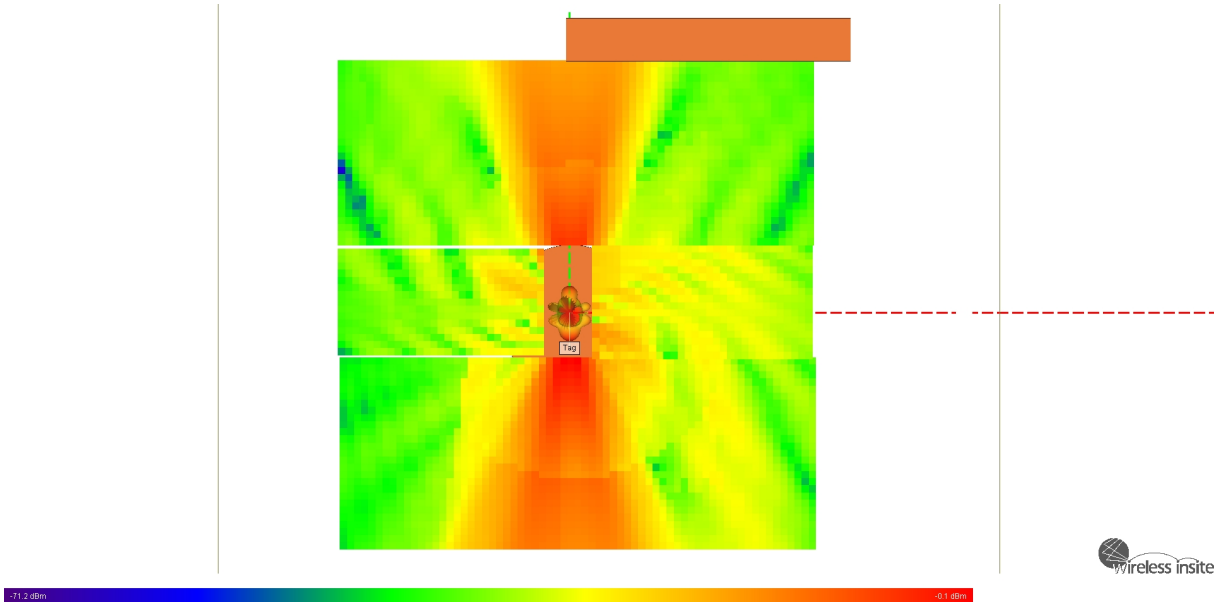

Figure 5.6: Directional antenna case (Horn)

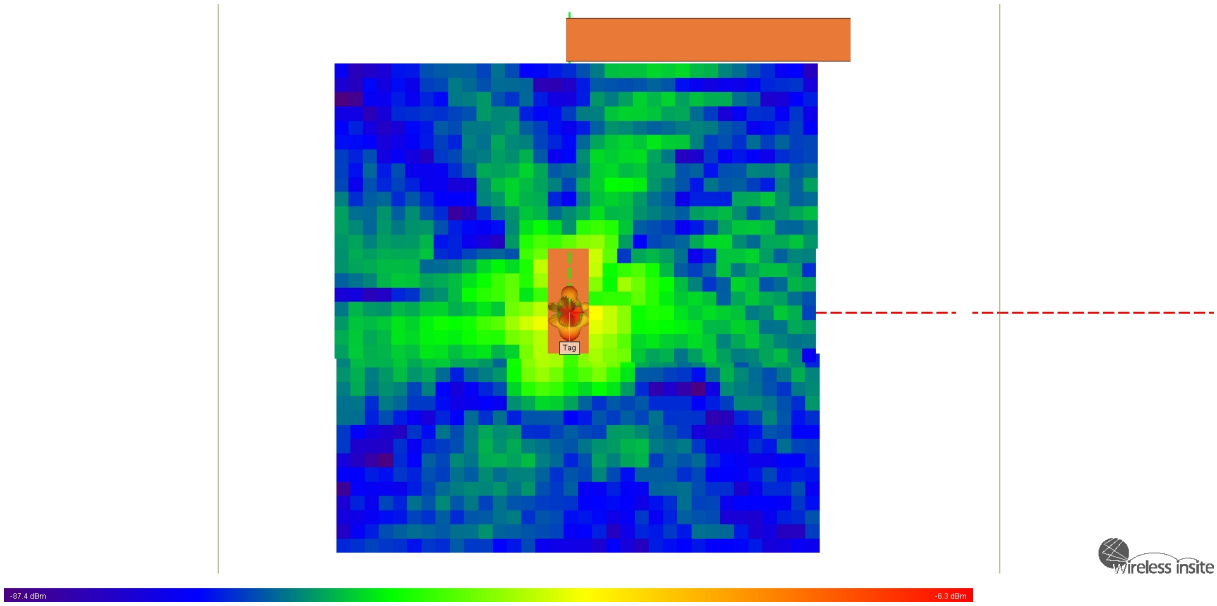

Figure 5.7: omni-Directional antenna case

The color coded results in Fig (5.6) and (5.7), shows the power received from the tag at each point considering the fully reflection mode where the tag have the highest RCS response. It is evident from the results that the use of a directive antenna shown in Fig. (5.6) leads to a higher interrogation area. This is could also be shown in equation (5.3). It must be noted that the interrogation zone differs at every frequency point, depending on the RCS radiation pattern.

It is also realized that the interrogation zone of the tag used in front and the back of the tag, in the directional reader antenna case. The tag does not scatter the incoming electromagnetic on the left and the right regions of the tag. If a ground based tag was used, as shown in Fig. (5.8), the ground plane will reflect all the incoming signal leading to only one direction of interrogation, represented by the red area.

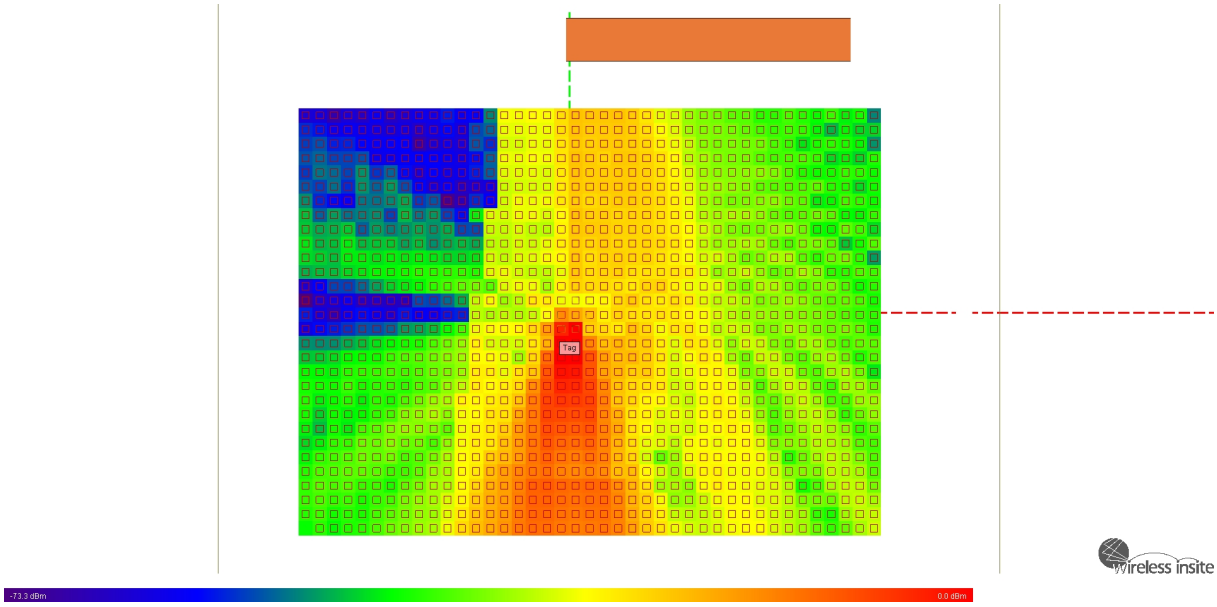

Figure 5.8: Directional antenna case with a ground based tag

5.4 Trilateration Estimation

In the chipless RFID there three main researches done in the localization of the tag. All of them uses trilateration for the localization of the tag [99–101]. Trilateration uses the distances among the locations to estimate the coordinate of the unknown location. In trilateration, the distances between reference locations (reader) and the unknown location (Tag) can be considered as the radii of many circles with centers at every reference location. Thus, the unknown location is the intersection of all the sphere surfaces as shown in Fig. (5.9).

Figure 5.9 shows three readers placed at random with known locations (x_n, y_n) where $n = 1, 2, 3$. the tag is placed in the interrogation zone of all the three readers. The main task of the localization algorithm is to calculate (x, y) by using (d_1, d_2, d_3). The simplest solution is to

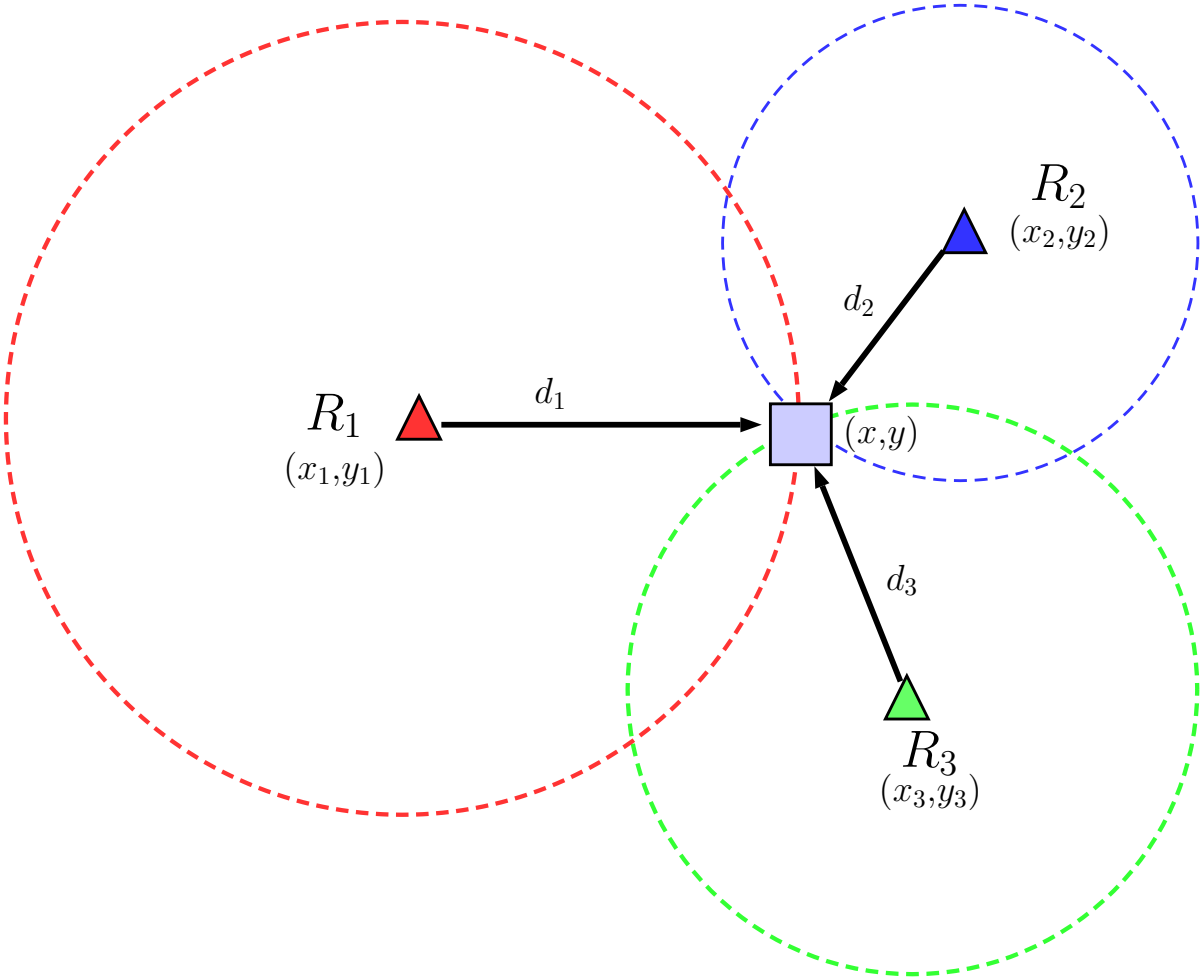

Figure 5.9: Trilateration estimation using three readers and a tag

use Pythagorean theorem.

$$\begin{aligned} d_1^2 &= (x_1 - x)^2 + (y_1 - y)^2 \\ d_2^2 &= (x_2 - x)^2 + (y_2 - y)^2 \\ d_3^2 &= (x_3 - x)^2 + (y_3 - y)^2 \end{aligned} \tag{5.4}$$

Rearrange the equations in 5.4 and solve for x and y, the location coordinate of the tag can be obtained as shown in the following expression.

$$x = \frac{AY_{32} + BY_{13} + CY_{21}}{2(x_1Y_{32} + x_2Y_{13} + x_3Y_{21})} \tag{5.5}$$

$$y = \frac{AY_{32} + BY_{13} + CY_{21}}{2(y_1Y_{32} + y_2Y_{13} + y_3Y_{21})} \tag{5.6}$$

where

$$\begin{aligned} A &= x_1^2 + y_1^2 - d_1^2 \\ B &= x_2^2 + y_2^2 - d_2^2 \\ C &= x_3^2 + y_3^2 - d_3^2 \end{aligned} \tag{5.7}$$

and

$$\begin{aligned} X_{32} &= (x_3 - x_2) \\ X_{13} &= (x_1 - x_3) \\ X_{21} &= (x_2 - x_1) \\ Y_{32} &= (y_3 - y_2) \\ Y_{13} &= (y_1 - y_3) \\ Y_{21} &= (y_2 - y_1) \end{aligned} \tag{5.8}$$

There are three possible scenarios:

- All three readers detect the tag.
- Two readers detect the tag.
- One or no reader detect the tag tags.

To use trilateration techniques, at least three reference nodes are required. The second and third scenarios are not able to fulfill the requirement [102]. This will prove to be a challenge in chipless RFID, since the probability of three readers detect the tag is very low. It will be substantially dependent on the location of the reader relative to the tag. To prove this theory, a simulation setup was made using WI.

In this setup, 12 readers were placed around the tag. The separation between each reader and the next is 30°. Moreover, at each angle 3 reader nodes are placed at distances of 2m, 1m, 20 cm. In this simulation, the tag 3D RCS is changed with the frequency. Two scenarios are implemented the forward and backward channel. The power received at each reader is monitored and the results are retrieved.

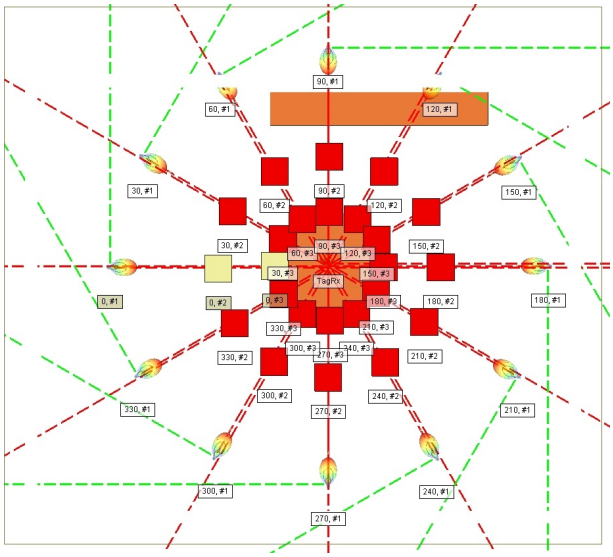

Figure 5.10: Trilateration technique setup in WI

The results show that the readers in front and behind the tag could only detect the tag while other readers failed to do so. This could also be validated using measurements done in the following subsection.

5.4.1 Measurements of angle dependency

To validate the angle dependency of the chipless tag, a testbed was created using a fabricated tag. The measurement was performed on three angles; 90, 30, 150. In the 90-degree scenario, the tag is facing the reader. In all scenarios, a spectrum generator and sensor is used to transmit and receive a sweeping sinusoidal signal to detect the tag which is 10 cm away.

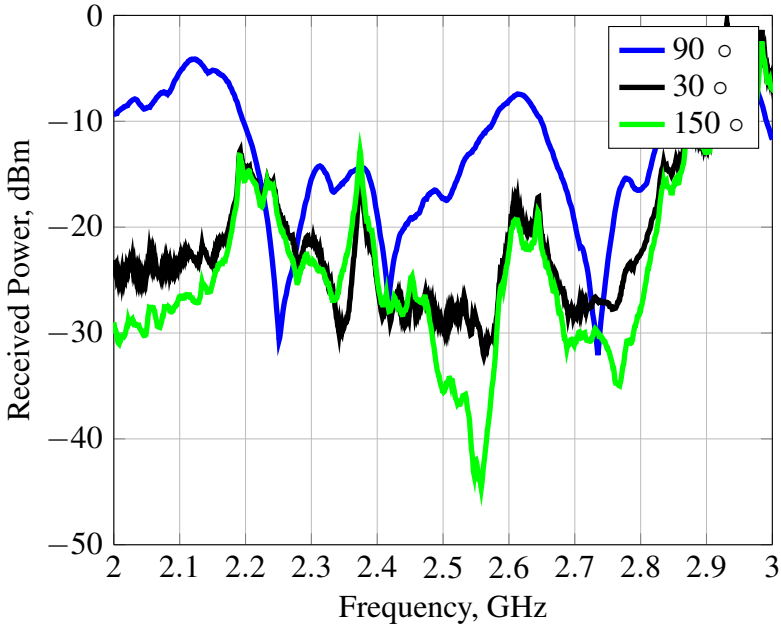

Figure 5.11: Measurement results of three tag rotation angles

The results of the measurements are shown in Fig. (5.11). The results clearly show that the tag was detected and identified in the 90-degree case. If those angles were chosen in a trilateration algorithm, the tag would be undetectable at two angles. This will lead to the algorithm to fail when localizing the tag.

5.5 Multiple Antenna Based Localization Techniques

To solve the trilateration limitations, it is proposed to design a localization system based on one reader with multiple antennas. The implemented system offers 1D localization, which calculates the range of the tag from the reader. Moreover, multiple antennas are utilized to calculate the angle of arrival of the backscattered signal, indicating the 2D location of the tag as shown in Fig. (5.12). In all techniques, both detection and localization are important, since any object from the environment could also reflect the signal. If there is no detection, this reflected signal could be mistaken for a tag.

This section will first highlight the ranging technique RSS. A simulation and measurements will be done to investigate the maximum distance that could be achieved by the algorithm. Moreover, the advantage and disadvantage of both techniques will be stated.

For 2D localization, AoA techniques will be utilized to determine the angle of arrival of the reflected signal. All available techniques will be studied to determine which is the best for our

application. In all localization techniques, 1D or 2D, only one notch will be considered.

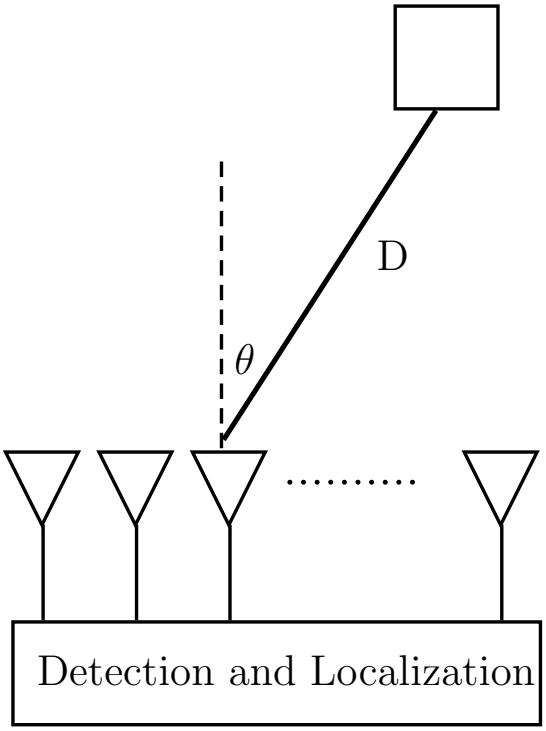

Figure 5.12: The use of multiple antennas for localizing the tag.

5.5.1 Reading Range Calculation

The first step in tag ranging is to calculate the achievable range for the recommended setup. For that, a simulation using WI and measurement using a function generator and a spectrum analyzer was used. In this setup, the tags are distributed in front of the reader. The antennas used for the readers are horn antennas for maximum gain, with an angle of 45 degrees.

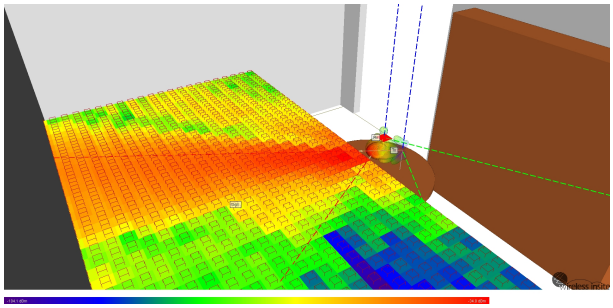

Figure 5.13: Forward channel power allocation

Algorithm 5.1 Algorithm for calculating the tag range

procedure WI FORWARD(x,y)
    Set Tx1 as the transmitter
    Transmit sine wave at power=20 dBm
    Set tag grid as the receiver
    Set received signal at each tag $= FORSignal(x,y)$
    Return $FORSignal(x,y)$
end procedure
procedure WI BACKWARD(FORSignal(x,y))
    Set tags as the transmitters
    Transmit $FORSignal(x,y)$
    Return $RXSignal(x,y)$
end procedure
▷ Main Code
Get Tag grid size= [x,y]
FORSignal=WI Forward(x,y)
RXSignal=WI Backward(FORSignal(x,y))
Remove clutter response
Set Reader Sensitivity =-110
Set RXSignal< Reader Sensitivity = -310

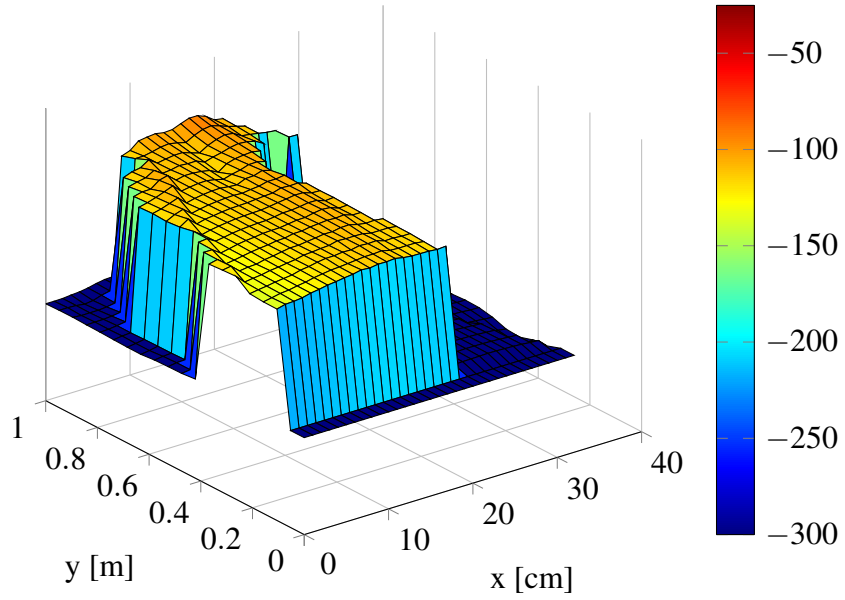

Figure 5.14: The detected tags after applying forward and backward channel.

For ranging calculation which includes environmental effects, channel gain, path loss and the chipless tag RCS pattern. An algorithm (5.1)was implemented to include the forward channel, shown in Fig. (5.13), and the backward channel. It was calculated that the tag could be detected in a range of 1 m. This includes the removal of clutter, transmission power of 20 dBm a reader sensitivity of -110 dBm. A greater range could be achieved if both a higher gain antenna, or a tag with a higher RCS value are used. Moreover, a more sensitive reader could provide a higher reading range.

5.5.2 RSS Measurements Using Chipless RFID

To calculate the range of the tag, RSS techniques should prove to be useful. In this algorithm a reference tag must be used at a known distance, to estimate the parameters of equation (5.1). In LOS indoor environments the pathloss exponent (η) ranges from 1.0 to about 2 in office environments. In NLOS scenarios the pathloss exponent typically ranges from 3 to 7 [103]. Ranging based on the received signal strength is strongly dependent on the estimation of the parameter the pathloss exponent which is variant in every environment. Therefore an accurate calibration is needed for the reference and no tag scenario. Equation (5.1) could be expressed in terms of the distance in the following equation:

$$\hat{d} = d_0(\frac{P_0}{P_r})^{\frac{1}{\eta}} \tag{5.9}$$

In the all the localization algorithms one notch was considered for efficiency. All the measurements were done using a function generator and a spectrum analyzer, where one tag was used and interrogated with a sweeping sinusoidal wave from 2 GHz to 3 GHz.

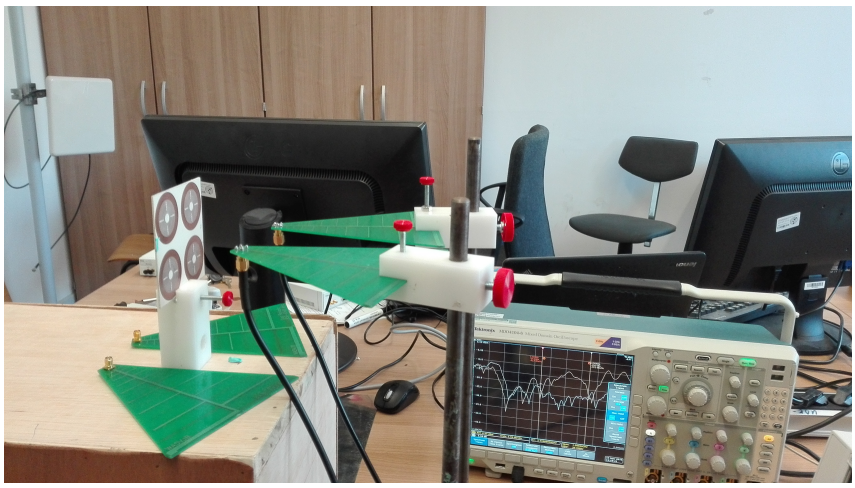

Figure 5.15: Localization test-bed designed in an indoor office setup.

The first task was to identify the best distance for the calibration process. Too close and we may risk being in the near field region of the reader antenna too far and we may risk having clutter and self-interference affect the measurements.

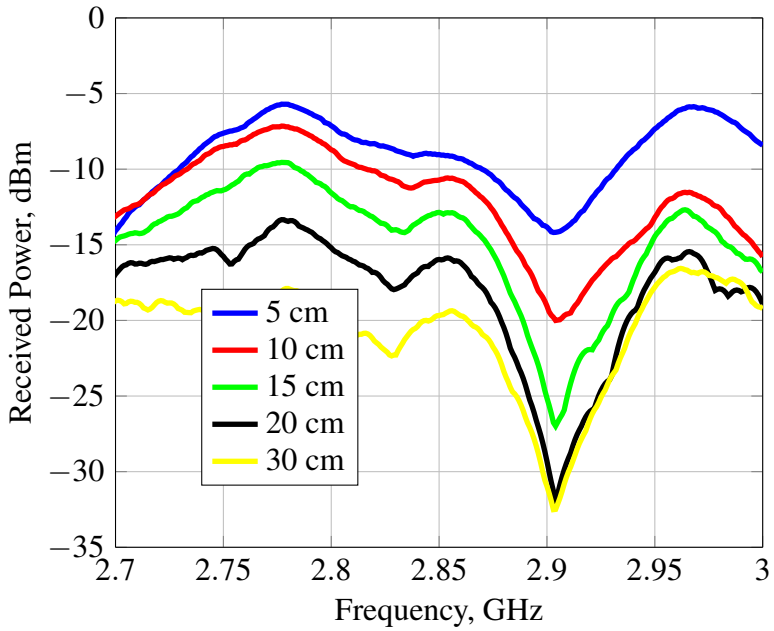

Figure 5.16: Calibrated tag measurements at 5 cm to 30 cm distance

Fig. (5.15) shows the measurement setup used and Fig. (5.16) are the calibrated results

extracted from the spectrum analyzer in sweep mode at a distance of 5 cm to 30 cm. Fig. (5.16) shows a peak where the tag is at full reflection mode at frequency 2.78 GHz and a notch at 2.9 GHz. These frequencies was chosen to fit our measurement equipment and the tag operation frequency.

In the ranging algorithm (5.2) the reader scans the first notch frequency in this case from 2.75 GHz to 2.95 GHz. Clutter removal techniques are then applied to the received signal to remove self interference. A notch detection algorithm is then applied to the equalized signal. This process is vital to avoid using ranging algorithms on any metal structures. The detection algorithms may vary from match filter; SVD or DTW, explained in chapter 4. The next step in the ranging process is analyzing the power at the peak. Using equation (5.9) the range could be determined.

The detection was performed 35 times at various distance. The error is then calculated using equation (5.10). Fig. (5.17) shows the calculated RSS measured values at η=1.5.

Algorithm 5.2 Algorithm for calculating the tag range using real test bed

1: **procedure** 5CM CALIBRATION
2: Scan tag from 2.75 GHz to 2.95 GHz.
3: Apply clutter removal technique
4: P_0 = Power(2.78)
5: calculate η
6: Return η
7: **end procedure**

▷ Main Code

8: Scan tag from 2.75 GHz to 2.95 GHz
9: Apply clutter removal technique
10: Apply detection algorithm
11: η=5cm calibration
12: Calculate Range

$$e_d = \hat{d} - d = d_0(\frac{P_0}{P_r})^{\frac{1}{\eta}} - d \tag{5.10}$$

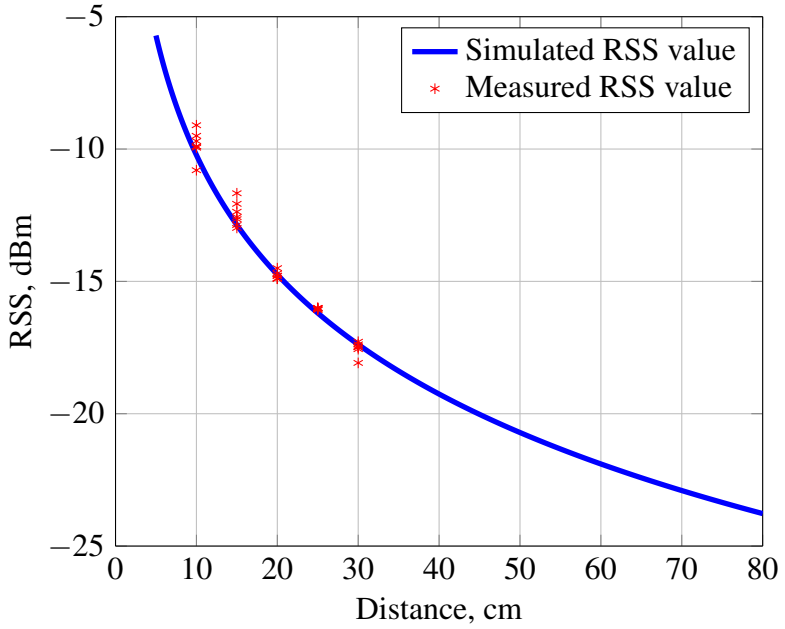

Figure 5.17: Measured vs simulated distance using empty room calibration.

5.5.3 Estimating Angle of Arrival using MPM

The problem of estimating the direction of arrival of the various sources impinging on an antenna array has received considerable attention in many fields including radar, sonar, radio astronomy, and mobile communications [104]. Each technology had its challenges and requirements, since each operates at different frequencies and environments. In chipless RFID using AoA proves to be quite a challenge, since all the reflected signals are highly correlated which would not work with many algorithms. Another challenge is in the operating frequency range of the chipless RFID. This is because the AoA algorithms get more complicated in an UWB scenario. Finally, the reflected signal is very week which could be undetectable by the array of antennas. These challenges will all be solved in this section.

Many methods and techniques have been developed to estimate the required parameters of plane wave signals. These methods can be divided into two broad categories

- Beamforming or Classical Methods
- Subspace Based Method

The main idea of the Classical Methods is to steer the array in one direction at a time and

measure the output power [105]. Where the received signal $y(t)$ after weighting is described by

$$y(t) = w^H x(t) \tag{5.11}$$

Two well known algorithms in this category are Bartlett Beam-former: [106] where the spacial spectrum is obtained by

$$P(\theta) = \frac{a^H(\theta)\hat{R}a(\theta)}{a^H(\theta)a(\theta)} \tag{5.12}$$

and CAPONS is defined by [107]:

$$P(\theta) = \frac{1}{a^H(\theta)\hat{R}^{-1}a(\theta)} \tag{5.13}$$

where $\hat{R}$ is the sample covariance matrix, while $a(\theta)$ is the steering matrix.

Subspace based methods are most widely used DOA estimation methods due to their computational simplicity and high resolution. These methods exploit the properties of noise and/or signal subspaces to estimate the required parameter. Well known algorithms in this category are:

- Multiple Signal Classification (MUSIC) [108]
- Estimation of Signal Parameters via Rotational Invariance Technique (ESPRIT) [109]
- Matrix Pencil (MP) method

All above techniques are covariance based algorithms which assume that0 the signals impinging on the array are not correlated or coherent, except for MP. For coherent or highly correlated signals the rank of the covariance matrix is reduced and the ability to resolve closely spaced sources is also dramatically decreased [110]. MP method operates directly on received data so as to estimate the required parameters and works well in the presence of fully correlated signals.

Matrix Pencil Method

MP method was first proposed by [52]. For a single measurement the output of the nth antenna is:

$$y_n = \sum_{i=1}^{I} A_i e^{j(n\Psi_i + \zeta_i)} + \nu \tag{5.14}$$

where A_i and ζ are the i_{th} signal's amplitude and phase. A Hankel matrix can be constructed from 5.14. with

$$\Psi_i = j\frac{2\pi}{\lambda} d\,cos(\theta_i) \tag{5.15}$$

$$\mathbf{Y} = \begin{bmatrix} y_0 & y_1 & \cdots & y_{L-1} \\ y_1 & y_2 & \cdots & y_L \\ \vdots & \vdots & \ddots & \vdots \\ y_{N-1} & y_{N-L+1} & \cdots & y_{N-1} \end{bmatrix} \tag{5.16}$$

where L is called the pencil parameter and its value should be between N/3 and N/2 for effective noise filtering, Where N is the number of antennas. The data matrix $\mathbf{Y}$ can be decomposed as

$$\mathbf{Y} = \mathbf{Z}_a \mathbf{R}_0 \mathbf{Z}_b \tag{5.17}$$

where

$$\mathbf{Z}_a = \begin{bmatrix} 1 & 1 & \cdots & 1 \\ e^{j\Psi_1} & e^{j\Psi_2} & \cdots & e^{j\Psi_I} \\ \vdots & \vdots & \ddots & \vdots \\ e^{(N-L)j\Psi_1} & e^{(N-L)j\Psi_2} & & e^{(N-L)j\Psi_I} \end{bmatrix} \tag{5.18}$$

and

$$\mathbf{Z}_a = \begin{bmatrix} 1 & e^{j\Psi_1} & \cdots & e^{(L-1)j\Psi_1} \\ 1 & e^{j\Psi_2} & \cdots & e^{(L-1)j\Psi_I} \\ \vdots & \vdots & \ddots & \vdots \\ 1 & e^{j\Psi_I} & & e^{(L-1)j\Psi_I} \end{bmatrix} \tag{5.19}$$

$$\mathbf{R}_0 = \begin{bmatrix} A_1 e^{j\zeta_1} & A_2 e^{j\zeta_2} & \cdots & A_I e^{j\zeta_I} \end{bmatrix} \tag{5.20}$$

For noisy data, a SVD can be used to reduce the effect of noise. After SVD,$\mathbf{Y}$ can be written as

$$\mathrm{SVD}(\mathbf{Y}) = \mathbf{U}\Sigma\mathbf{V}^{\mathrm{H}} \tag{5.21}$$

where $\mathbf{U}$ and $\mathbf{V}$ are unitary matrices whose columns are left and right singular vectors of $\mathbf{Y}$, respectively, and Σ contains the singular values of $\mathbf{Y}$ located on its main diagonal.

$$\mathrm{SVD}(\mathbf{Y}) = \mathbf{U}_s\Sigma_s\mathbf{V}_s^{\mathrm{H}} + \mathbf{U}_n\Sigma_n\mathbf{V}_n^{\mathrm{H}} \tag{5.22}$$

where $\mathbf{U}_s$ and $\mathbf{V}_s$ contain the left and right singular vectors of Y corresponding to $\mathbf{I}$ largest

singular values, respectively. Similarly, $\mathbf{U}_n$ and $\mathbf{V}_n$ contain the left and right singular vectors of $\mathbf{Y}$ corresponding to remaining singular values respectively.

$$\mathbf{U}_1 = \mathbf{U}_s : \text{ with last row deleted} \tag{5.23}$$

$$\mathbf{U}_2 = \mathbf{U}_s : \text{ with first row deleted} \tag{5.24}$$

then the eigenvalues of matrix $\mathbf{U}_1^{\dagger}\mathbf{U}_2$ yield the angle of arrival of the incoming signals on the antenna array.

$$\theta_{1,\cdots,I} = \text{eigenval}(\mathbf{U}_1^{\dagger}\mathbf{U}_2) \tag{5.25}$$

Using both ranging and DoA algorithms localization was performed on chipless tags at different locations in the interrogation zone. In Fig. (5.18) MPM algorithm was used to calculate the angle of the tag. The algorithm located all the tags successfully except one. This is due to wrong RSS ranging.

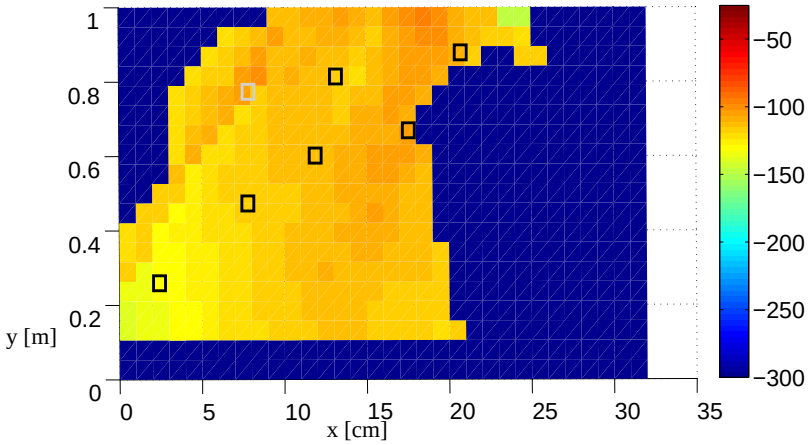

Figure 5.18: localization using ranging and MPM, gray boxes represent wrong detected tags and black is correct.

5.5.4 Measurement Setup

For real-time measurements, a USRP test bed was created inside an indoor environment. Three USRP were used, two for the receiver (B210) and one as the transmitter (N210) as shown in Fig. (5.19). For synchronization of all USRP devices, an Octoclock with a 10 MHz source was used.

All the signal processing and was performed on a laptop containing GNURadio.

For localization, only one notch was considered. This eliminates the scanning of the full tag bandwidth making the localization process much faster. The first process done by the reader was notch detection using algorithms discussed in [111]. The notch and the peak frequency was recorded, and the localization process starts by applying RSS for the range and the MPM for AoA detection. Furthermore to remove clutter a spacial filter and the PN-Sequence was preformed [85].

The results shown in Fig. (5.20), shows the original position of the tag (blue circles) and the detected position (red triangles) in a 50 cm by 50 cm interrogation zone. The interrogation zone is precalculated using WI and measurements calibration.

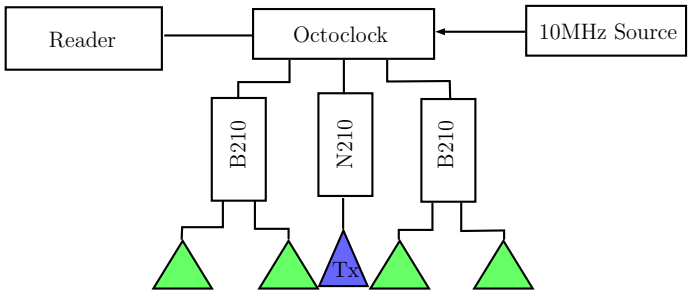

Figure 5.19: A description drawing showing the measurement setup using USRP

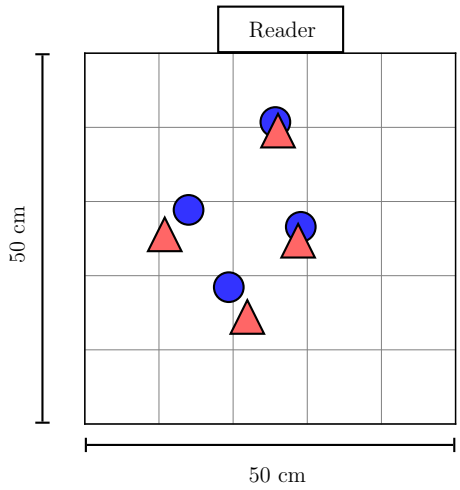

Figure 5.20: Chipless RFID tag localization measurement results (blue is the actual position and red is the calculated position)

6 Conclusion and Future Work

In this chapter, the conclusion achieved throughout the dissertation is summarized, and the future work is stated.

6.1 Conclusion

This thesis discussed three main points related to FC chipless RFID. The first pint is the clutter effect and how it greatly affects the tag backscattering response. The second aspect was notch detection and we proved that without an efficient detection technique the tag will not be identified. The third aspect was tag localization, were AoA techniques with RSS to determine the location of the tag.

Chapter 3 starts by formulating the channel and concluded that two signals distort the backscattered signal from the tag. The two interference signals are the clutter response and coupling. It was found that to get the actual performance of the tag; the 3D model has to be taken into consideration. The 3D was exported from an EM simulation tool and inserted in a ray tracer software. Moreover, to prove our theories, a test bed is created using USRP, where two clutter removal techniques were investigated. These two algorithms are empty room calibration and PN sequence using Rake receiver equalizer. In the empty room calibration, it was concluded that a high number of averaging is required to get an accurate reading from the channel. In empty room calibration, the environment has to be constant, if there any change in the environment or the measurement setup the system has to be re-calibrated. As a solution, PN sequence was introduced to counter the deficiency of empty room calibration. To remove the clutter a Rake receiver. This method is considered like time gating with CW signals. After simulation and measurements, it was concluded that the PN sequence shows great results and without the use of any empty room measurement.

In Chapter 4 proves that notch detection is an important part of the identification process. The first conclusion from this chapter is that the operating frequency band should be windowed. This window should either contain a notch or a full reflection. This concept must be considered even when designing the tag. The second step is to apply notch detection techniques on this window. It was also shown that the larger the notch the P_d is, as long as the notch is contained inside the window. If part of the notch is in the other window, then the overall detection will be significantly decreased. Three different notch detection algorithms were also presented in this chapter. The three algorithms are matched filter, SVD and DTW. Each algorithm was made to solve a disadvantage in the other. It was shown that matched filter, although easy to implement, could not resolve different notch widths. Resolving different notch widths is essential for increasing the capacity of the tag, where the information of the tag is in its width and its position. The algorithm that showed the best success in notch width detection are DTW and SVD techniques. Although, SVD showed the best performance in a single notch detection, where the information is only in the frequency position of the notch. Since the tag geometry is necessary for the response of the notch, any manufacturing errors or wrong reader calibration could cause the position of the notch to shift. This shift should be studied regarding the decoding. The best performance for detecting the notch even if there were shifts are the matched filter and DTW. The SVD showed the worst results for the overall P_d for detecting shifted notches. The last conclusion taken from this chapter is that the matched filter is the less complicated algorithm then comes the SVD and then DTW.

Chapter 5 discusses the localization algorithms for chipless RFID. It starts by reinforcing the conclusion mentioned in chapter 3 that the 3D RCS should always be taken into consideration when modeling the tag. The interrogation zone is then calculated using the 3D RCS, with a mathematical presentation of the link budget. The difference in range between an Omni and a directional antenna was also shown. In this investigation, directional antenna showed a higher interrogation area. The chapter then investigates two different localization algorithms. The first is trilateration, where at least three readers are required to detect the location of the tag. This algorithm was concluded inefficient for some types of tags. Since most of the tags could not be detected in all the angles. This was when a different approach was introduced. This algorithm uses the angle of arrival and RSS measurements. To validate this algorithm first, RSS was measured in 1D ranging. It shows that detecting the full reflection mode of the tag is sufficient for ranging the tag. The second part is then locating the AoA. All AOA algorithm was investigated to test their efficiency in an indoor chipless tag localization. It was concluded that MPM is the

best algorithm to detect the correlated angle of arrivals. In all localization algorithms, the tag had to be detected using one of the algorithms mentioned in chapter 4.

6.2 Future Work

For future work, it is recommended to design a tool specially designed for chipless RFID. This tool would include all the properties of the chipless RFID from EM simulation of the tag to the channel estimation and even protocol design. This tool could take some functionality from other well-known software. Another recommendation is in the channel chipless RFID modeling. In this thesis deterministic models were used, it is recommended that a statistical model should be built. This model has to accurate to decrease the need for real measurements.

For the chipless RFID to replace the signature of the tag should represent more bits. Decoding a large number of bits should be studied and investigated. Moreover, the reading range should be significantly increased. This could be done by higher sensitive readers and more directive antenna.

List of Publications and Awards

Journal Papers

[1] El-Hadidy, M., El-Awamry, A., Fawky, A., Khaliel, M., and Kaiser, T. (2016) Real-world testbed for multi-tag UWB chipless RFID system based on a novel collision avoidance MAC protocol. Trans Emerging Tel Tech

[2] A. Fawky, M. Khaliel, A. El-Awamry and T. Kaiser, "'Novel Notch Detection and Identification Techniques for Frequency Coded Chipless RFID Readers," *submitted in* IET Communications, 2016, pp. 1-20.

[3] A. Fawky, M. Khaliel, A. El-Awamry and T. Kaiser, "Chipless RFID Localization using Angle of Arrival Techniques," *to be submitted in* IET Communications, 2016, pp. 1-22.

[4] A. El-Awamry, M. Khaliel, A. Fawky and T. Kaiser, "Multi-Tag Identification and Protocol Evaluation Framework for the FC-Chipless RFID System," *submitted in* IET Communications, 2016, pp. 1-18.

[5] A. El-Awamry, M. Khaliel, A. Fawky and T. Kaiser, "Adaptive Spectrum Scanning Techniques for Reducing the Identification Time of the Frequency Coded Chipless RFID System," *submitted in* Transactions on Emerging Telecommunications Technologies (Wiley), 2016, pp. 1-14.

[6] M. Khaliel, A. El-Awamry, A. Fawky and T. Kaiser, "Novel Physically Modulated Frequency Coded Chipless RFID Tags for High Coding Capacity and Robust Detection," *submitted in* IEEE Transactions on Microwave Theory and Techniques, 2016.

[7] M. Khaliel, A. Fawky, A. El-Awamry and T. Kaiser, "Long Reading Range Frequency Coded Chipless RFID System based on Reflectarray Antennas," *submitted in* IEEE Transactions on Microwave Theory and Techniques, 2016.

Conference Papers

[1] A. El-Awamry, M. Khaliel, A. Fawky, M. El-Hadidy and T. Kaiser, "Novel Adaptive Sliding Window Algorithm Reducing Latency for Multi-tag Chipless RFID Systems," Radio Science Meeting (Joint with AP-S Symposium), 2015 USNC-URSI, Vancouver, BC, Canada, 2015, pp. 206-206.

[2] A. Fawky, M. Khaliel, A. El-Awamry, M. El-Hadidy and T. Kaiser, "Novel Pseudo-Noise Coded Chipless RFID System for Clutter Removal and Tag Detection," 2015 IEEE International Conference on RFID (RFID), San Diego, CA, 2015, pp. 100-104.

[3] A. El-Awamry, M. Khaliel, A. Fawky, M. El-Hadidy and T. Kaiser, "Novel Notch Modulation Algorithm for Enhancing the Chipless RFID Tags Coding Capacity," 2015 IEEE International Conference on RFID (RFID), San Diego, CA, 2015, pp. 25-31.

[4] M. El-Hadidy, A. El-Awamry, A. Fawky, M. Khaliel and T. Kaiser, "A Novel Collision Avoidance MAC Protocol for Multi-tag UWB Chipless RFID Systems based on Notch Position Modulation," 2015 9th European Conference on Antennas and Propagation (EuCAP), Lisbon, 2015, pp. 1-5.

[5] A. El-Awamry, A. Fawky, M. El-Hadidy and T. Kaiser, "Smart Notch Detection Techniques for Robust Frequency Coded Chipless RFID Systems," 2015 9th European Conference on Antennas and Propagation (EuCAP), Lisbon, 2015, pp. 1-5.

[6] M. Khaliel, A. El-Awamry, A. Fawky, M. El-Hadidy and T. Kaiser, "A Novel Co/Cross-polarizing Chipless RFID Tags for High Coding Capacity and Robust Detection," 2015 IEEE International Symposium on Antennas and Propagation and USNC/URSI National Radio Science Meeting, Vancouver, BC, 2015, pp. 159-160.

[7] B. Nagy, A. Fawky, M. Khaliel, M. El-Hadidy and T. Kaiser, "Novel Pseudo-Noise coded chipless RFID system for clutter removal and tag detection," The 8th European Conference on Antennas and Propagation (EuCAP 2014), The Hague, 2014, pp. 2808-2811.

[8] A. Fawky, M. Khaliel, M. El-Hadidy and T. Kaiser, "UWB Chipless RFID System Performance Based on Real World 3D-Deterministic Channel Model and ZF Equalization," The 8th European Conference on Antennas and Propagation (EuCAP 2014), The Hague, 2014, pp. 1765-1768.

[9] M. El-Hadidy, A. Fawky, B. Nagy, M. Khaliel, E. Abdallah, H. Elhennawy, and T. Kaiser, "Evaluation of UWB Chipless RFID System Performance Considering Indoor Multipath Propagation Channeland Real World Aspects," 34th Progress In Electromagnetics Research Symposium PIERS, Stockholm, Sweden, Aug. 12-15, 2013, pp. 616-620.

[10] M. El-Hadidy, B. Nagy, M. Khaliel, A. Fawky, E. Abdallah, H. Elhennawy, and T. Kaiser, "Novel Methodology for Increasing the Reading Range of the UWB Passive RFID Chipless Tags Considering Power regulations," 34th Progress In Electromagnetics Research Symposium PIERS, Stockholm, Sweden, Aug. 12-15, 2013, pp. 630-632.

[11] M. Khaliel, A. El-Awamry, A. Fawky and T. Kaiser, "Printable High Coding Capacity Chipless RFID Tags for Low Cost Item Tagging," submitted in 14th IEEE International Conference on Networking, Sensing and Control, Italy, 2017, pp. 1-5.

[12] M. Khaliel, A. El-Awamry, A. Fawky and T. Kaiser, "Long Reading Range Chipless RFID System Based on Reflectarray Antennas," submitted in European Conference on Antennas and Propagation (EuCAP), Paris, 2017, pp. 1-5.

[13] A. El-Awamry, M. Khaliel, A. Fawky and T. Kaiser, "A Novel Multi-Tag Identification Technique for Frequency Coded Chipless RFID Systems Based on Look-Up-Table Approach," submitted in European Conference on Antennas and Propagation (EuCAP), Paris, 2017, pp. 1-5.

[14] A. Fawky, M. Khaliel, A. El-Awamry and T. Kaiser, "Frequency Coded Chipless RFID Tag Localization Using Multiple Antennas," submitted in European Conference on Antennas and Propagation (EuCAP), Paris, 2017, pp. 1-5.

[15] A. El-Awamry, A. Fawky, M. Khaliel and T. Kaiser, "A Novel Adaptive Spectrum Scanning Technique for Reducing the Identification Time of the UWB Chipless RFID System," submitted in 14th IEEE International Conference on Networking, Sensing and Control, Italy, 2017, pp. 1-5.

[16] A. Fawky, A. El-Awamry, M. Khaliel and T. Kaiser, "Novel Notch Detection Techniques for Frequency Coded Chipless RFID," submitted in 14th IEEE International Conference on Networking, Sensing and Control, Italy, 2017, pp. 1-5.

Organized IEEE Workshops

[1] "Chipless RFID Future and Challenges," 2015 9th European Conference on Antennas and Propagation (EuCAP), Lisbon, 2015

[2] "Chipless RFID System and Testbed: Reader and Tag Antennas, Reader and Tag Design, Multi-Tag Scenarios, Modulation, Clutter Effects and Channel Estimation, Signaling and Real-world Testbed," Radio Science Meeting (Joint with AP-S Symposium), 2015 USNC-URSI, Vancouver, BC, Canada, 2015

Awards

1. Awarded a three year Deutscher Akademischer Austauschdienst (DAAD) PhD. student scholarship under the Deutsch-Arabische Forschungspartnerschaft program grants in ID4EGYPT Project.

2. The paper "A Novel Collision Avoidance MAC Protocol for Multi-Tag UWB Chipless RFID Systems based on Notch Position Modulation," is nominated for the **best student paper award** at 2015 9th European Conference on Antennas and Propagation (EuCAP) conference.

Bibliography

[1] J. D. Griffin and G. D. Durgin, "Complete link budgets for backscatter-radio and rfid systems," *IEEE Antennas and Propagation Magazine*, vol. 51, no. 2, pp. 11–25, April 2009.

[2] Debasis Bandyopadhyay and Jaydip Sen, "Internet of things: Applications and challenges in technology and standardization," *Wireless Personal Communications*, vol. 58, no. 1, pp. 49–69, 2011.

[3] Fan Wu, Frank Kuo, and Liu-Wei Liu, "The application of rfid on drug safety of inpatient nursing healthcare," in *Proceedings of the 7th International Conference on Electronic Commerce*, New York, NY, USA, 2005, ICEC '05, pp. 85–92, ACM.

[4] E. Perret, *Radio Frequency Identification and Sensors: From RFID to Chipless RFID*, Wiley, 2014.

[5] M. M. Perez, G. V. Gonzalez, J. R. V. Hermida, I. M. Herranz, and C. Dafonte, "Improving the locating precision of an active wifi rfid system to obtain traceability of patients in a hospital," in *2016 30th International Conference on Advanced Information Networking and Applications Workshops (WAINA)*, March 2016, pp. 833–837.

[6] C. H. Liu and J. Y. Lo, "The study for the rfid with bluetooth positioning system," in *Information Sciences and Interaction Sciences (ICIS), 2010 3rd International Conference on*, June 2010, pp. 386–391.

[7] A. Bansal, A. Aneja, J. Bansal, S. Sharma, and R. Ankur, "Rfid zigbee based interplatform train tracking system," in *India Educators' Conference (TIIEC), 2013 Texas Instruments*, April 2013, pp. 268–270.

[8] Morrison E Babbage C, Morrision P, "On the principles and development of the calculator and other seminal writing," *Dover Publications*, 1961.

[9] Klaus Finkenzeller, *RFID Handbook: Fundamentals and Applications in Contactless Smart Cards and Identification*, Wiley Publishing, 2nd edition, 2003.

[10] N. C. Karmaker, "Tag, you're it radar cross section of chipless rfid tags," *IEEE Microwave Magazine*, vol. 17, no. 7, pp. 64–74, July 2016.

[11] Reza Rezaiesarlak and Majid Manteghi, *Chipless RFID: Design Procedure and Detection Techniques*, Springer Publishing Company, Incorporated, 2014.

[12] Stevan Preradovic and Nemai Chandra Karmakar, *Multiresonator-Based Chipless RFID: Barcode of the Future*, Springer Publishing Company, Incorporated, 2014.

[13] V. P. Plessky and L. M. Reindl, "Review on saw rfid tags," *IEEE Transactions on Ultrasonics, Ferroelectrics, and Frequency Control*, vol. 57, no. 3, pp. 654–668, March 2010.

[14] Y. y. Zhong, Z. j. Chen, X. c. Wang, C. Han, and J. Fu, "Anti-collision saw tags based on cidt," in *Piezoelectricity, Acoustic Waves, and Device Applications (SPAWDA), 2015 Symposium on*, Oct 2015, pp. 137–142.

[15] V. P. Plessky, Z. J. Davis, M. Lamothe, and S. G. Suchkov, ," pp. 392–395, Sept.

[16] R. Nair, E. Perret, and S. Tedjini, "Novel encoding in chipless rfid using group delay characteristics," in *Microwave Optoelectronics Conference (IMOC), 2011 SBMO/IEEE MTT-S International*, Oct 2011, pp. 896–900.

[17] S. Preradovic, I. Balbin, and N. Karmakar, "The development and design of a novel chipless rfid system for low-cost item tracking," in *2008 Asia-Pacific Microwave Conference*, Dec 2008, pp. 1–4.

[18] S. Preradovic and N. C. Karmakar, "Design of fully printable planar chipless rfid transponder with 35-bit data capacity," in *Microwave Conference, 2009. EuMC 2009. European*, Sept 2009, pp. 013–016.

[19] S. Preradovic, S. Roy, and N. Karmakar, "Fully printable multi-bit chipless rfid transponder on flexible laminate," in *2009 Asia Pacific Microwave Conference*, Dec 2009, pp. 2371–2374.

[20] M. S. Bhuiyan, A. Azad, and N. Karmakar, "Dual-band modified complementary split ring resonator (mcsrr) based multi-resonator circuit for chipless rfid tag," in *Intelligent Sensors, Sensor Networks and Information Processing, 2013 IEEE Eighth International Conference on*, April 2013, pp. 277–281.

[21] P. Narkcharoen and S. Pranonsatit, "The applications of fill until full (fuf) for multiresonator-based chipless rfid system," in *Electrical Engineering/Electronics, Computer, Telecommunications and Information Technology (ECTI-CON), 2011 8th International Conference on*, May 2011, pp. 176–179.

[22] "Rf barcodes using multiple frequency bands," in *IEEE MTT-S International Microwave Symposium Digest, 2005.*, June 2005, pp. 4 pp.–.

[23] A. Vena, E. Perret, and S. Tedjini, "High-capacity chipless rfid tag insensitive to the polarization," *IEEE Transactions on Antennas and Propagation*, vol. 60, no. 10, pp. 4509–4515, Oct 2012.

[24] M. A. Islam and N. C. Karmakar, "A novel compact printable dual-polarized chipless rfid system," *IEEE Transactions on Microwave Theory and Techniques*, vol. 60, no. 7, pp. 2142–2151, July 2012.

[25] D. Dardari, R. D'Errico, C. Roblin, A. Sibille, and M.Z. Win, "Ultrawide bandwidth rfid: The next generation?," *Proceedings of the IEEE*, vol. 98, no. 9, pp. 1570–1582, 2010.

[26] A. Lazaro, D. Girbau, and D. Salinas, "Radio link budgets for uhf rfid on multipath environments," *Antennas and Propagation, IEEE Transactions on*, vol. 57, no. 4, pp. 1241–1251, 2009.

[27] J.D. Griffin and G.D. Durgin, "Link envelope correlation in the backscatter channel," *Communications Letters, IEEE*, vol. 11, no. 9, pp. 735–737, 2007.

[28] Li Jiang, Lin Li, and Guo-Qing Zhao, "A novel method for lpi radar signal sorting in multipath channel," in *Industrial Electronics (ISIE), 2012 IEEE International Symposium on*, 2012, pp. 1100–1104.

[29] M.A. Assad, M. Heidari, and K. Pahlavan, "Effects of channel modeling on performance evaluation of wifi rfid localization using a laboratory testbed," in *Global Telecommunications Conference, 2007. GLOBECOM '07. IEEE*, 2007, pp. 366–370.

[30] Yulin Deng, Wing Cheong Lau, and Onching Yue, "Design and evaluation of rfid counting algorithms under time-correlated channels," in *Consumer Communications and Networking Conference (CCNC), 2013 IEEE*, 2013, pp. 443–448.

[31] Kin Seong Leong, Mun Leng Ng, and P.H. Cole, "The reader collision problem in rfid systems," in *Microwave, Antenna, Propagation and EMC Technologies for Wireless Communications, 2005. MAPE 2005. IEEE International Symposium on*, 2005, vol. 1, pp. 658–661 Vol. 1.

[32] A.G. Dimitriou, A. Bletsas, A.C. Polycarpou, and J.N. Sahalos, "On efficient uhf rfid coverage inside a room," in *Antennas and Propagation (EuCAP), 2010 Proceedings of the Fourth European Conference on*, 2010, pp. 1–5.

[33] S. Duangsuwan and S. Promwong, "A rfid reader suppressive interferences due to multipath," *PIERS Proceedings*, pp. 1472 – 1475, 2012.

[34] John G. Proakis and Dimitris G. Manolakis, *Digital signal processing (3rd ed.): principles, algorithms, and applications*, Prentice-Hall, Inc., Upper Saddle River, NJ, USA, 1996.

[35] M. El-Hadidy and T. Kaiser, "An uwb channel model considering angular antenna impulse response and polarization," in *Antennas and Propagation, 2007. EuCAP 2007. The Second European Conference on*, 2007, pp. 1–5.

[36] M.A. Islam, Y. Yap, N. Karmakar, and A.K.M. Azad, "Orientation independent compact chipless rfid tag," in *RFID-Technologies and Applications (RFID-TA), 2012 IEEE International Conference on*, 2012, pp. 137–141.

[37] G. Tiberi, S. Bertini, W. Q. Malik, A. Monorchio, D. J. Edwards, and G. Manara, "An efficient ray tracing propagation simulator for analyzing ultrawideband channels," in *2007 IEEE International Conference on Ultra-Wideband*, Sept 2007, pp. 794–799.

[38] S. Preradovic and N.C. Karmakar, "Design of short range chipless rfid reader prototype," in *Intelligent Sensors, Sensor Networks and Information Processing (ISSNIP), 2009 5th International Conference on*, Dec 2009, pp. 307–312.

[39] M. Khaliel, A. Fawky, M. El-Hadidy, and T. Kaiser, "Uwb reflectarray antenna for chipless rfid applications," in *Radio Science Conference (NRSC), 2014 31st National*, April 2014, pp. 17–20.

[40] P. Kalansuriya, N. C. Karmakar, and E. Viterbo, "On the detection of frequency-spectra-based chipless rfid using uwb impulsed interrogation," *IEEE Transactions on Microwave Theory and Techniques*, vol. 60, no. 12, pp. 4187–4197, Dec 2012.

[41] M. Popperl, C. Carlowitz, M. Vossiek, C. Mandel, and R. Jakoby, "An ultra-wideband time domain reflectometry chipless rfid system with higher order modulation schemes," in *2016 German Microwave Conference (GeMiC)*, March 2016, pp. 401–404.

[42] A. Ramos, E. Perret, O. Rance, S. Tedjini, A. Lazaro, and D. Girbau, "Temporal separation detection for chipless depolarizing frequency-coded rfid," *IEEE Transactions on Microwave Theory and Techniques*, vol. 64, no. 7, pp. 2326–2337, July 2016.

[43] Yaakov Kraftmakher, "Noise reduction by signal accumulation," *The Physics Teacher*, vol. 44, no. 8, pp. 528–530, 2006.

[44] A. Vena, E. Perret, and S. Tedjni, "A depolarizing chipless rfid tag for robust detection and its fcc compliant uwb reading system," *Microwave Theory and Techniques, IEEE Transactions on*, vol. 61, no. 8, pp. 2982–2994, Aug 2013.

[45] R. Koswatta and N.C. Karmakar, "Development of digital control section of rfid reader for multi-bit chipless rfid tag reading," in *Electrical and Computer Engineering (ICECE), 2010 International Conference on*, Dec 2010, pp. 554–557.

[46] A. Vena, E. Perret, and S. Tedjni, "A depolarizing chipless rfid tag for robust detection and its fcc compliant uwb reading system," *Microwave Theory and Techniques, IEEE Transactions on*, vol. 61, no. 8, pp. 2982–2994, Aug 2013.

[47] A. Vena, E. Perret, and S. Tedjini, "A compact chipless rfid tag using polarization diversity for encoding and sensing," in *RFID (RFID), 2012 IEEE International Conference on*, April 2012, pp. 191–197.

[48] Chi Xu and Choi L. Law, "Toa estimator for uwb backscattering rfid system with clutter suppression capability," *EURASIP J. Wirel. Commun. Netw.*, vol. 2010, pp. 46:1–46:13, Apr. 2010.

[49] C. Candan and A.O. Yilmaz, "Efficient methods of clutter suppression for coexisting land and weather clutter systems," *Aerospace and Electronic Systems, IEEE Transactions on*, vol. 45, no. 4, pp. 1641–1650, Oct 2009.

[50] Xiaolong Chen, Jian Guan, Ningbo Liu, and You He, "Maneuvering target detection via radon-fractional fourier transform-based long-time coherent integration," *Signal Processing, IEEE Transactions on*, vol. 62, no. 4, pp. 939–953, Feb 2014.

[51] Enrico Paolini, Andrea Giorgetti, Marco Chiani, Riccardo Minutolo, and Mauro Montanari, "Localization capability of cooperative anti-intruder radar systems.," *EURASIP J. Adv. Sig. Proc.*, vol. 2008, 2008.

[52] C.M. Nijas, U. Deepak, P.V. Vinesh, R. Sujith, S. Mridula, K. Vasudevan, and P. Mohanan, "Low-cost multiple-bit encoded chipless rfid tag using stepped impedance resonator," *Antennas and Propagation, IEEE Transactions on*, vol. 62, no. 9, pp. 4762–4770, Sept 2014.

[53] K.L. Yung, C.Y. Chan, and D.K.W. Cheng, "Chipless microwave identification tag," Oct. 29 2009, US Patent App. 12/396,127.

[54] M.A. Islam, Y. Yap, N. Karmakar, and A.K.M. Azad, "Orientation independent compact chipless rfid tag," in *RFID-Technologies and Applications (RFID-TA), 2012 IEEE International Conference on*, Nov 2012, pp. 137–141.

[55] A. Fawky, M. Mohammed, M. El-Hadidy, and T. Kaiser, "Uwb chipless rfid system performance based on real world 3d-deterministic channel model and zf equalization," in *Antennas and Propagation (EuCAP), 2014 8th European Conference on*, April 2014, pp. 1765–1768.

[56] Henry Stark and John W. Woods, *Probability and Random Processes with Applications to Signal Processing (3rd Edition)*, Prentice Hall, 3 edition, Aug. 2001.

[57] N. Benvenuto, E. Costa, and E. Obetti, "Performance comparison of chip matched filter and rake receiver for wcdma systems," in *Global Telecommunications Conference, 2001. GLOBECOM '01. IEEE*, 2001, vol. 5, pp. 3060–3064 vol.5.

[58] M. Goresky and A.M. Klapper, "Fibonacci and galois representations of feedback-with-carry shift registers," *Information Theory, IEEE Transactions on*, vol. 48, no. 11, pp. 2826–2836, Nov 2002.

[59] W.Q. Malik, D.J. Edwards, and C.J. Stevens, "Experimental evaluation of rake receiver performance in a line-of-sight ultra-wideband channel," in *Ultra Wideband Systems,*

2004. Joint with Conference on Ultrawideband Systems and Technologies. Joint UWBST IWUWBS. 2004 International Workshop on, May 2004, pp. 217–220.

[60] S. Genovesi, F. Costa, A. Monorchio, and G. Manara, "Phase-only encoding for novel chipless rfid tag," in *RFID Technology and Applications Conference (RFID-TA), 2014 IEEE*, Sept 2014, pp. 68–71.

[61] I. Balbin and N.C. Karmakar, "Phase-encoded chipless rfid transponder for large-scale low-cost applications," *Microwave and Wireless Components Letters, IEEE*, vol. 19, no. 8, pp. 509–511, Aug 2009.

[62] S. Preradovic, N. Karmakar, and M. Zenere, "Uwb chipless tag rfid reader design," in *RFID-Technology and Applications (RFID-TA), 2010 IEEE International Conference on*, June 2010, pp. 257–262.

[63] M. Manteghi, "A novel approach to improve noise reduction in the matrix pencil algorithm for chipless rfid tag detection," in *Antennas and Propagation Society International Symposium (APSURSI), 2010 IEEE*, July 2010, pp. 1–4.

[64] R. Rezaiesarlak and M. Manteghi, "A new detection technique for identifying chipless rfid tags," in *Radio Science Meeting (USNC-URSI NRSM), 2014 United States National Committee of URSI National*, Jan 2014, pp. 1–1.

[65] R. Rezaiesarlak and M. Manteghi, "Short-time matrix pencil method for chipless rfid detection applications," *Antennas and Propagation, IEEE Transactions on*, vol. 61, no. 5, pp. 2801–2806, May 2013.

[66] P. Kalansuriya, N. Karmakar, and E. Viterbo, "Signal space representation of chipless rfid tag frequency signatures," in *Global Telecommunications Conference (GLOBECOM 2011), 2011 IEEE*, Dec 2011, pp. 1–5.

[67] Leon W. Couch, II, *Digital and Analog Communication Systems*, Prentice Hall PTR, Upper Saddle River, NJ, USA, 3rd edition, 1990.

[68] Letao Xu, Dejun Feng, and Xuesong Wang, "Matched-filter properties of linear-frequency-modulation radar signal reflected from a phase-switched screen," *Radar, Sonar Navigation, IET*, vol. 10, no. 2, pp. 318–324, 2016.

[69] A. Johnston, "Improvements to a pulse compression radar matched filter," *Radio and Electronic Engineer*, vol. 53, no. 4, pp. 138–140, April 1983.

[70] S. Sussman, "A matched filter communication system for multipath channels," *Information Theory, IRE Transactions on*, vol. 6, no. 3, pp. 367–373, June 1960.

[71] Xuedong Huang, Alex Acero, and Hsiao-Wuen Hon, *Spoken Language Processing: A Guide to Theory, Algorithm, and System Development*, Prentice Hall PTR, Upper Saddle River, NJ, USA, 1st edition, 2001.

[72] K. Barczewska and A. Drozd, "Comparison of methods for hand gesture recognition based on dynamic time warping algorithm," in *Computer Science and Information Systems (FedCSIS), 2013 Federated Conference on*, Sept 2013, pp. 207–210.

[73] Meinard Muller, *Information retrieval for music and motion*, Springer, New York, 2007.

[74] Ahmed A. Elawamry, *Realistic Chipless RFID: Protocol, Encoding and System Latency*, Ph.D. thesis, Duisburg-Essen University, 2016.

[75] Maher Khaliell, *Realistic Chipless RFID: Physically Modulated Tags and Reflectarray Readers*, Ph.D. thesis, Dusburg-Essen University, 2016.

[76] M. El-Hadidy, A. El-Awamry, A. Fawky, M. Khaliel, and T. Kaiser, "A novel collision avoidance mac protocol for multi-tag uwb chipless rfid systems based on notch position modulation," in *2015 9th European Conference on Antennas and Propagation (EuCAP)*, May 2015, pp. 1–5.

[77] C. Feng, W. Zhang, L. Li, L. Han, X. Chen, and R. Ma, "Angle-based chipless rfid tag with high capacity and insensitivity to polarization," *IEEE Transactions on Antennas and Propagation*, vol. 63, no. 4, pp. 1789–1797, April 2015.

[78] M. M. Khan, F. A. Tahir, and H. M. Cheema, "High capacity polarization sensitive chipless rfid tag," in *2015 IEEE International Symposium on Antennas and Propagation USNC/URSI National Radio Science Meeting*, July 2015, pp. 1770–1771.

[79] M. Khaliel, A. El-Awamry, A. Fawky, M. El-Hadidy, and T. Kaiser, "A novel co/cross-polarizing chipless rfid tags for high coding capacity and robust detection," in *2015 IEEE International Symposium on Antennas and Propagation USNC/URSI National Radio Science Meeting*, July 2015, pp. 159–160.

[80] M. Zomorrodi and N. C. Karmakar, "Image-based chipless rfid system with high content capacity for low cost tagging," in *2014 IEEE International Microwave and RF Conference (IMaRC)*, Dec 2014, pp. 41–44.

[81] M. Zomorrodi and N. C. Karmakar, "Cross-polarized printable chipless rfid tag with superior data capacity," in *Microwave Conference (EuMC), 2014 44th European*, Oct 2014, pp. 766–769.

[82] C. M. Nijas, U. Deepak, R. Sujith, and P. Mohanan, "Multi resonance based chipless rfid tag with high data encoding capacity," in *General Assembly and Scientific Symposium (URSI GASS), 2014 XXXIth URSI*, Aug 2014, pp. 1–4.

[83] A. El-Awamry, M. Khaliel, A. Fawky, M. El-Hadidy, and T. Kaiser, "Novel notch modulation algorithm for enhancing the chipless rfid tags coding capacity," in *2015 IEEE International Conference on RFID (RFID)*, April 2015, pp. 25–31.

[84] M. Khaliel, M. El-Hadidy, and T. Kaiser, "Printable depolarizing chipless rfid tag based on dgs resonators for suppressing the clutter effects," in *Antennas and Propagation (EUCAP), 2015 9th European Conference on*, 2015.

[85] A. Fawky, M. Khaliel, A. El-Awamry, M. El-Hadidy, and T. Kaiser, "Novel pseudo-noise coded chipless rfid system for clutter removal and tag detection," in *2015 IEEE International Conference on RFID (RFID)*, April 2015, pp. 100–104.

[86] V. Wolfe, W. Frobe, V. Shrinivasan, and T. Y. Hsieh, "Detecting and locating cell phone signals from avalanche victims using unmanned aerial vehicles," in *Unmanned Aircraft Systems (ICUAS), 2015 International Conference on*, June 2015, pp. 704–713.

[87] J. Yan and J. Yan, "Design and experiment of the passive rfid system in joint total asset visibility system," in *Instrumentation, Measurement, Computer, Communication and Control, 2011 First International Conference on*, Oct 2011, pp. 39–42.

[88] H. Lee, S. H. Kim, and H. W. Lee, "Advanced technologies for smart exhibition guide services," in *Information and Communication Technology Convergence (ICTC), 2015 International Conference on*, Oct 2015, pp. 864–867.

[89] Y. K. Yuce and K. H. Gulkesen, "Caregivernet: A novel social support intervention for locating and securing wandering alzheimer's patients as soon as possible," in *2013 9th*

International Wireless Communications and Mobile Computing Conference (IWCMC), July 2013, pp. 1405–1411.

[90] Y. Zheng, Y. Zang, and K. Pahlavan, "Uwb localization modeling for electronic gaming," in *2016 IEEE International Conference on Consumer Electronics (ICCE)*, Jan 2016, pp. 170–173.

[91] M. Khaliel, M. El-Hadidy, and T. Kaiser, "Printable depolarizing chipless rfid tag based on dgs resonators for suppressing the clutter effects," in *2015 9th European Conference on Antennas and Propagation (EuCAP)*, May 2015, pp. 1–5.

[92] T. Gigl, G. J. M. Janssen, V. Dizdarevic, K. Witrisal, and Z. Irahhauten, "Analysis of a uwb indoor positioning system based on received signal strength," in *2007 4th Workshop on Positioning, Navigation and Communication*, March 2007, pp. 97–101.

[93] Y. Shimizu and Y. Sanada, "Accuracy of relative distance measurement with ultra wideband system," in *Ultra Wideband Systems and Technologies, 2003 IEEE Conference on*, Nov 2003, pp. 374–378.

[94] R. C. Qiu, "A generalized time domain multipath channel and its application in ultra-wideband (uwb) wireless optimal receiver design-part ii: physics-based system analysis," *IEEE Transactions on Wireless Communications*, vol. 3, no. 6, pp. 2312–2324, Nov 2004.

[95] S. Gezici, Zhi Tian, G. B. Giannakis, H. Kobayashi, A. F. Molisch, H. V. Poor, and Z. Sahinoglu, "Localization via ultra-wideband radios: a look at positioning aspects for future sensor networks," *IEEE Signal Processing Magazine*, vol. 22, no. 4, pp. 70–84, July 2005.

[96] Zafer Sahinoglu, Sinan Gezici, and Ismail Gvenc, *Ultra-wideband Positioning Systems: Theoretical Limits, Ranging Algorithms, and Protocols*, Cambridge University Press, New York, NY, USA, 2011.

[97] Nemai Chandra Karmakar, *Handbook of smart antennas for RFID systems / edited by Nemai Chandra Karmakar*, Wiley Hoboken, N.J, 2010.

[98] S. M. Kim and Y. H. Kim, "Three octave ultra-wideband 3-port circulator in 0.11 cmos," *Electronics Letters*, vol. 49, no. 10, pp. 648–650, May 2013.

[99] R. E. A. Anee and N. C. Karmakar, "Chipless rfid tag localization," *IEEE Transactions on Microwave Theory and Techniques*, vol. 61, no. 11, pp. 4008–4017, Nov 2013.

[100] R. Rezaiesarlak and M. Manteghi, "A space-frequency technique for chipless rfid tag localization," *IEEE Transactions on Antennas and Propagation*, vol. 62, no. 11, pp. 5790–5797, Nov 2014.

[101] N. Zhang, M. Hu, L. Shao, and J. Yang, "Localization of printed chipless rfid in 3-d space," *IEEE Microwave and Wireless Components Letters*, vol. 26, no. 5, pp. 373–375, May 2016.

[102] Chuan-Hsian Pu Chuan-Chin Pu and Hoon-Jae Lee, *Emerging Communications for Wireless Sensor Networks*, InTech, 2011.

[103] Andreas F Molisch, Kannan Balakrishnan, Chia-Chin Chong, Shahriar Emami, Andrew Fort, Johan Karedal, Juergen Kunisch, Hans Schantz, Ulrich Schuster, and Kai Siwiak, "Ieee 802.15. 4a channel model-final report," *IEEE P802*, vol. 15, no. 04, pp. 0662, 2004.

[104] Nuri Yilmazer and Tapan K. Sarkar, "2dd unitary matrix pencil method for efficient direction of arrival estimation," *Digit. Signal Process.*, vol. 16, no. 6, pp. 767–781, Nov. 2006.

[105] B. D. Van Veen and K. M. Buckley, "Beamforming: a versatile approach to spatial filtering," *IEEE ASSP Magazine*, vol. 5, no. 2, pp. 4–24, April 1988.

[106] M. S. Bartlett, "Smoothing periodograms from time series with continuous spectra," *Nature*, 1948.

[107] C. Vaidyanathan and K. M. Buckley, "Performance analysis of the mvdr spatial spectrum estimator," *IEEE Transactions on Signal Processing*, vol. 43, no. 6, pp. 1427–1437, Jun 1995.

[108] R. Schmidt, "Multiple emitter location and signal parameter estimation," *IEEE Transactions on Antennas and Propagation*, vol. 34, no. 3, pp. 276–280, Mar 1986.

[109] A. Paulraj, R. Roy, and T. Kailath, "A subspace rotation approach to signal parameter estimation," *Proceedings of the IEEE*, vol. 74, no. 7, pp. 1044–1046, July 1986.

[110] Sheng Hong, Xianrong Wan, and Hengyu Ke, "Spatial difference smoothing for coherent sources location in mimo radar," *Signal Process.*, vol. 109, no. C, pp. 69–83, Apr. 2015.

[111] A. El-Awamry, A. Fawky, M. El-Hadidy, M. Khaliel, and T. Kaiser, "Smart notch detection techniques for robust frequency coded chipless rfid systems," in *9th European Conference on Antennas and Propagation EuCAP 2015*, April 2015.